NASA CONTRACTOR REPORT

NASA CR-2312

NASA CR-2312

QUASI-OPTIMUM DESIGN OF A SIX DEGREE OF FREEDOM MOVING BASE SIMULATOR CONTROL SYSTEM

by Bernard Friedland, Chong-Kuan Ling, and Maurice F. Hutton

Prepared by
SINGER COMPANY
Little Falls, N.J.
for Ames Research Center

NATIONAL AERONAUTICS AND SPACE ADMINISTRATION • WASHINGTON, D. C. • OCTOBER 1973

1. Report No. NASA CR-2312	2. Government Accession No.	3. Recipient's Catalog No.
4. Title and Subtitle Quasi-Optimum Design of a Six Degree of Freedom Moving Base Simulator Control System		5. Report Date October 1973 6. Performing Organization Code
7. Author(s) Bernard Friedland, Chong-Kuan Ling, and Maurice F. Hutton		8. Performing Organization Report No. 10. Work Unit No.
9. Performing Organization Name and Address Singer Company Kearfott Division Little Falls, New Jersey		11. Contract or Grant No. NAS 2-3636 13. Type of Report and Period Covered Contractor Report
12. Sponsoring Agency Name and Address National Aeronautics and Space Administration Washington, D.C. 20546		14. Sponsoring Agency Code

15. Supplementary Notes

16. Abstract

The design of a "washout" control system for a moving-base simulator is treated by a quasi-optimum control technique developed by Firedland (NASA CR-527 and CR-1099). An earlier version of the washout system, limited to longitudinal motion, was described in NASA CR-1613 and this work extends the design to a complete six-degree-of-freedom simulator. The broad objective of the design is to reproduce the sensed motion (angular velocity and specific force) as accurately as possible without causing the simulator (cab) excursions to exceed specified limits. A performance criterion is established that weights magnitude and direction errors in specific force and in angular velocity and attempts to maintain the excursion within set limits by penalizing excessive excursions. A FORTRAN routine for realizing the washout law was developed and typical time-histories using the washout routine were simulated for a range of parameters in the penalty-and weighting-functions. These time histories and the listing of the routine are included in the report. Evaluation of this class of washout laws in actual pilot simulations was not undertaken, and such evaluation is recommended for future investigation.

17. Key Words (Suggested by Author(s))	18. Distribution Statement
Simulator, Moving-base simulator, Optimal Control, Washout Control Law	UNCLASSIFIED-UNLIMITED

19. Security Classif. (of this report)	20. Security Classif. (of this page)	21. No. of Pages	22. Price*
UNCLASSIFIED	UNCLASSIFIED	149	Domestic, $4.50 Foreign, $7.00

*For sale by the National Technical Information Service, Springfield, Virginia 22151

PREFACE

An earlier report [1] describes the application of a quasi-optimum control technique to the design of a control system for a three degree-of-freedom motion simulator. This technique, developed under this contract, NAS 2-3636 and an earlier contract, NAS 2-3648, was applied to design a complete six degree-of-freedom motion simulation in the investigation described herein. This report contains the analytical results and simulated time histories that would be obtained with various parameter settings for several types of missions. To facilitate experimental evaluation of the control law, a description and listing of the washout subroutine is given in Appendix IV.

The authors are grateful for the assistance provided by Mr. J. G. Douvillier and by Dr. E. C. Stewart, who served as Contract Technical Monitor.

CONTENTS

Section		Page
	PREFACE	i
1.	INTRODUCTION	1
2.	ANALYSIS	5
	2.1 Description of Simulation Problem	5
	2.2 Coordinate Systems and Transformations	14
	2.3 Mathematical Formulation of the Control Problem	20
	2.4 Performance Indices	30
	2.5 Quasi-Optimum Washout System Design	43
	2.5.1 The Two-Point Boundary Value Problem	43
	2.5.2 Physical Implication of the Mathematical Formulation	50
	2.5.3 Quasi-Optimum Solution of the Two-Point Boundary Value Problem	53
	2.6 Summary and System Implementation	59
	2.6.1 Summary of the Simulator Control System Design	59
	2.6.2 Analysis of the Linear Design Case	64
	2.6.3 Computer Simulation Program	66
3.	PERFORMANCE SIMULATION	69
	3.1 Description of the Reference Aircraft Motion	69
	3.2 Simulated Time Histories of Cab Motion	78
	3.3 Summary and Discussion of Simulation Results	109
4.	CONCLUSION AND RECOMMENDATIONS	113
	REFERENCE	115
	APPENDIX I: DERIVATION OF OPTIMUM CONTROLS, $\vec{a}$, $\bar{\upsilon}$	117
	APPENDIX II: DERIVATION OF QUASI-OPTIMUM CORRECTION FACTORS	119
	APPENDIX III: OPTIMUM SINGULAR CONTROLS	131
	APPENDIX IV: FORTRAN SUBROUTINE OF THE SIMULATOR CONTROL SYSTEM	135

1. INTRODUCTION

In controlling the motion of an aircraft, the pilot uses both visual and kinesthetic cues. Visual cues provide information about the position of the aircraft with respect to a suitable frame of reference; kinesthetic cues provide information about the motion (velocity, acceleleration) of the aircraft with respect to the reference frame. The pilot processes the data from the visual and kinesthetic sensors in a sophisticated (and little understood) manner in such a way that his action upon the aircraft controls causes the aircraft to behave as he desires.

Since the primary objective of the pilot is to control the position of the aircraft, it is reasonable to suppose that the pilot relies primarily upon visual cues; kinesthetic cues, although very useful, are not indispensible. Presumably, this is the reason that fixed-base (non-moving) simulators, which provide accurate visual cues, (but no kinesthetic cues) have been used with great success in a variety of aircraft and space applications.

Owing to the absence of motion cues in fixed-base simulators, however, the experience of the pilot in such simulators is not identical to what he would experience in an actual aircraft, and hence there are many instances in which the pilot's performance is not the same as it would be in an actual aircraft, and in which he may complain of the lack of fidelity of the simulation. It is generally believed that in the absence of motion cues, the pilot after an initial training period in the simulator, alters his method of mental data processing in an attempt to maintain his performance at the level he would achieve in the actual aircraft. In effect, the pilot synthesizes or interpolates the information he expects from his kinesthetic sensors. To accomplish this, however, requires greater mental effort; accordingly, the pilot becomes more rapidly fatigued, and he generally describes the task as being more difficult to perform.

The recognized shortcomings of fixed-base simulators have led to the increasing use of simulators which can move in response to the pilot's commands. The introduction of additional motion into simulators, however, has not alleviated all the problems of fixed-base simulators. There are even situations in which the pilot indicates preference for a

fixed-base simulation over a moving-base simulation. The major difficulty with moving-base simulators is that their motion is generally not identical to that of the aircraft being simulated, because the simulator is confined to a physical volume which is much smaller than the volume in which the aircraft is free to maneuver (The exception to this general situation is the so-called case of "one-to-one" motion, in which the pilot's task and aircraft are selected so that the aircraft could be maintained within a volume not larger than the volume available for motion of the simulator. An example of such a situation is a helicopter with a hovering task.)

It is evident that fidelity of the motion cues can be increased by increasing the volume in which the simulator is free to maneuver. The important question in regard to design of motion simulators is thus how to make most effective use of a given maneuverability volume.

To make effective use of the volume in which the simulator moves, some knowledge of the nature of the kinesthetic sensors of motion is required. It is generally believed that the principal sensors of motion in the human being are in the labyrinth structure of the ear, and comprise the semicircular canals and the otoliths. The former are believed to act in the manner of rate gyros to sense the angular velocity of the pilot's head and the latter act like linear accelerometers to sense the specific force at the pilot's head. Motion of the body is also sensed as a result motion of the organs in the abdominal cavity and due to pressure on the body surface (the "seat of the pants"), but it is believed that the motion cues derived from other than the ear labyrinth are relatively insignificant.

Various studies have been made to determine the characteristics of the labyrinthine sensors and it has been concluded that these are fairly complex nonlinear dynamic systems. Moreover, the characteristics of the physical sensors themselves, even if obtainable, would not be adequate to determine how the human being senses motion, because the signals from the sensors are processed by the sophisticated digital computer which is the brain. Sensor models have been constructed to account for the signal processing in the brain, but these are not very well established. Hence, for the purpose of this investigation, we have assumed that the motion cues of significance are simply angular velocity and specific force. Each are vector quantities and are refered to a set of reference axes fixed

in the pilot and moving with him.

The ideal motion simulator would produce in the simulator cab the same angular velocity vector and specific force vector as would result in the aircraft in response to the pilot's control inputs. The difference between the angular velocity vector of the simulator and the angular velocity vector in the aircraft is an error as is the difference between the specific force vector in the cab and in the aircraft. If these error vectors are both zero, the motion simulation is perfect ("one-to-one"). The objective of the simulator control system design is to keep these errors as small as possible.

One of the difficulties in designing an optimum simulator control system is that there are two (2) vector-valued error components (angular velocity and specific force) or a total of 6 scalar error signals. It is thus necessary to devise a single scalar measure of error to account for the 6 components which may be present. Since the typical pilot is usually able to discriminate between types of motion simulations and can assess their relative performance, it is possible that such a measure of error exists. If it does exist, it may depend on the particular task, the pilot's experience, the nature of the visual cues, and many other factors. Hence determination of the "natural" measure of error, i.e. the measure of error which governs the pilot's subjective evaluation of simulator quality, is unrealistic. The only feasible approach is to use a "reasonable" measure of error. The approach adopted in this study is to regard the total measure of error as the weighted sum of two scalars, one representing specific force, and one representing angular velocity, i.e.

$$E = M_{\beta} + k\, M_{\omega}$$

where M_{β} is the contribution to the total error due to errors in the specific force vector, M_{ω} is the contribution due to errors in the angular velocity vector and k is a constant which determines the importance of angular velocity relative to specific force. The scalars M_{β} and M_{ω} are determined from the corresponding vectors on the basis of the following empirical considerations:

- The direction of the error is significant. For example, if the true specific force is 0.5 g and the simulated specific force is 1.5 g (i.e. the error magnitude is 1 g), this is less serious than when the simulated specific force is - 0.5 g (i.e., the error is still 1 g in magnitude but the simulated specific force is in the opposite direction to the true specific force).

- The specific force in the vertical direction when the aircraft is not accelerating vertically is 1 g (which is also the specific force experienced by a person at rest on the ground). One is not normally aware of this vertical specific force when standing. In other words, it is reasonable to assume that the brain "biases-out" the normal 1 g component of vertical specific force, and hence that the vertical specific force sensation is the actual specific force less 1 g.

Based on these considerations several alternative analytical expressions for the measure of error in specific force and angular velocity have been developed and are described in Section 2. 4.

Using these error measures and the methods of optimum control theory, a set of control laws were devised.

2. ANALYSIS

2.1 Description of Simulation Problem

In the operation of a moving-base flight simulation, a pilot manipulates a set of flight controls and the simulator cab in which he is situated moves in a manner which tends to reproduce the sensation of motion which the pilot would experience if he were in the actual aircraft and he manipulated the flight controls in the same manner. Ideally, the motion of the cab should be identical to that of the aircraft. Under conditions which permit the cab motion to reproduce the aircraft motion perfectly ("one-to-one" simulation) the sensation of motion in the simulator is the same as the sensation of motion in the actual aircraft. Generally, however, simulators are used to simulate flight tasks in which one-to-one simulation is physically impossible because the cab is confined to remain inside a fairly small physical volume. The simulator control system thus must be designed, not to reproduce the motion of the aircraft being simulated, since this is impossible, but rather to provide a sensation of motion which is as close as possible to the sensation of motion in the actual aircraft, but without causing the cab to exceed the physical limits of its motion.

The moving-base simulator of concern in this investigation is of the type currently in use at the Ames Research Center; the cab is built into a gimbal system which provides three rotational degrees of freedom and the whole gimbal assembly is in turn provided with three translational degrees of freedom by a system of three mutually perpendicular tracks. (See Figure 2-1). Each degree of freedom of the cab motion can be independently controlled by the cab arive system. A digital computer is used to simulate the dynamics of the aircraft which permits the dynamics to be modeled to any degree of accuracy desired. The inputs to this computer are the flight commands resulting from the pilot's manipulation of the flight controls in the cab. The computer outputs are the state variables (velocity, angular rotation, and etc.) describing the motion of the aircraft which in turn are used by the simulator control to compute the signals needed to drive the cab motion. It is the design of the simulator control that is the subject of this study. Figure 2-2 shows a functional block diagram of the overall simulator system.

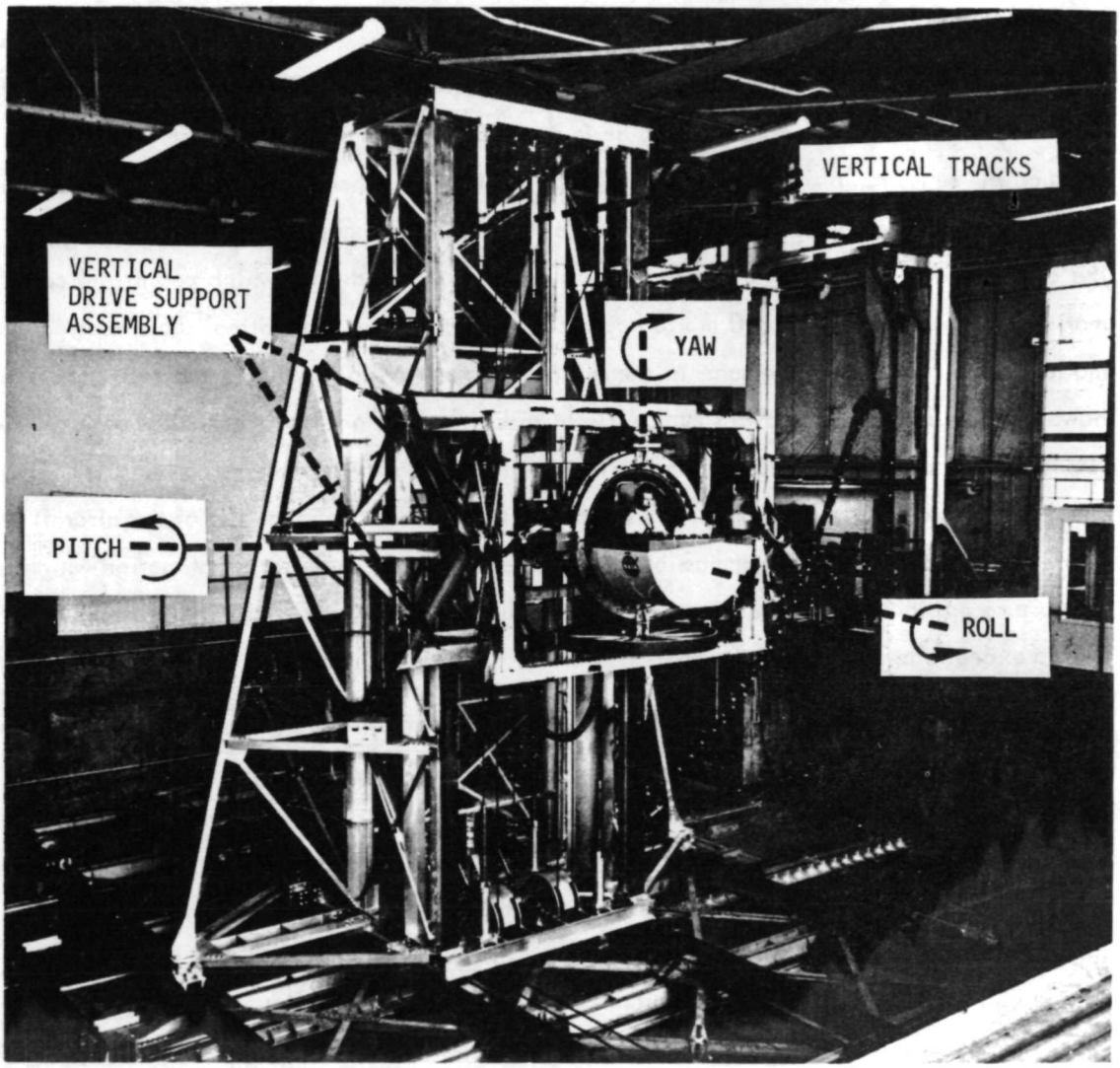

Figure 2-1

The Ames All-Axis Motion Simulator

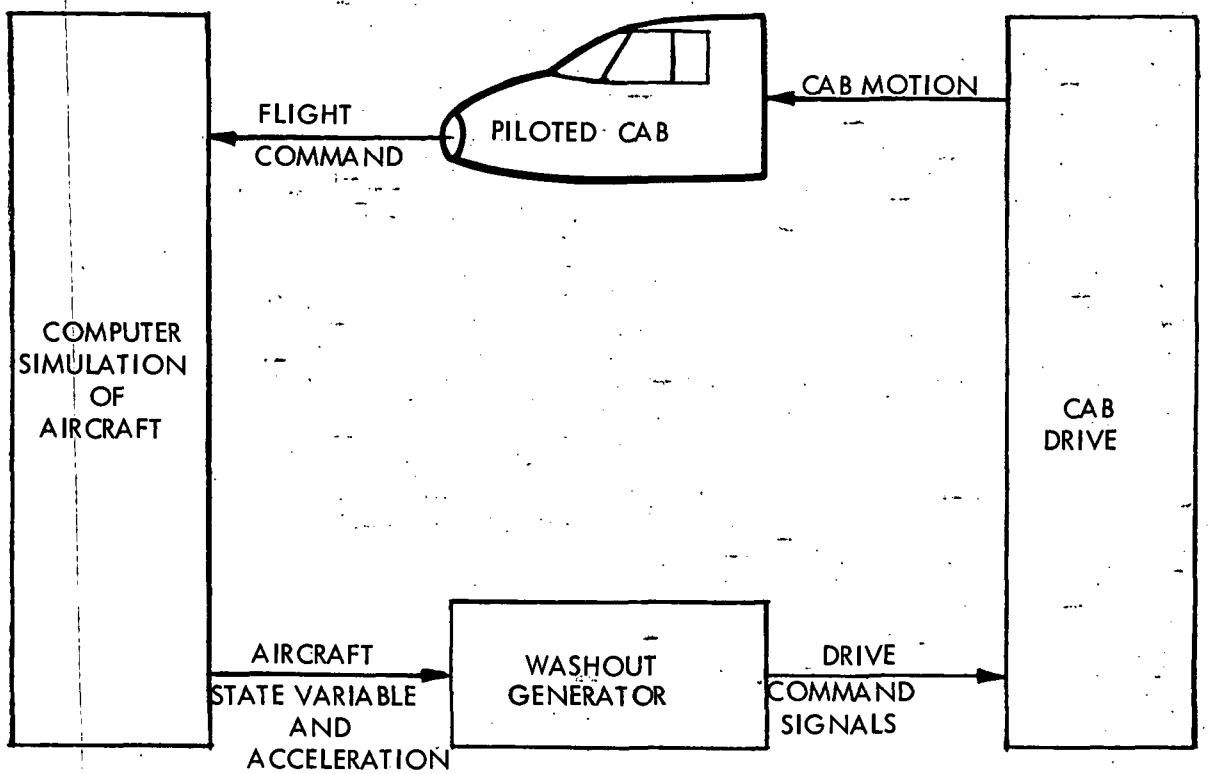

Figure 2-2

Functional Control System Block Diagram

Since each degree of freedom of the cab is driven by an electromechanical system which is designed as a high-speed position servo, it is reasonable to assume that the position (i.e. gimbal angles for rotational degrees of freedom, translations along tracks for translational degrees of freedom) of the cab is identical to the drive system position commands, so long as the latter do not exceed the motion limits. If the motion limits are exceeded, mechanical switches are operated to engage a system designed to arrest the cab motion safely. When the safety switches are engaged, the simulation is ended, the cab is returned to a neutral position, and, after various safety checks are made, the simulation is again initiated. To avoid engaging the safety switches, the drive system has an electrical system designed to anticipate the engagement of the mechanical safety system and to cutoff power before cab motion causes the latter to be engaged. Accordingly, from the operational viewpoint, the simulator control should be designed so that the cab drive command signals do not cause either the electrical or mechanical safety limits to be exceeded.

Because of the physical construction of the simulator, the position of the cab at any instant of time is approximately described by the three translations of the movable gimbal structure on the system of rails, and three gimbal angles. These quantities and their time derivatives (twelve in all) are a set of state variables natural to the motion of the cab. They are, however, not particularly well-suited for describing the sensible motion of the aircraft. For the latter, a more suitable set of state variables are the components of the vehicle linear and angular velocity vectors resolved along a set of axes fixed in the aircraft at the pilot's station (6 quantities) and 3 angles relating the position of these body axes to a set of reference axes. With regard to the sensation of motion, the position in space of the aircraft is not important. For that matter, velocity, per se, is not important; it is acceleration that is responsible for sensation of motion: linear translation at constant velocity does not contribute to the sensation of motion. This fact is particularly convenient with regard to simulation of the forward motion of the aircraft. Under quescent conditions (cruise, for example) the aircraft moves at constant forward velocity which is not sensible, except through visual reference. Only changes from this quiescent state are detectable; consequently, the constant forward component of velocity is not required in the simulation. As a consequence, the simulation is accomplished by subtracting the forward component of velocity of the aircraft from the total

velocity vector before driving the cab. The effect can be visualized by the assumption that the aircraft flies in a wind tunnel in which the air mass moves at a constant velocity equal to that of the forward speed of the aircraft. When the thrust of the engines is adjusted so that the aircraft is stationary with respect to the wind tunnel, the situation is aerodynamically identical to the motion of the aircraft in a windless airmass but with constant forward velocity.

In consequence of these considerations, the control system for the motion simulator in a situation in which one-to-one motion simulation is possible has the form shown in Figure 2-3. The aircraft acceleration and angular velocity vectors, in body axes are transformed to accelerations of the cab along its axes of travel and to cab gimbal rates, respectively. The former are integrated once to provide the velocity components of the cab. After subtracting the constant forward speed $\bar{v}_x$ of the aircraft, the velocity components are again integrated to produce the position commands for the linear drive system. Concurrently, the cab gimbal rates are integrated once to yield the cab gimbal angle commands which are used to drive gimbal servos.

When the task or set of tasks to be simulated is such that one-to-one motion is not permissible, however, the linear and angular drive signals cannot be generated as shown in Figure 2-3. Instead, it is necessary to "wash-out" some of the aircraft motion before generating the cab servo drive signals. The placement of the wash-out system (or "wash-out circuits") is shown in Figure 2-4.

In the design of the wash-out circuits, three techniques are conventionally used: scaling, high-pass filtering, and "residual tilts". Scaling consists of multiplying each component of the vector acceleration or angular velocity by a constant scale factor less than unity. This causes an attenuated sensation of motion, but the sensed directions of the vectors in the simulator are the same as in the aircraft. High-pass filtering is employed to eliminate the d-c and low-frequency components of acceleration which lead to large excursions. To compensate for the loss of sustained (i.e. low-frequency) accelerations due to high-pass filtering, residual tilts are sometimes used. The idea here is to use the components of the gravity vector in the forward and lateral directions which result when the cab is tilted to simulate the sensation of sustained acceleration in these directions.

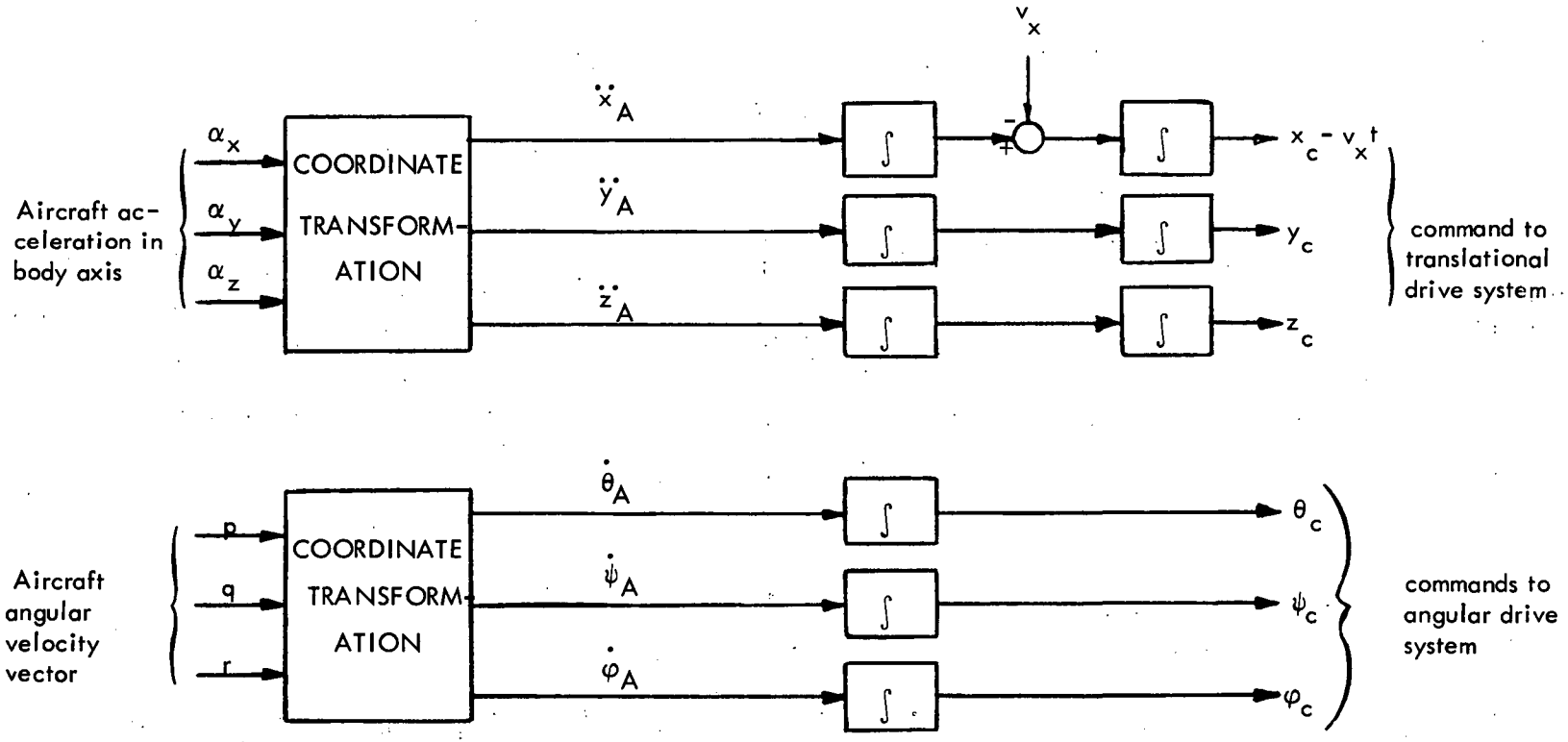

Figure 2-3

Simulator Control Without Washout

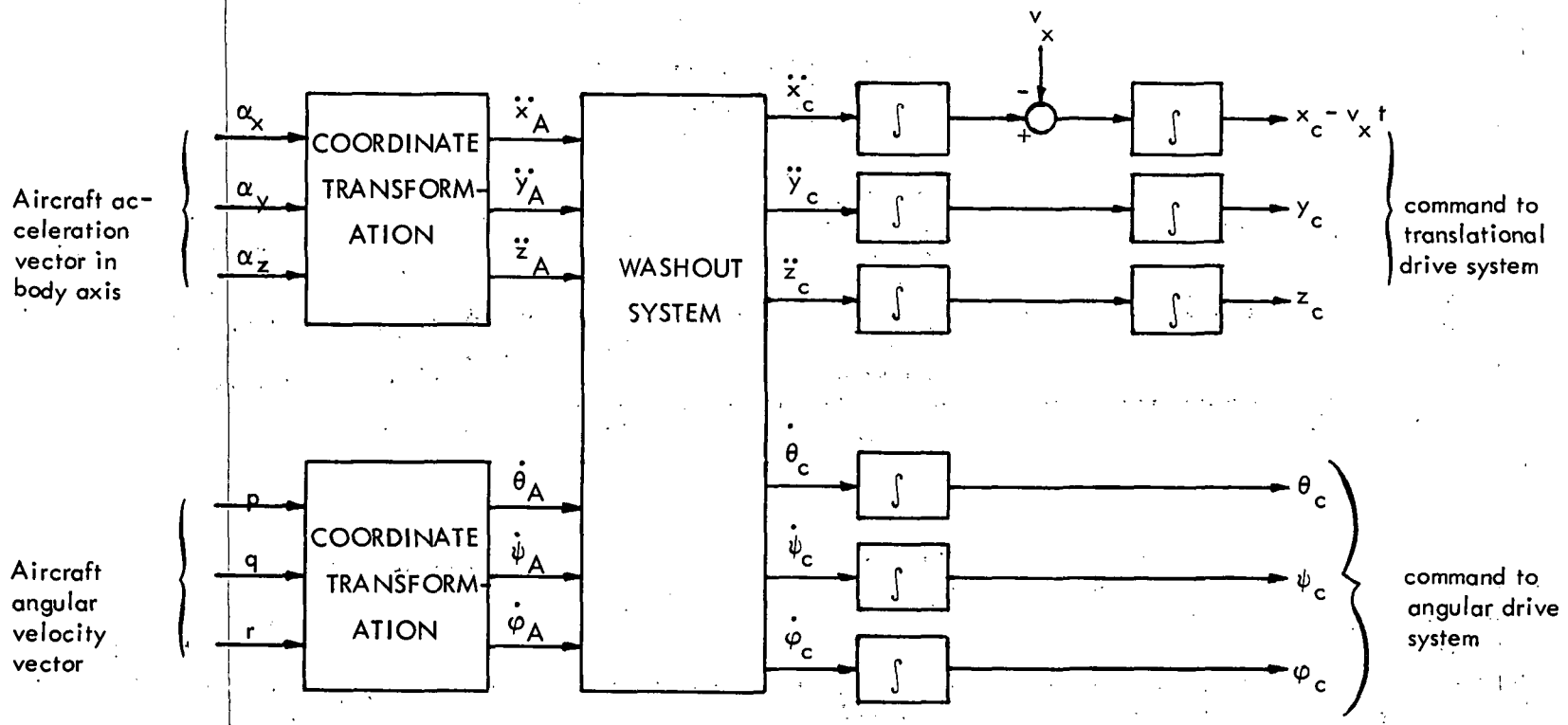

Figure 2-4

Simulator Control Showing Placement of Washout Circuit

The amount of scaling, filtering and tilting which is employed in a particular simulation is currently determined empirically, using a combination rules-of-thumb developed out of prior experience and adjustments on the simulation of an aircraft in an actual mission. It has been generally recognized that this design technique may not use the capabilities of the simulator to the fullest extent: that a more systematic approach might provide greater fidelity of motion within the confines of the same volume, or might be useful for a larger variety of tasks. The purpose of this investigation is to study the possibility of using the techniques of optimum control theory as a method of systematizing the design of improved wash-out systems.

If a single control system is to be used for a broad spectrum of tasks, it would appear that the desired performance is essentially nonlinear (with respect to the functional dependence between the wash-out and the aircraft motion). For those tasks or phases of a task in which one-to-one simulation is possible, one-to-one motion should be used. When one-to-one simulation is not possible, the minimum amount of wash-out which keeps the cab within its permissible motion limits should be used. The basic question in designing the control system is: What aspects of the aircraft motion must be followed accurately by the simulator, and what aspects can be sacrificed without degrading the realism of the simulation? It is generally accepted that one of the most important factors governing the realism of a simulation is the kinesthetic sensation of motion. Although there is a continuing discussion of what "sensed" quantities really are, a consensus of the opinion is that the linear acceleration and the angular velocity, as measured with respect to axes fixed in the pilot are the most pertinent factors sensed by human kinesthetic sensory organs. Thus, simply stated, the control problem is to endeavor to find a control law which, while keeping the cab excursions within specified physical boundaries, minimizes the errors in the motion sensations. If a suitable cost or penalty function of the errors in the motion sensations can be determined in addition to an analytical model for representing the errors in the motion sensation, then it is possible to apply the optimum control technique. Since this approach is considered the most likely candidate to yield the "best" simulator control law, it was adopted for this investigation.

During the initial phase of the investigation of applying the quasi-optimum control technique to the wash-out circuit design (1968-1969), a relatively simple case of one-degree-of-freedom longitudinal motion was considered to establish the feasibility of using the technique. In the present phase of the investigation, the general six degree-of-freedom motion simulation is considered. In order to treat the six degree-of-freedom problem realistically, it was necessary to modify the analytical approach used in the first phase because the earlier approach led to hopelessly complicated calculations in the more realistic problem. The problem formulation in the present case is substantially more realistic in that a trade-off between the angular and the linear motions is allowed to utilize the effect of "residual tilt" and that the washout control system is independent of the aircraft dynamics, although "good" setting of the parameters in the wash-out circuit may depend on aircraft dynamics as well as the specific mission.

In the following subsections, the different phases of the analysis leading to the simulator control design are discussed in detail and these include the following:

- Definition of the various coordinate systems and their mutual transformations.
- Formulation of the problem in a manner suitable for application of the optimum control technique including a discussion of the notation and pertinent quantities.
- Development of various cost or penalty functions of the errors in the sensed motion which provide a realistic measure of the "goodness" of the performance and, on the other hand, are mathematically tractable as a performance indices for the optimum control technique.
- Application of the quasi-optimum control technique to obtain the simulator control law.
- Discussion of an implimentation scheme for realizing the simulator control design.

2.2 Coordinate Systems and Transformations

There are two sets of axes of significance in the motion simulation: a set of "inertial" axes fixed with respect to the ground and a set of axes fixed in the vehicle and moving with it:

(1) Inertial Coordinates - The assumed "inertial" reference frame is a cartesian coordinate system with its origin at the center of the moving-base simulator track assembly and oriented so that each axis coincides with one direction of translational motion of the simulator. The positive directions of the x, y, z axes are chosen, respectively, to coincide with forward, right side and downward motions. The translational motions of both the cab and the aircraft are defined with respect to the same inertial coordinate system.

(2) Body Coordinates - The body axis forms a cartesian coordinate system fixed with respect to the vehicle where the origin is located at the pilot's seat in the cockpit of the vehicle. The directions of the axes are in the same sense as the inertial reference (i.e. forward, right, and down), but with respect to the pilot rather than ground. Since there are two vehicles, the simulator cab and the actual aircraft, there are correspondingly two sets of body coordinates. The two sets of body coordinates are illustrated in Figure 2-5 where subscripts "A" and "c" are used to denote "aircraft" and "cab", respectively.

The displacements of the vehicles from the inertial frame are denoted by position vectors $\vec{r}_A$ and $\vec{r}_c$ * . The angular orientations of the vehicles are described by the Euler angles (yaw, pitch, and roll) relating each respective system of body coordinates to the inertial coordinates. Any vector defined in the inertial coordinates can always be transformed into either of the systems of body coordinates by means of an orthogonal direction cosine matrix. Elements in the direction cosine matrix are functions of the Euler angles where the particular functions depend on the sequence of rotations from the inertial directions to the directions of the body axis that have been adopted.

---

* In this report, variables with an arrow ($\rightarrow$) on top denote physical vectors with magnitude and direction (velocity, force, and etc.) whereas variables with a bar (-) on top merely denote column vectors with three elements where the three elements may not be the x, y, z components of a physical vector.

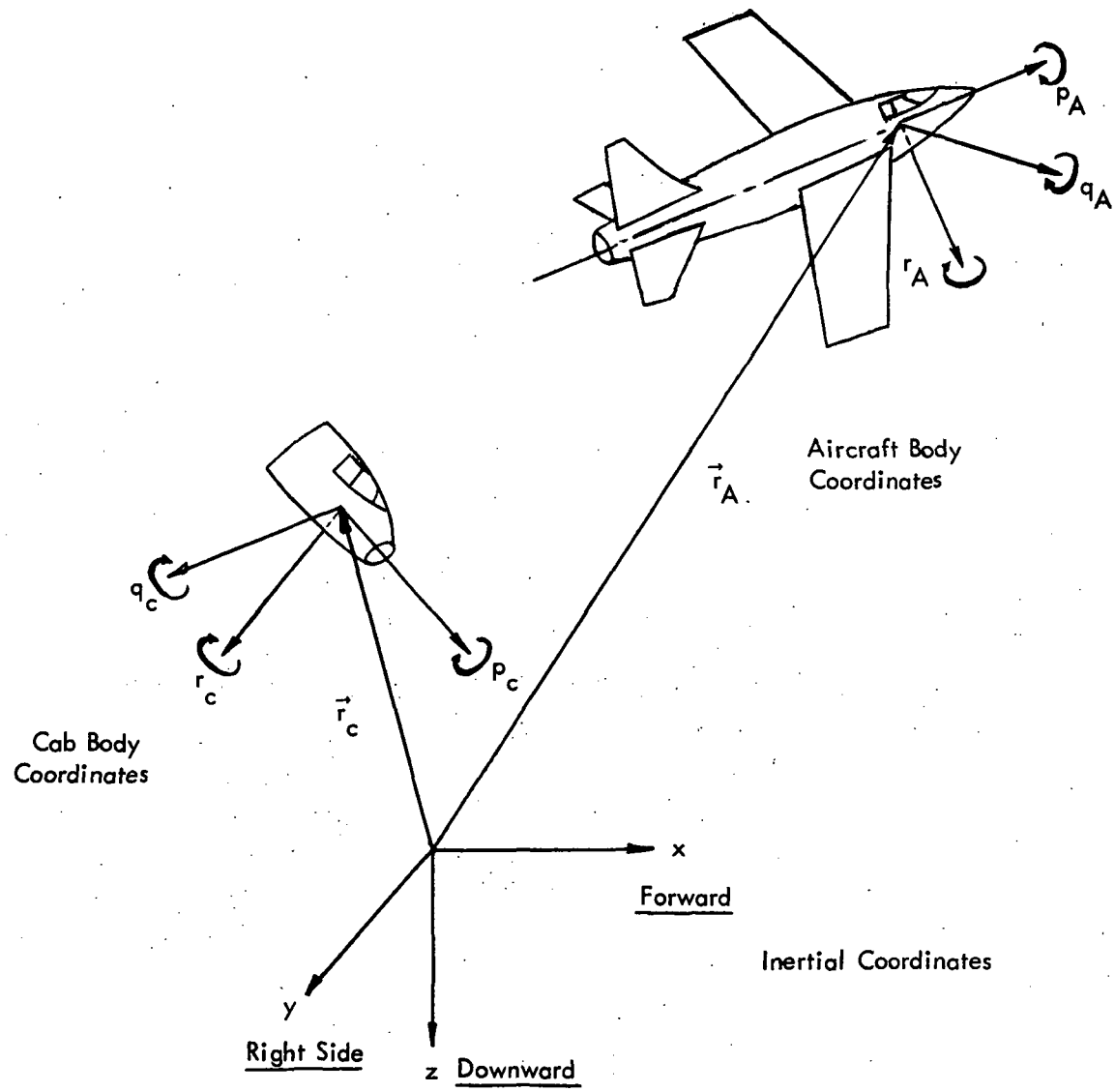

Figure 2-5

Coordinate Systems

In accordance with the physical structure of the existing gimbal assembly, as shown in Figure 2-6, the angular orientation of the cab is described by the three gimbal angles:

Outer gimbal:	Pitch (θ)
Middle gimbal:	Yaw (ψ)
Inner gimbal:	Roll (φ)

Thus, for computational convenience, the Euler angle transformations in this report for both the cab and the aircraft are defined according to the following sequence of rotations: (Pitch — Yaw — Roll). In mathematical notation, let

$$\bar{\lambda}_i = \begin{bmatrix} \varphi_i \\ \theta_i \\ \psi_i \end{bmatrix} = \text{Euler angle vector}$$

$\vec{n}_i$ = a vector in the inertial coordinate system

$\vec{\mu}_i$ = the transformed vector of $\vec{n}_i$ in the body coordinate system

where i = A for the aircraft

i = c for the cab

then the vector $\vec{\mu}_i$ is obtained from $\vec{n}_i$ by the transformation

$$\vec{\mu}_i = C(\bar{\lambda}_i)\,\vec{n}_i \tag{2.1}$$

where the transformation matrix $C(\bar{\lambda}_i)$ is the orthogonal direction cosine matrix given by

$$C(\bar{\lambda}_i) = \begin{bmatrix} \cos\psi_i \cos\theta_i & \sin\psi_i & -\cos\psi_i \sin\theta_i \\ \sin\Phi_i \sin\theta_i - \sin\psi_i \cos\varphi_i \cos\theta_i & \cos\Phi_i \cos\psi_i & \sin\Phi_i \cos\theta_i + \cos\Phi_i \sin\psi_i \sin\theta_i \\ \cos\Phi_i \sin\theta_i + \sin\Phi_i \sin\psi_i \cos\theta_i & -\sin\Phi_i \cos\psi_i & \cos\Phi_i \cos\theta_i - \sin\Phi_i \sin\psi_i \sin\theta_i \end{bmatrix} \tag{2.2}$$

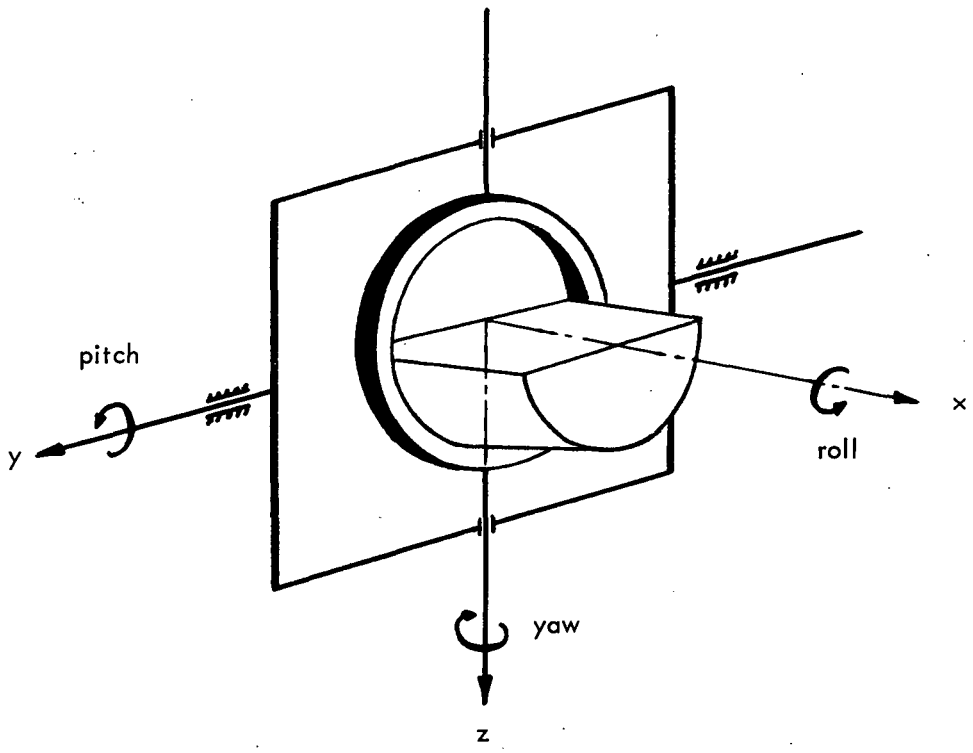

Figure 2-6

Gimbal System for the Ames Simulator

The orthogonal property of $C(\bar{\lambda}_i)$, i.e.

$$C^{-1}(\bar{\lambda}_i) = C'(\bar{\lambda}_i) \tag{2.3}$$

is used frequently in subsequent calculations #.

It is noted that this particular sequence of rotations is specific to the physical structure of the existing gimbal system and is not the generally adopted sequence of rotations used in the description of aircraft motion. The conventional sequence of rotations is (yaw, pitch, roll). If the conventional set of Euler angles are denoted by $\bar{\lambda}^*_A = (\varphi^*_A, \theta^*_A, \psi^*_A)'$, then these are related to the Euler angles $\bar{\lambda}_A = (\varphi_A, \theta_A, \psi_A)'$, used here as defined in (2.1) and (2.2) by

$$\begin{aligned}
\varphi_A &= \tan^{-1}\left(\frac{\sin\varphi^*_A \cos\psi^*_A - \cos\varphi^*_A \sin\theta^*_A \sin\psi^*_A}{\cos\varphi^*_A \cos\psi^*_A + \sin\varphi^*_A \sin\theta^*_A \sin\psi^*_A}\right) \\
\theta_A &= \tan^{-1}\left(\frac{\sin\theta^*_A}{\cos\theta^*_A \cos\psi^*_A}\right) \\
\psi_A &= \sin^{-1}(\cos\theta^*_A \sin\psi^*_A)
\end{aligned} \tag{2.4}$$

Let $\vec{\omega}_i$ be the angular velocity vector of the vehicle with p_i, q_i and r_i as its components in forward, right side and downward axis of the body coordinates respectively. The components p_i, q_i and r_i, customarily refered to as "roll rate", "pitch rate" and "yaw rate", respectively, are related to the gimbal angle rates $\dot{\bar{\lambda}}_i = (\dot{\varphi}_i, \dot{\theta}_i, \dot{\psi}_i)'$ by

---

The superscripts (-1) and (′) used in conjunction with a vector or a matrix denote, respectively, the inverse and the transpose of the particular vector or matrix.

$$\begin{bmatrix} p_i \\ q_i \\ r_i \end{bmatrix} = \begin{bmatrix} 1 & \sin\psi_i & 0 \\ 0 & \cos\varphi_i \cos\psi_i & \sin\varphi_i \\ 0 & -\sin\varphi_i \cos\psi_i & \cos\varphi_i \end{bmatrix} \begin{bmatrix} \dot{\varphi}_i \\ \dot{\theta}_i \\ \dot{\psi}_i \end{bmatrix} \tag{2.5}$$

For notational convenience, let

$$F(\bar{\lambda}_i) = \begin{bmatrix} 1 & \sin\psi_i & 0 \\ 0 & \cos\varphi_i \cos\psi_i & \sin\varphi_i \\ 0 & -\sin\varphi_i \cos\psi_i & \cos\varphi_i \end{bmatrix} \tag{2.6}$$

then (2.5) can be written in vector notation as

$$\vec{\omega}_i = F(\bar{\lambda}_i)\dot{\bar{\lambda}}_i \tag{2.7}$$

The matrix $F(\bar{\lambda}_i)$ is not orthogonal in general since the three components $\dot{\varphi}_i$, $\dot{\theta}_i$ and $\dot{\psi}_i$ of the Euler angle rate vector $\dot{\bar{\lambda}}_i$ are not orthogonal components of a physical vector. The inverse of $F(\bar{\lambda}_i)$ which will be encountered frequently in subsequent calculations, is given by

$$F^{-1}(\bar{\lambda}_i) = \begin{bmatrix} 1 & -\tan\psi_i \cos\varphi_i & \tan\psi_i \sin\varphi_i \\ 0 & \cos\varphi_i / \cos\psi_i & -\sin\varphi_i / \cos\psi_i \\ 0 & \sin\varphi_i & \cos\varphi_i \end{bmatrix}$$

It should be noted that the orientation of all the angular quantities used in this report are defined in accordance with the right-hand convention as shown in Figure 2-6.

2.3 Mathematical Formulation of the Control Problem

The general control problem is formulated as a set of first order differential equations relating the state of the dynamic system to the control variables and also an explicit expression of the performance index in terms of the state variables and control variables defined in the differential equations. The objective of the system design is to find the control law for computing the control variables from the state variables which minimizes the performance index. The system of differential equations defining the dynamic system under investigation is described below. Several choices for the explicit expression of the performance index is given in the next section.

The first step in the mathematical formulation of the dynamics is to derive the differential equations describing the motion of the simulator cab plus explicit expressions relating the sensed motion felt by the pilot in the simulator cab to the actual motion of the cab. There is a corresponding set of variables and differential equations describing the actual and sensed motion of the reference aircraft. The equations for each vehicle are distinguished by the subscript A or c which will be used throughout the report to indicate reference to the aircraft or to the cab, respectively.

Since we are interested in how well the cab motion duplicates the aircraft motion, it is convenient to introduce a third set of variables defined as the difference between two corresponding quantities for the cab and for the aircraft. These variables will be referred to as the "error" quantities and will be denoted by the absence of a subscript.

Since we are generally dealing with variables or quantities composed of three components, the development will utilize three-component vectors. In the definitions given below, it should be noted that, for both the cab and the aircraft, some of the quantities are defined in their respective body coordinates and the other quantities are defined in the inertial coordinates fixed with respect to the ground. To express these quantities in a format convenient for an optimum design approach, we let

$$\vec{r}_i = \begin{bmatrix} x_i \\ y_i \\ z_i \end{bmatrix}$$ = position vector of vehicle in inertial reference axes.

$$\vec{v}_i = \begin{bmatrix} v_{ix} \\ v_{iy} \\ v_{iz} \end{bmatrix} = \dot{\vec{r}}_i$$ = veclocity vector of vehicle in inertial reference axis.

$$\bar{\lambda}_i = \begin{bmatrix} \Phi_i \\ \theta_i \\ \psi_i \end{bmatrix}$$ = Euler angle vector relating vehicle body axes to inertial reference axes.

$$\bar{u}_i = \begin{bmatrix} u_{i\Phi} \\ u_{i\theta} \\ u_{i\psi} \end{bmatrix} = \begin{bmatrix} \dot{\Phi}_i \\ \dot{\theta}_i \\ \dot{\psi}_i \end{bmatrix} = \dot{\bar{\lambda}}_i$$ = Euler angle rate

$$\vec{a}_i = \begin{bmatrix} f_{ix} \\ f_{iy} \\ f_{iz} \end{bmatrix} = \ddot{\vec{r}}_i - \vec{g}$$ = specific force(pound per unit mass) acting on vehicle

$$\vec{\alpha}_i = \begin{bmatrix} \alpha_{ix} \\ \alpha_{iy} \\ \alpha_{iz} \end{bmatrix} = C(\bar{\lambda}_i)\,\vec{a}_i$$ = "sensed" specific force
= reading from accelerometers mounted at the pilot's seat.

$$\vec{\beta}_i = \begin{bmatrix} \beta_{ix} \\ \beta_{iy} \\ \beta_{iz} \end{bmatrix} = \vec{\alpha}_i + \vec{g} = \text{"unbiased" sensed specific force.}$$

$$\vec{\omega}_i = \begin{bmatrix} p_i \\ q_i \\ r_i \end{bmatrix} = F(\bar{\lambda}_i)\,\bar{u}_i = \text{"sensed" angular velocity vector of vehicle}$$
$$= \text{reading of rate gyros mounted on the vehicle's body axes.}$$

where

i = A for aircraft

i = c for cab

$$\vec{g} = \begin{bmatrix} 0 \\ 0 \\ g \end{bmatrix} = \text{gravitational acceleration vector in inertial reference}$$

$g = 32.2$ ft/sec^2 $= 9.81$ m/sec^2

$C(\bar{\lambda}_i)$ = orthogonal transformation matrix which transforms a vector in inertial reference axes to a vector in body axes as defined in (2.2)

$F(\bar{\lambda}_i)$ = transformation matrix which transforms an Euler angle rate vector into an angular velocity vector as defined in (2.6)

The error quantities which indicate the difference between the motion (both actual and sensed) of the cab and the aircraft are defined by

$$\begin{aligned}
\vec{r} &= \vec{r}_c - \vec{r}_A \\
\vec{v} &= \vec{v}_c - \vec{v}_A = \dot{\vec{r}}_c - \dot{\vec{r}}_A = \dot{\vec{r}} \\
\vec{a} &= \vec{a}_c - \vec{a}_A = \ddot{\vec{r}}_c - \ddot{\vec{r}}_A = \ddot{\vec{r}} \\
\vec{\beta} &= \vec{\beta}_c - \vec{\beta}_A = \vec{\alpha}_c - \vec{\alpha}_A = \vec{\alpha} \\
\bar{\lambda} &= \bar{\lambda}_c - \bar{\lambda}_A \\
\bar{u} &= \bar{u}_c - \bar{u}_A = \dot{\bar{\lambda}}_c - \dot{\bar{\lambda}}_A = \dot{\bar{\lambda}} \\
\vec{\omega} &= \vec{\omega}_c - \vec{\omega}_A
\end{aligned} \qquad (2.8)$$

In the above equations, it is noted that the components of the vectors $\vec{r}_t$, $\vec{v}_t$, $\vec{a}_t$, $\vec{g}$ are defined with respect to the inertial reference axes whereas the components of $\vec{\alpha}_t$, $\vec{\beta}_t$ are defined with respect to the corresponding body axes.

The quantity $\vec{\beta}_t$, obtained by adding $\vec{g}$ to $\vec{\alpha}_t$, is considered a more salient measure of translational acceleration sensed by the human pilot rather than $\vec{\alpha}_t$, since it is argued that a pilot who is accustomed to being in a 1 g environment does not really sense the effect of a 1 g force acting vertically downward with respect to himself. In other words, the pilot's "vertical accelerometer" only senses deviations in the specific force from the normal 1 g force. In the subsequent development, the unbiased sensed specific force $\vec{\beta}_t$ will be considered to be the sensed translational acceleration felt by the pilot.

Obviously, the sensed errors $\vec{\beta}$ and $\vec{\omega}$ are a consequence of the actual motion errors $\ddot{\vec{r}}$ and $\dot{\bar{\lambda}}$. The actual motion errors are in turn generated by the presence of the washout signals. In other words, from (2.8), the relation

$$\begin{aligned} \ddot{\vec{r}} &= \vec{a} \\ \dot{\bar{\lambda}} &= \bar{u} \end{aligned} \tag{2.9}$$

establishes the fact that

$\vec{a}$ = translational acceleration washout signal

$\bar{u}$ = angular rate washout signal

From (2.8) and (2.9), it follows that the differential equation governing the actual motion of the cab are

$$\begin{aligned} \ddot{\vec{r}}_c &= \vec{a} + \ddot{\vec{r}}_A \\ \dot{\bar{\lambda}}_c &= \bar{u} + \dot{\bar{\lambda}}_A \end{aligned} \tag{2.10}$$

The differential equations (2.9) represent the dynamic system required for the optimum design procedure where the washout signals $\bar{u}$ and $\vec{a}$ are the control variables. The differential equations (2.10), which form the basis for the realization of the designed washout control system, suggest a general control system configuration as shown in Figure 2-7. As indicated in Figure 2-7, the command signals generated as a result of the pilot's manipulation of the flight controls in the simulator cab are processed by the digital computer to compute the corresponding motion of the reference aircraft. The variables defining the motion of the aircraft are in turn processed by the washout circuit to compute $\vec{a}$ and $\bar{u}$. The washout signals $\vec{a}$ and $\bar{u}$ are then combined with the aircraft motion according to (2.10) to produce the command signals controlling the motion of the cab. The two integrators shown in Figure 2-7 are necessary since the servomechanisms of the cab drive system are designed to follow the translational position commands $\vec{r}_c$ and the gimbal angle commands $\bar{\lambda}_c$. A more detailed block diagram showing the physical implementation of the control system is given in Section 2.6.1 after the equations describing the washout circuit have been derived. (See Figure 2-19)

As discussed previously, a simulation is regarded as perfect if the sensed motion errors are zero ($\vec{\beta} = \vec{\omega} = 0$). Consequently, the goal of a wash-out control system is to minimize $\vec{\beta}$ and $\vec{\omega}$. It is noted, however, that since $\vec{\beta}$ and $\vec{\omega}$ are physical vectors with magnitude and direction, the question of whether a particular value of $\vec{\beta}$ (or $\vec{\omega}$) is smaller than another value of $\vec{\beta}$ (or $\vec{\omega}$) in the minimization process requires further interpretation. This question is resolved by introducing two scaler functions, $M_\beta(\vec{\beta})$ and $M_\omega(\vec{\omega})$, which in some sense, measures the "size" of $\vec{\beta}$ and $\vec{\omega}$ with respect to the fidelity of the simulation. If these penalty functions are to be used in the performance index required for the optimum control technique, then the functions M_β and M_ω must possess the following properties:

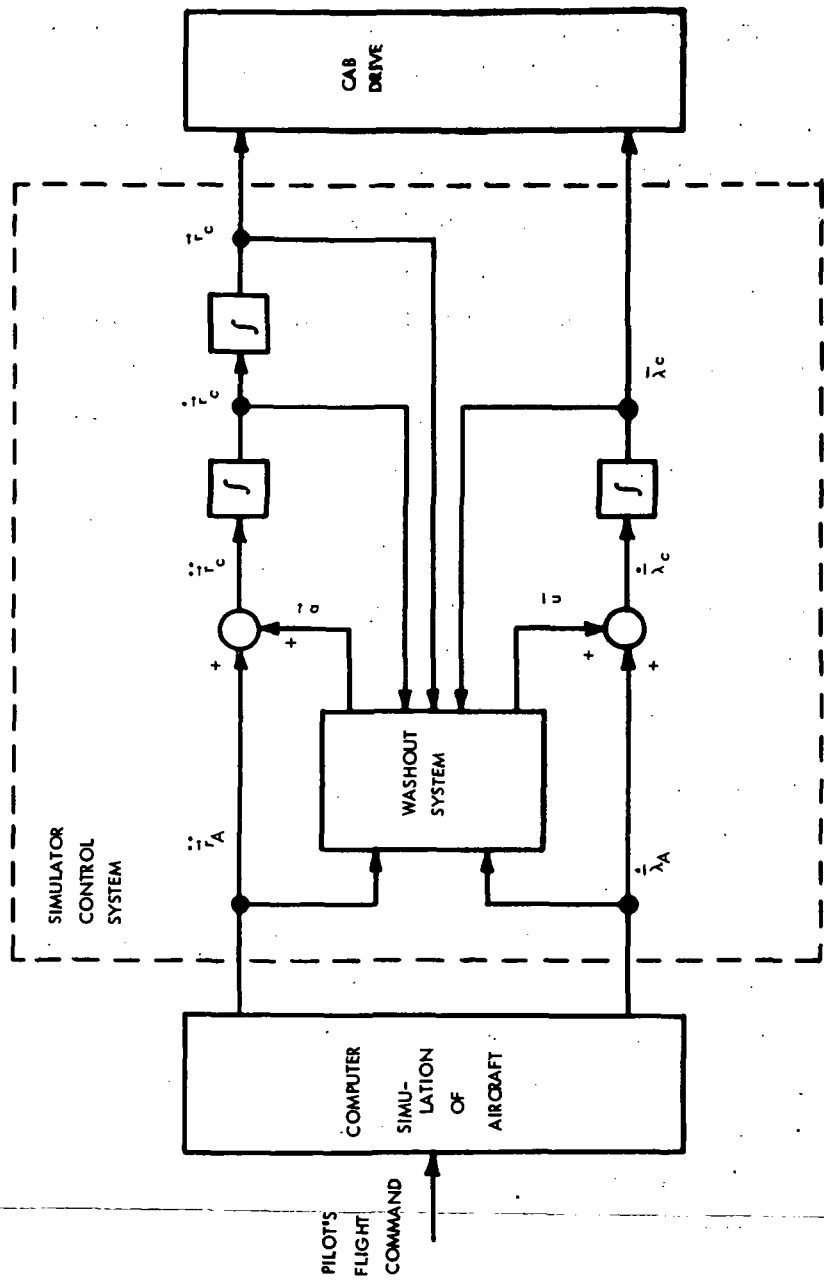

Figure 2-7
General Configuration of Simulator Control System

$$M_\beta > 0, \quad \frac{\partial M_\beta}{\partial \vec{\beta}} \neq 0, \quad \frac{\partial^2 M_\beta}{\partial \vec{\beta}^2} > 0 \quad \text{for } \vec{\beta} \neq 0$$

$$M_\beta = 0, \quad \frac{\partial M_\beta}{\partial \vec{\beta}} = 0, \quad \frac{\partial^2 M_\beta}{\partial \vec{\beta}^2} > 0 \quad \text{for } \vec{\beta} = 0 \tag{2.11}$$

$$M_\omega > 0, \quad \frac{\partial M_\omega}{\partial \vec{\omega}} \neq 0, \quad \frac{\partial^2 M_\omega}{\partial \vec{\omega}^2} > 0 \quad \text{for } \vec{\omega} \neq 0$$

$$M_\omega = 0, \quad \frac{\partial M_\omega}{\partial \vec{\omega}} = 0, \quad \frac{\partial^2 M_\omega}{\partial \vec{\omega}^2} > 0 \quad \text{for } \vec{\omega} = 0 \tag{2.12}$$

From (2.11) and (2.12), it follows that the penalty functions M_β and M_ω increase monotonically with increases in the sensed motion errors $\vec{\beta}$ and $\vec{\omega}$, respectively. A more detailed discussion of the penalty functions, including explicit expressions for M_β and M_ω is given in the next section.

Another aspect necessary to complete the formulation of the control problem is the consideration of physical constraints. The cab motion is, in general, constrained by limits on the translational distances and by limits on the gimbal rotations, both the angles and perhaps the angular rates. Nevertheless, experiences with the existing simulators has indicated that except for the excursion limits, the other limitations seldom cause difficulties. For this reason, and for mathematical convenience, only excursion constraints will be considered.

In order to account in the performance index for the constraints on the cab motion, a penalty function $L(\vec{r}_c)$ is defined in a similar fashion to M_β and M_ω except that $L(\vec{r}_c)$ depends only on the magnitude of $\vec{r}_c$. The optimum control technique requires that the penalty function be chosen to possess the following properties:

$$L(\vec{r}_c) \geq 0, \frac{\partial^2 L}{\partial \vec{r}_c^{\,2}} > 0 \qquad (2.13)$$

Several specific forms of $L(\vec{r}_c)$ will be considered in a subsequent section.

Based on the penalty functions, introduced above, a performance index S is defined as

$$S = \int_t^{t+T} (M_\beta + k M_\omega + \epsilon L)\, d\tau \qquad (2.14)$$

where t = present time, T = fixed time span, and k, ϵ are constant adjustable weighting factors. The control laws $\vec{a}$ and $\bar{u}$ are determined by means of the optimum control technique so that the scaler S is a minimum (or near minimum) for any given values of k and ϵ. For the trivial case, $\epsilon = 0$, i.e., when no boundary constraint is imposed on the cab motion, the control law should provide a perfect simulation. For large ϵ, the cab excursions being highly penalized, the control law should generate abnormal motion cues. In this sense the parameter ϵ can be regarded as a control on the amount of wash-out, adjusted in accordance with the available distances permitted for travel of the simulator.

The parameter k which weighs M_ω in the performance index S in (2.14) provides a means of adjusting the trade-off between translational and angular motions, since the effect of "residual tilt" is embodied in the linear combination of the penalty functions M_β and M_ω. The technique of residual tilt can be illustrated by an example where the reference aircraft is flying at a trim attitude ($\bar{\lambda}_A = 0$) with a forward acceleration of $\ddot{x}_A$ ($\ddot{y}_A = \ddot{z}_A = 0$) as illustrated in Figure 2-8a. Suppose that the simulator cab has no translational motion, but is pitched downward by an angle θ_c as illustrated in Figure 2-8b. In the pitched down condition, the simulator pilot will sense a forward translational acceleration of $g \sin\theta_c$ as a result of gravity. If the pitch angle θ_c is chosen so that $\ddot{x}_A = g \sin\theta_c$ then the simulator pilot would sense the same motion as felt in the actual aircraft, if it is assumed that the simulator pilot is unaware of or ignores the fact that the cab is pitched downward. There is also an upward translational acceleration of $g(1 - \cos\theta_c)$ sensed by the simulator pilot as a result of pitching downward, but this upward translational acceleration

is much smaller than the forward translational acceleration as long as the pitch angle does not become too large and thus can be ignored. Therefore, by pitching the cab upward or downward, it is possible to simulate a translational acceleration along the longitudinal axis (x) of the aircraft. Similarly, by rolling the cab, it is possible to simulate a translational acceleration along the lateral axis (y) of the aircraft. Clearly, residual tilt can only simulate translational accelerations which are smaller than 1 g (g = 32.2 ft/sec^2 = 9.81 m/sec^2).

The disadvantage of residual tilt is the unrealistic angular motion required to impliment the technique. In cases where high fidelity of translational motion sensing is demanded, but the limited cab motion imposes a severe handicap, the technique of residual tilt may result in a better overall simulation of the sensed motion even though abnormal angular motion is imposed in order to compensate for the limited translational accelerations. The problem of determining the optimum trade-off between translational and angular cab motion which yields the greatest fidelity of the simulation forms the primary basis for using the optimum control approach.

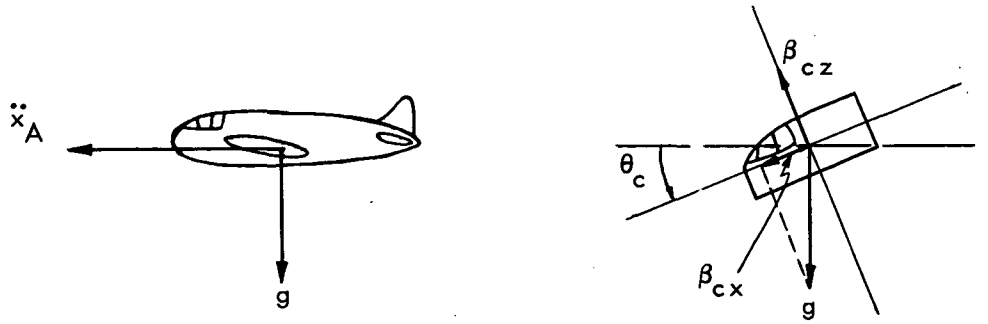

$$\vec{\beta}_A = \begin{bmatrix} \ddot{x}_A \\ 0 \\ 0 \end{bmatrix}$$

(a) Reference Aircraft

$$\vec{\beta}_c = \begin{bmatrix} g \sin\theta_c \\ 0 \\ g \quad (1 - \cos\theta_c) \end{bmatrix}$$

(b) Simulator Cab

Figure 2-8

Illustration of the Effect of Residual Tilt

To summarize, the equations describing the optimum control problem for designing the washout control are

Dynamic System:

$$\ddot{\vec{r}} = \vec{a}$$
$$\dot{\bar{\lambda}} = \bar{u} \qquad (2.15)$$

Performance Index:

$$S = \int_{t}^{t+T} (M_{\beta} + k M_{\omega} + \epsilon L)\, d\tau \qquad (2.16)$$

Find:

$\vec{a}$ and $\bar{u}$ so that S is minimized

Simulator Motion:

$$\ddot{\vec{r}}_c = \ddot{\vec{r}}_A + \vec{a}$$
$$\dot{\bar{\lambda}}_c = \dot{\bar{\lambda}}_A + \bar{u} \qquad (2.17)$$

In solving the optimum control problem, it will be assumed that a flight simulation always starts from a trim condition and the cab attitude is aligned so that the initial conditions $\dot{\vec{r}}(t) = \dot{\vec{r}}_A(t)$, $\vec{r}(t) = \vec{r}_A(t)$, and $\bar{\lambda}(t) = 0$ hold. It is also assumed that all aircraft quantities needed for the control law can be obtained from the computer simulating its motion.

2.4 Performance Indices

One of the major task in attempting to apply an optimum control method to the control of the six degree-of-freedom simulator is the search for an appropriate performance index. To start with, the state-of-the-art dictates that a precise definition of what constitutes a sensed motion cue is still an open physiological question. Even with the assumption that the motion cues sensed by the pilot are the same quantities as can be measured by three linear accelerometers and by three rate gyros, the fact that these quantities are vector valued makes it difficult, if not impossible, to find a single functional expression which provides a realistic measure of how well the simulator is able to duplicate the motion sensations. The search for a realistic performance index in functional form is further compounded by the necessary requirement of mathematical tractability. As often the case in the application of the optimum control technique, a final form of the performance index is chosen among other promising candidates because of its functional simplicity.

As indicated previously, the basic form assumed for the performance index is

$$S = \int_{t}^{t+T} (M_{\beta} + k M_{\omega} + \epsilon L)\, d\tau \qquad (2.18)$$

In this section, analytical expressions for the penalty functions M_{β}, M_{ω} and L will be defined in accordance with (2.11) - (2.13), and their properties analyzed. It is emphasized that the penalty functions discussed below were selected from a larger set of candidates, some of which may appear physically more realistic but were excluded from further consideration because of their functional complexity.

2.4.1 Sensed Acceleration Penalty M_β

To establish a meaningful penalty function in terms of the measurable sensed quantities, $\vec{\beta}_A$ and $\vec{\beta}_c$ (Figure 2-9), it is observed that the following properties should be considered:

(a) M_β should be scaled relative to $\vec{\beta}_A$, i.e. if all vectored quantities in M_β are multiplied by the same constant, the value of M_β should remain unchanged. In other words, for a given error $\vec{\beta}$, the penalty is higher for small $\vec{\beta}_A$ and lower for large $\vec{\beta}_A$.

(b) M_β should depend only on the orientation of $\vec{\beta}_c$ relative to $\vec{\beta}_A$ and not upon the absolute orientation per se.

(c) It should be possible to represent M_β as a function of the magnitude of the error vector $|\vec{\beta}|$ and the phase angle ξ between $\vec{\beta}_c$ and $\vec{\beta}_A$.

Based on these propositions, a general form of M_β which thus would be suitable as a penalty measure is

$$M_\beta = f_m\left(\frac{\beta}{\beta_A}\right) + K_\beta f_p(\xi) \qquad (2.19)$$

where the functionals f_m and f_p account, respectively, for the magnitude and phase errors, and the weighting factor K_β is used to adjust the relative importance between the magnitude and phase errors. The effect of the parameter K_β on the penalty imposed by M_β for differences between the sensed motion of the cab and the aircraft, can be shown by a vector diagram comparing the sensed acceleration vectors $\vec{\beta}_c$ and $\vec{\beta}_A$. An example of such a vector diagram is given in Figure 2-10 where the vectors $\vec{\beta}_c$ and $\vec{\beta}_A$ are normalized with respect to the magnitude β_A of $\vec{\beta}_A$, ($\beta_A = |\vec{\beta}_A|$), and where the unit vector $\vec{\beta}_A/\beta_A$ is used as a basis of reference. In Figure 2-10, six different possible values of the normalized vector $\vec{\beta}_c/\beta_A$ denoted by the indices 1 through 6 are shown for comparison with $\vec{\beta}_A/\beta_A$. The circles with their center at the tip of the vector $\vec{\beta}_A/\beta_A$ depict the contours for which the magnitudes of the error vector $\vec{\beta}/\beta_A$ remain constant. Obviously, if K_β were zero, the penalty imposed on sensed cab motions represented by the vectors

$$\left(\frac{\vec{\beta}_c}{\beta_A}\right)_1, \quad \left(\frac{\vec{\beta}_c}{\beta_A}\right)_4, \quad \left(\frac{\vec{\beta}_c}{\beta_A}\right)_5, \quad \text{and} \quad \left(\frac{\vec{\beta}_c}{\beta_A}\right)_6$$

are the same despite the fact that cases 1 and 4 have a phase error of ξ, while cases 5 and 6 have zero phase error. With nonzero K_β, however, the penalty corresponding to 1 and 4 is greater than the penalty corresponding to cases 5 and 6 by an amount of $K_\beta f_p(\xi)$.

In Figure 2-10, the cab motions depicted by case 1 and case 4 have the same magnitude error and phase error; the same is also true for the pair of cases 2 and 3 and the pair of cases 5 and 6. For cases 1, 2, 5, the magnitude of the cab motion is smaller than that of the aircraft, whereas the corresponding cases 4, 3, 6 have larger magnitude of motion as shown from the lengths of the vectors. In practice, however, the magnitudesof the cab motion is in general smaller than that of the aircraft. An excessively large magnitude of cab motion at a particular time interval will have to be compensated by an excessively small or even negative motion thereafter in order that the position of the cab does not cross the boundary limits. Thus, it would appear logical to place higher penalties on cases 3, 4, 6 where the magnitudes of the sensed cab motion are larger than for the aircraft.

The above discussion can be summarized by sketching contours of constant penalty, M_β = constant, as shown in Figure 2- 11.

Another important property that should be considered in selecting M_β is that of assigning greater penalty for large phase errors. This is related to the notion that maintaining $\vec{\beta}_c$ in the same general direction as $\vec{\beta}_A$ is at least as significant, if not more so, than magnitude errors. Thus, in the region where the phase error is greater than, say, $\frac{\pi}{2}$, the contours of M_β should display a pattern as shown in Figure 2-12.

With these requirements in mind, various choices of M_β are discussed below.

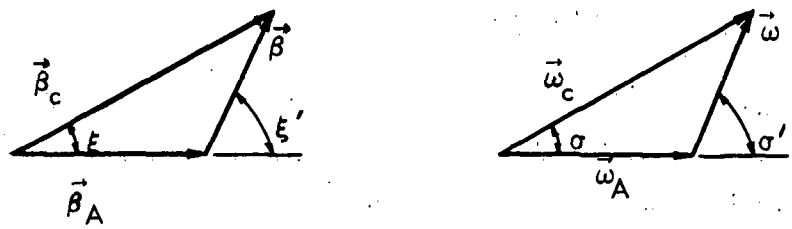

Figure 2-9

Vector Diagram for Sensed Quantities

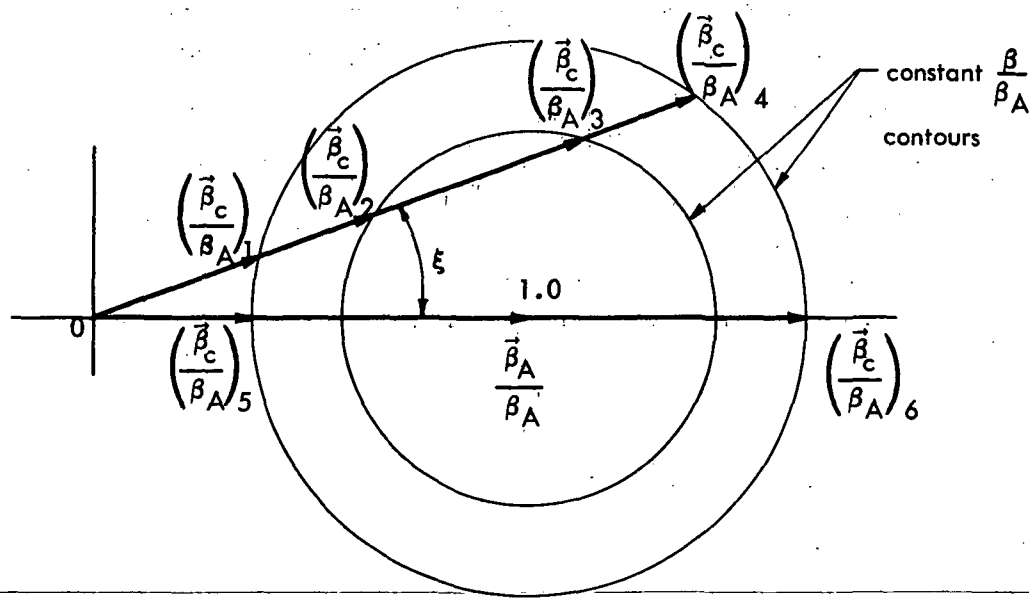

Figure 2-10

Normalized Vector Diagram to Illustrate Relative Motions

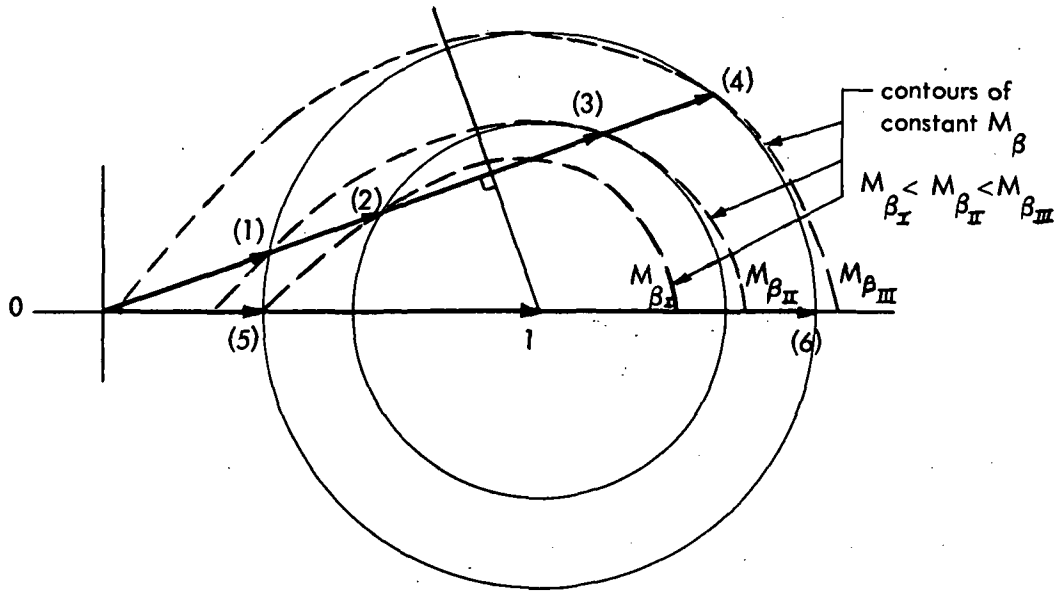

Figure 2-11

Contours of Constant M_β

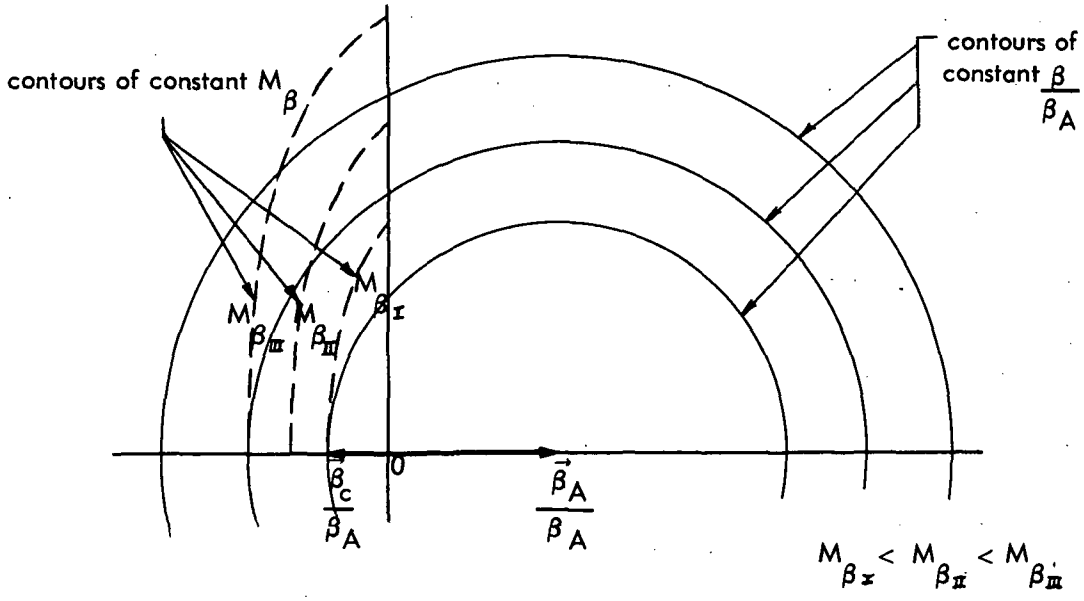

Figure 2-12

Contours of Constant M_β

(A). Penalty Function "A"

$$M_\beta = \frac{1}{\beta_A^2}\left\{ \frac{\beta^2}{2} + K_\beta[\beta\beta_A(1-\cos\xi')] \right\}^n \qquad n = 1, 2, \ldots$$

$$= \frac{\beta^2}{2\beta_A^2} + K_\beta \left(\frac{\beta}{\beta_A} - \frac{\vec{\beta}_A'\vec{\beta}}{\beta_A^2} \right)^n \qquad (2.20)$$

where

$$\beta^2 = \vec{\beta}'\vec{\beta} \ , \quad \beta = |\vec{\beta}| \ , \text{ etc.}$$

To aid in plotting the constant M_β contours, let

$$x = \frac{\beta}{\beta_A}\cos\xi'$$

$$y = \frac{\beta}{\beta_A}\sin\xi' \qquad (2.21)$$

then (2.20) is rewritten as

$$M_\beta = \frac{1}{2}(x^2+y^2) + K_\beta\left(\sqrt{x^2+y^2} - x\right)^n \qquad (2.22)$$

Figure 2-13 shows the M_β contours for n = 1, K_β = 0.02, 0.5 and 12.5

$$M_\beta = \frac{1}{2}(x^2+y^2) + K_\beta\left(\sqrt{x^2+y^2} - x\right) \qquad (2.23)$$

Figure 2-14 shows the case for n = 2 and K_β = 0.5

$$M_\beta = \frac{1}{2}(x^2+y^2) + K_\beta\left(\sqrt{x^2+y^2} - x\right)^2 \qquad (2.24)$$

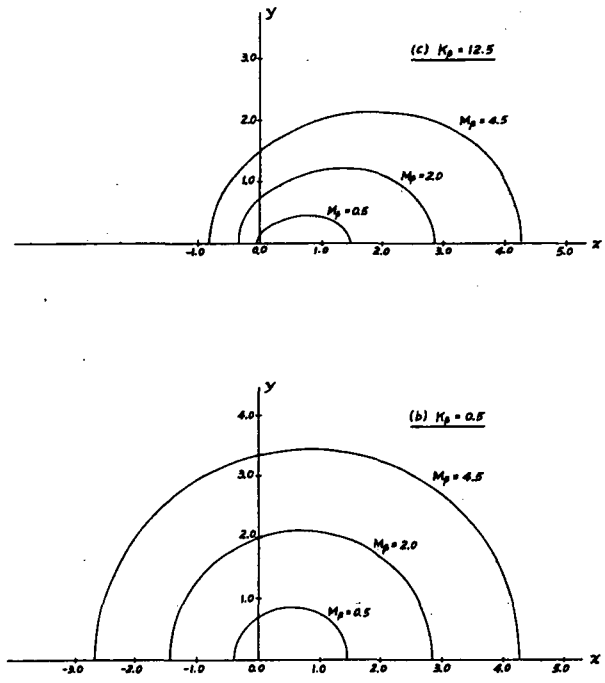

Figure 2-13

Contours of Constant M_β for Penalty Function "A" (n=1.0)

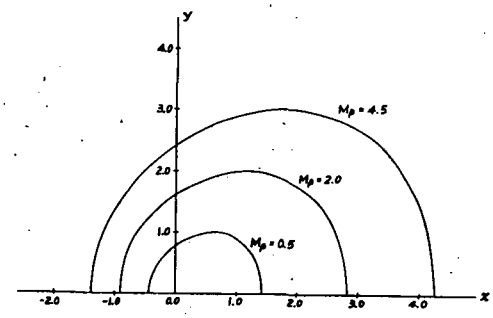

Figure 2-14

Contours of Constant M_β for Penalty Function "A" (n=2, $K_\beta = 0.5$)

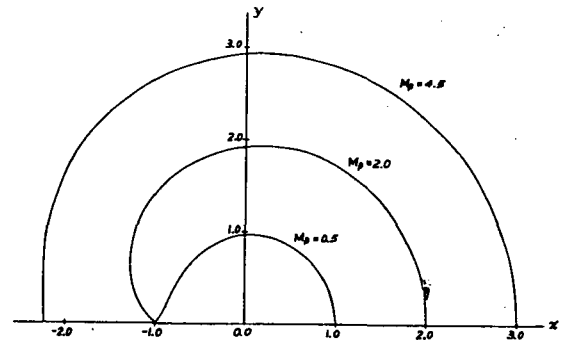

Figure 2-15

Contours of Constant M_β for Penalty Function "B" ($K_\beta = 0.5$)

(B) Penalty Function "B"

$$M_\beta = \frac{\beta^2}{2\beta_A^2} + K_\beta (1 - \cos \xi)^n \quad , \quad n = 1, 2, \ldots$$

$$= \frac{\beta^2}{2\beta_A^2} + K_\beta \left(1 - \frac{\vec{\beta}_c' \vec{\beta}_A}{\beta_c \beta_A}\right)^n \qquad (2.25)$$

Let

$$x = \frac{\beta}{\beta_A} \cos \xi' = \frac{\vec{\beta}' \vec{\beta}_A}{\beta_A^2}$$

$$y = \frac{\beta}{\beta_A} \sin \xi' = \left| \frac{\vec{\beta}}{\beta_A} - x \frac{\vec{\beta}_A}{\beta_A} \right| = \sqrt{\frac{\beta^2}{\beta_A^2} - x^2} \qquad (2.26)$$

then

$$M_\beta = \frac{1}{2}(x^2 + y^2) + K_\beta \left(1 - \frac{1 + x}{\sqrt{(1+x)^2 + y^2}}\right)^n \qquad (2.27)$$

and the set of curves for $n = 1$ and $K_\beta = 0.5$ is shown in Figure 2-15 .

(C) Penalty Function "C"

$$M_\beta = \frac{\beta^2}{2\beta_A^2} + K_\beta \left[\frac{\beta}{\beta_A} \cos \xi' \left(1 - K_1 \frac{\beta}{\beta_A} \cos \xi'\right)\right]^2$$

$$= \frac{\beta^2}{2\beta_A^2} + K_\beta \left(\frac{\vec{\beta}_A' \vec{\beta}}{\beta_A^2}\right)^2 \left(1 - K_1 \frac{\vec{\beta}_A' \vec{\beta}}{\beta_A^2}\right)^2 \qquad (2.28)$$

In terms of x and y.

$$M_\beta = \frac{1}{2}(x^2 + y^2) + K_\beta x^2 (1 - K_1 x)^2 \qquad (2.29)$$

Figure 2- 16 shows the M_β contours for different combinations of K_β and K_1.

(D) Penalty Function "D"

$$M_\beta = \frac{\beta^2}{2\beta_A^2}\left[1 + K_\beta\left(1 - K_1\frac{\beta}{\beta_A}\cos\xi'\right)^2\right]$$

$$= \frac{\beta^2}{2\beta_A^2}\left[1 + K_\beta\left(1 - K_1\frac{\vec{\beta}_A'\,\vec{\beta}}{\beta_A^2}\right)^2\right] \qquad (2.30)$$

In terms of x and y.

$$M_\beta = \frac{1}{2}(x^2 + y^2)\left[1 + K_\beta(1 - K_1 x)^2\right] \qquad (2.31)$$

Figure 2- 17 shows the M_β contours for different combinations of K_β and K_1.

2.4.2 Sensed Angular Penalty M_ω

It is assumed that the angular penalty M_ω takes the same form as the acceleration penalty M_β. Therefore, all of the discussions concerning M_β also applies to M_ω. The various possible choices used for the function M_ω are summarized below:

"A": $$M_\omega = \frac{\omega^2}{2\omega_A^2} + K_\omega\left(\frac{\omega}{\omega_A} - \frac{\vec{\omega}_A'\,\vec{\omega}}{\omega_A^2}\right)^n \qquad n = 1, 2, \ldots \qquad (2.32)$$

"B": $$M_\omega = \frac{\omega^2}{2\omega_A^2} + K_\omega\left(1 - \frac{\vec{\omega}_c'\,\vec{\omega}_A}{\omega_c\,\omega_A}\right)^n \qquad n = 1, 2, \ldots \qquad (2.33)$$

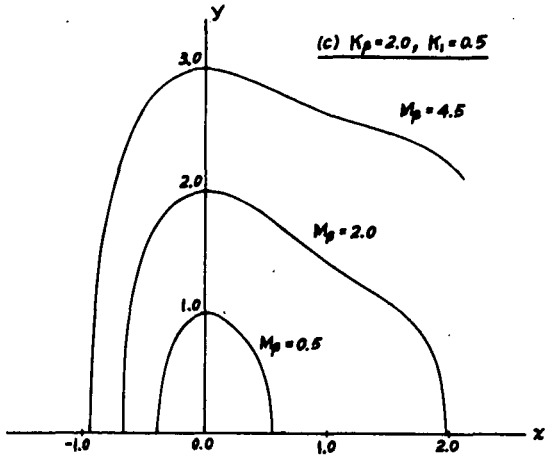

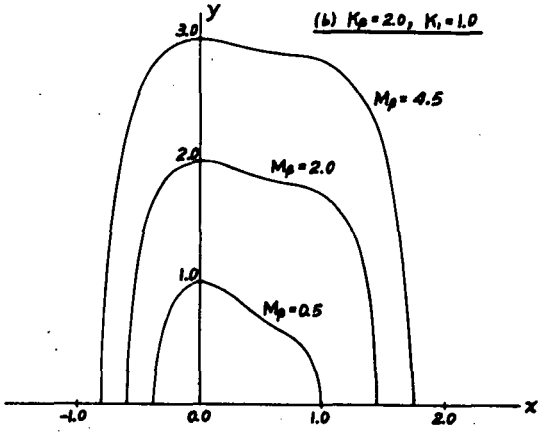

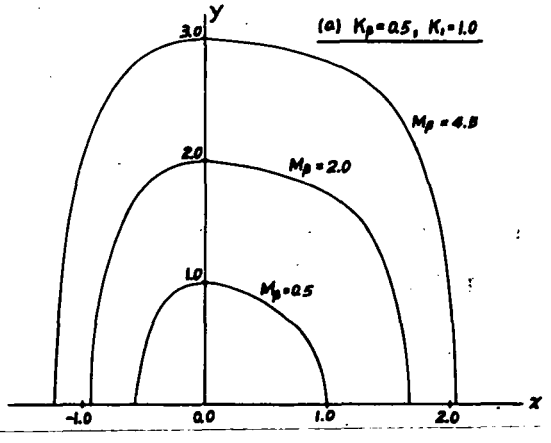

Figure 2-16

Contours of Constant M_β for Penalty Function "C"

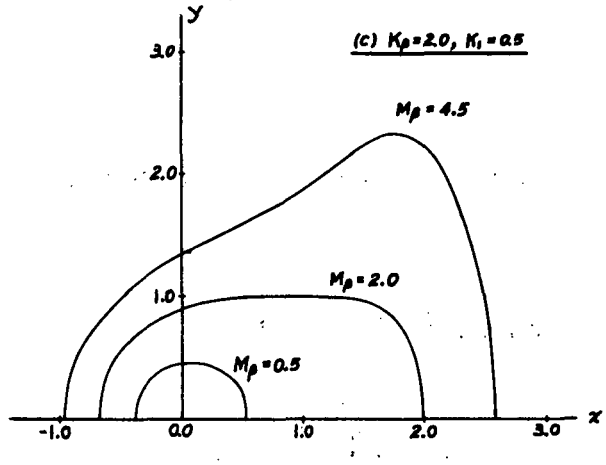

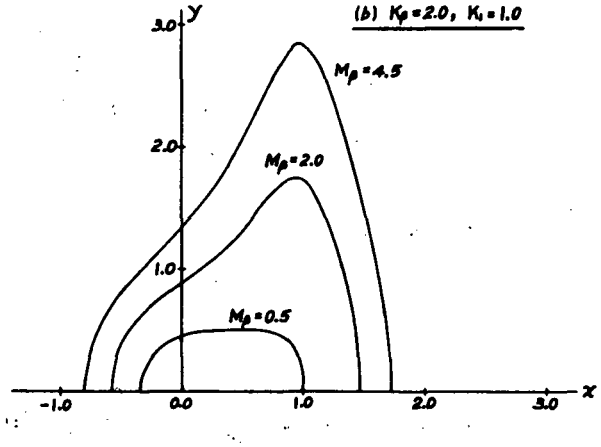

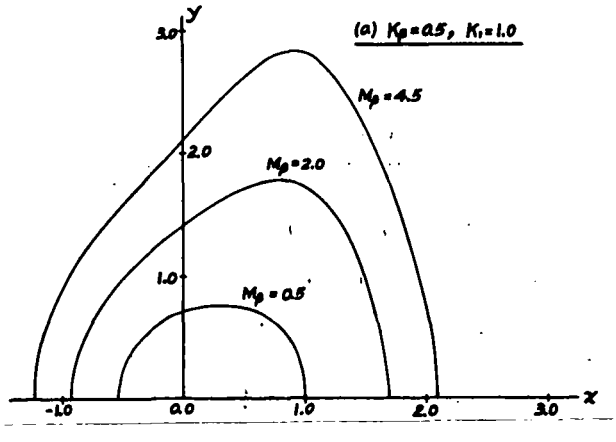

Figure 2-17

Contours of Constant M_β for Penalty Function "D"

$$\text{"C"}: \quad M_\omega = \frac{\omega^2}{2\omega_A^2} + K_\omega \left(\frac{\vec{\omega}_A' \vec{\omega}}{\omega_A^2} \right)^2 \left(1 - K_1 \frac{\vec{\omega}_A' \vec{\omega}}{\omega_A^2} \right) \tag{2.34}$$

$$\text{"D"}: \quad M_\omega = \frac{\omega^2}{2\omega_A^2} \left[1 + K_\omega \left(1 - K_1 \frac{\vec{\omega}_A' \vec{\omega}}{\omega_A^2} \right)^2 \right] \tag{2.35}$$

2.4.3 Excursion Penalty $L(\vec{r}_c)$

The basic requirement in the choice of $L(\vec{r}_c)$ is that of assigning heavy penalty for large cab excursions and small penalty when travelling well within the allowable boundary. There are two possible types of the limiting penalty described below.

(a) "Soft" Limiting Penalty:

$$L(\vec{r}_c) = \frac{1}{2} \left[\left(\frac{x_c}{d_x} \right)^{2n} + \left(\frac{y_c}{d_y} \right)^{2n} + \left(\frac{z_c}{d_z} \right)^{2n} \right] \quad , n \geq 1 \tag{2.36}$$

where d_x, d_y, d_z are adjustable parameters, whose values depend on the actual lengths of the allowable excursion limits. For $n = 1$, (2.36) reduces to

$$L(\vec{r}_c) = \frac{1}{2} \vec{r}_c' D \vec{r}_c \tag{2.37}$$

with

$$D = \begin{bmatrix} \frac{1}{d_x^2} & 0 & 0 \\ 0 & \frac{1}{d_y^2} & 0 \\ 0 & 0 & \frac{1}{d_z^2} \end{bmatrix}$$

(b) "Hard" Limiting Penalty:

$$L(\vec{r}_c) = L_x + L_y + L_z \tag{2.38}$$

where

$$L_x = \begin{cases} 0 & , \quad |x_c| < d_x \\ |x_c - d_x| & , \quad |x_c| \geq d_x \end{cases}$$

$$L_y = \begin{cases} 0 & , \quad |y_c| < d_y \\ |y_c - d_y| & , \quad |y_c| \geq d_y \end{cases} \tag{2.39}$$

$$L_z = \begin{cases} 0 & , \quad |z_c| < d_z \\ |z_c - d_z| & , \quad |z_c| \geq d_z \end{cases}$$

Figure 2- 18 illustrates these two types of penalty functions.

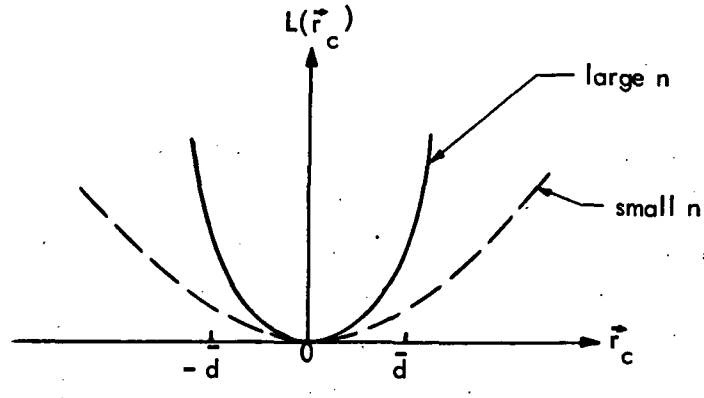

(a) Soft Limiting Case

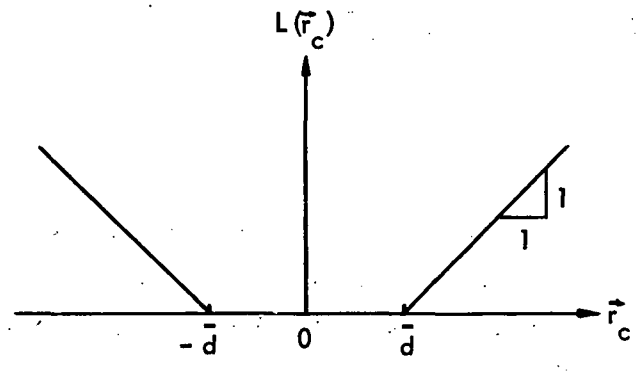

(b) Hard Limiting Case

Figure 2-18

Excursion Penalty Functions

2.5 Quasi-Optimum Washout System Design

In this section, the optimum control problem, as formulated in Sections 2.3 and 2.4, will be solved using the quasi-optimum control technique. Although it would be desirable to consider all the penalty functions defined in Section 2.4 so that the relative merits of the resulting washout systems could be evaluated by actual flight simulation, only one case will be considered in detail due to the limited amount of time available. In particular, the penalty functions considered in this report are (2.20), (2.32) and (2.36) with n = 1, i.e.

$$M_\beta(\vec{\beta}(\vec{a}, \bar{\lambda}), \vec{\beta}_A(\tau)) = \frac{\beta^2}{2\beta_A^2} + K_\beta\left(\frac{\beta}{\beta_A} - \frac{\vec{\beta}_A' \vec{\beta}}{\beta_A^2}\right) \tag{2.40}$$

$$M_\omega(\vec{\omega}(\bar{u}, \bar{\lambda}), \vec{\omega}_A(\tau)) = \frac{\omega^2}{2\omega_A^2} + K_\omega\left(\frac{\omega}{\omega_A} - \frac{\vec{\omega}_A' \vec{\omega}}{\omega_A^2}\right) \tag{2.41}$$

$$L(\vec{r}_c) = \frac{1}{2}\vec{r}_c' D \vec{r}_c \tag{2.42}$$

In subsection 2.5.1, the maximum principle is applied to reduce the optimum control problem to a two-point boundary value problem whose physical interpretation is discussed in subsection 2.5.2. Finally, in subsection 2.5.3, the quasi-optimum control technique is applied to solve the two-point boundary value problem for the controls $\vec{a}$ and $\bar{u}$ in closed form.

2.5.1 The Two-Point Boundary Value Problem

The control problem to be treated consists of the error dynamics

$$\begin{aligned} \ddot{\vec{r}} &= \vec{a} \\ \dot{\bar{\lambda}} &= \bar{u} \end{aligned} \tag{2.43}$$

and the performance index

$$S = \int_t^{t+T} (M_\beta + k M_\omega + \epsilon L)\, d\tau \qquad (2.44)$$

which is rewritten in state variable form, by letting $r_0 = S$

$$\begin{aligned}
\dot{r}_0 &= M_\beta + k M_\omega + \epsilon L \\
\dot{\vec{r}} &= \vec{v} \\
\dot{\vec{v}} &= \vec{a} \\
\dot{\bar{\lambda}} &= \bar{u} \\
\dot{\tau} &= 1 \\
\dot{\epsilon} &= 0
\end{aligned} \qquad (2.45)$$

The initial time is taken as the present time t and the time interval T is assumed fixed. The assumed initial conditions are

$$\begin{aligned}
r_0(t) &= 0 \\
\vec{r}(t) &= \vec{r}_A(t) \\
\vec{v}(t) &= \vec{v}_A(t) \\
\bar{\lambda}(t) &= 0 \\
\tau(t) &= t \\
\epsilon(t) &= \epsilon
\end{aligned} \qquad (2.46)$$

and the assumed terminal conditions are

$$\begin{aligned}
r_0(t+T) &= \text{free} \quad , \quad \bar{\lambda}(t+T) = \text{free} \\
\vec{r}(t+T) &= \text{free} \quad , \quad \tau(t+T) = t+T \\
\vec{v}(t+T) &= \text{free} \quad , \quad \epsilon(t+T) = \text{free}
\end{aligned} \qquad (2.47)$$

The Hamiltonian for the dynamic system described by (2.45) is

$$h = p_0(M_\beta + k\, M_\omega + \epsilon L) + \bar{p}_r' \vec{v} + \bar{p}_r' \vec{a} + \bar{p}_\lambda' \bar{u} + p_\tau \qquad (2.48)$$

where the adjoint variables $\bar{p}$ are defined by

$$\begin{aligned}
\dot{p}_0 &= 0 \\
\dot{\bar{p}}_r &= -\epsilon p_0 \frac{\partial L(\vec{r}_c)}{\partial \vec{r}} \\
\dot{\bar{p}}_v &= -\bar{p}_r \\
\dot{\bar{p}}_\lambda &= -p_0 \left(\frac{\partial M_\beta(\vec{a}, \bar{\lambda}, \tau)}{\partial \bar{\lambda}} + k \cdot \frac{\partial M_\omega(\bar{u}, \bar{\lambda}, \tau)}{\partial \bar{\lambda}} \right) \qquad (2.49) \\
\dot{p}_\tau &= -p_0 \left(\frac{\partial M_\beta(\vec{a}, \bar{\lambda}, \tau)}{\partial \tau} + k \cdot \frac{\partial M_\omega(\bar{u}, \bar{\lambda}, \tau)}{\partial \tau} + \epsilon \cdot \frac{\partial L(\vec{r}, \tau)}{\partial \tau} \right) \\
\dot{p}_\epsilon &= -p_0 L(\vec{r}_c)
\end{aligned}$$

subject to the boundary conditions

$$\begin{aligned}
p_0(t+T) &= -1 \\
\bar{p}_r(t+T) &= 0 \\
\bar{p}_v(t+T) &= 0 \qquad (2.50) \\
\bar{p}_\lambda(t+T) &= 0 \\
p_\tau(t+T) &= \text{free} \\
p_\epsilon(t+T) &= 0
\end{aligned}$$

The solution of the two-point boundary value problem defined by (2. 45) – (2. 50) is highly complicated in its original form due to the irrational form of the penalty functions (2. 40) and (2.41). It will be shown that by means of a nonlinear transformation, the original problem can be reduced to one which may be more readily solved and which in turn provides physical insight into the structure of the system.

The first step is to apply the maximum principle to obtain the optimum controls $\vec{a}$ and $\bar{u}$. This entails computing the partial derivatives of the hamiltonian h, given by (2. 48) with respect to $\vec{a}$ and $\bar{u}$, respectively, and then setting the derivatives to zero. The resulting equations are

$$\frac{\partial M_\beta}{\partial \vec{a}} = \bar{p}_v \qquad (2.\ 51\ )$$

$$\frac{\partial M_\omega}{\partial \bar{u}} = \bar{p}_\lambda / k \qquad (2.\ 52\ )$$

where the adjoint variable p_0 was easily found to be $p_0 = -1$ from (2.49) and (2.50). Substitution of M_β and M_ω from (2. 40) and (2. 41) into (2. 51) and (2. 52), respectively, results in an expression which can be solved for $\vec{a}$ and $\bar{u}$. The final equations for $\vec{a}$ and $\bar{u}$ (see Appendix I for the details of the derivation) are

$$\vec{a} = \left[1 - \frac{K_\beta}{\sqrt{\beta_A^2 p_v^2 + 2 K_\beta \vec{\beta}_A' C(\bar{\lambda}_c) \bar{p}_v + K_\beta^2}} \right] \left(\beta_A^2 \bar{p}_v + K_\beta C'(\bar{\lambda}_c) \vec{\beta}_A \right) + C'(\bar{\lambda}_c) \vec{\alpha}_A - \vec{a}_A \qquad (2.\ 53\ )$$

$$\bar{u} = \left\{ 1 - \frac{K_\omega}{\sqrt{\omega_A^2 \bar{p}_\lambda' F^{-1}(\bar{\lambda}_c) [F'(\bar{\lambda}_c)]^{-1} \bar{p}_\lambda / k^2 + 2 K_\omega \vec{\omega}_A' [F'(\bar{\lambda}_c)]^{-1} \bar{p}_\lambda / k + K_\omega^2}} \right\} \cdot$$

$$\left\{ \omega_A^2 F^{-1}(\bar{\lambda}_c) [F'(\bar{\lambda}_c)]^{-1} \bar{p}_\lambda / k + K_\omega F^{-1}(\bar{\lambda}_c) \vec{\omega}_A \right\} + F^{-1}(\bar{\lambda}_c) \vec{\omega}_A - \bar{u}_A \qquad (2.\ 54\ )$$

or, in functional form

$$\vec{a} = \vec{a}(\bar{p}_v, \bar{\lambda}, \bar{\lambda}_A(\tau), \vec{a}_A(\tau))$$

$$\bar{u} = \bar{u}(\bar{p}_\lambda, \bar{\lambda}, \bar{\lambda}_A(\tau), \bar{u}_A(\tau)) \qquad (2.\ 55\ )$$

Using the optimum control laws (2. 53) and (2. 54), the closed-loop two-point boundary value problem can be obtained by substituting these controls into (2. 45) and (2. 49). It is noted from (2. 45), (2. 49) and (2. 55) that the pertinent variables are $\vec{r}$, $\vec{v}$, $\bar{\lambda}$, $\bar{p}_r$, $\bar{p}_v$ and $\bar{p}_\lambda$ and that they are uncoupled from the rest of the state and adjoint variables. In order to obtain the closed-loop equations in terms of the pertinent variables, we evaluate the partial derivatives in (2. 49) by noting that

$$\frac{\partial M_\beta}{\partial \bar{\lambda}} = \left(\frac{\partial \vec{\beta}}{\partial \bar{\lambda}}\right)' \frac{\partial M_\beta}{\partial \vec{\beta}}$$

$$\frac{\partial M_\omega}{\partial \bar{\lambda}} = \left(\frac{\partial \vec{\omega}}{\partial \bar{\lambda}}\right)' \frac{\partial M_\omega}{\partial \vec{\omega}} \qquad (2.56)$$

But, from (2. 51) and (2. 52), we have

$$\frac{\partial M_\beta}{\partial \vec{a}} = \left(\frac{\partial \vec{\beta}}{\partial \vec{a}}\right)' \frac{\partial M_\beta}{\partial \vec{\beta}} = \bar{p}_v$$

$$\frac{\partial M_\omega}{\partial \bar{u}} = \left(\frac{\partial \vec{\omega}}{\partial \bar{u}}\right)' \frac{\partial M_\omega}{\partial \vec{\omega}} = \bar{p}_\lambda / k \qquad (2.57)$$

or

$$\frac{\partial M_\beta}{\partial \vec{\beta}} = \left[\left(\frac{\partial \vec{\beta}}{\partial \vec{a}}\right)'\right]^{-1} \bar{p}_v$$

$$\frac{\partial M_\omega}{\partial \vec{\omega}} = \left[\left(\frac{\partial \vec{\omega}}{\partial \bar{u}}\right)'\right]^{-1} \bar{p}_\lambda / k \qquad (2.58)$$

and

$$\frac{\partial \vec{\beta}}{\partial \vec{a}} = C(\bar{\lambda}_c)$$

$$\frac{\partial \vec{\omega}}{\partial \bar{u}} = F(\bar{\lambda}_c) \qquad (2.59)$$

$$\frac{\partial \vec{\beta}}{\partial \bar{\lambda}} = \frac{\partial C(\bar{\lambda}_c)}{\partial \bar{\lambda}} \vec{a}_c$$

$$\frac{\partial \vec{\omega}}{\partial \bar{\lambda}} = \frac{\partial F(\bar{\lambda}_c)}{\partial \bar{\lambda}} \bar{u}_c \qquad (2.60)$$

Substitution of (2. 58) – (2.60) into (2. 56) yields

$$\frac{\partial M_\beta}{\partial \bar{\lambda}} = \vec{a}_c' \left[\frac{\partial C(\bar{\lambda}_c)}{\partial \bar{\lambda}} \right]' C(\bar{\lambda}_c) \bar{p}_v$$

$$\frac{\partial M_\omega}{\partial \bar{\lambda}} = \bar{u}_c' \left[\frac{\partial F(\bar{\lambda}_c)}{\partial \bar{\lambda}} \right]' [F'(\bar{\lambda}_c)]^{-1} \bar{p}_\lambda / k \qquad (2.61)$$

Further substitution of (2. 61) into (2. 49) obtains the closed-loop two-point boundary value problem for the pertinent variables

$$\dot{\vec{r}} = \vec{v}$$
$$\dot{\vec{v}} = \vec{a}$$
$$\dot{\bar{\lambda}} = \bar{u} \qquad (2.62)$$
$$\dot{\bar{p}}_r = \epsilon \frac{\partial L(\vec{r}_c)}{\partial \vec{r}}$$
$$\dot{\bar{p}}_v = -\bar{p}_r \qquad (2.63)$$
$$\dot{\bar{p}}_\lambda = \bar{u}_c' \left[\frac{\partial F(\bar{\lambda}_c)}{\partial \bar{\lambda}} \right]' [F'(\bar{\lambda}_c)]^{-1} \bar{p}_\lambda + \vec{a}_c' \left[\frac{\partial C(\bar{\lambda}_c)}{\partial \bar{\lambda}} \right]' C(\bar{\lambda}_c) \bar{p}_v$$

where $\vec{a}$ and $\bar{u}$ are given by (2. 53) and (2. 54), respectively, and where the initial conditions and boundary conditions are given, respectively, in (2. 46) and (2. 50). The objective is to solve for $\bar{p}_v$ and $\bar{p}_\lambda$ in terms of the state vectors $\vec{r}$, $\vec{v}$ and $\bar{\lambda}$ from the coupled differential equations (2. 62) and (2. 63). Substitution of the expressions for $\bar{p}_v$ and $\bar{p}_\lambda$ into the control laws for $\vec{a}$ and $\bar{u}$ shown in (2. 53) and (2. 54), will result in the feedback configuration necessary to realize the washout circuit.

The nonlinear transformation required to solve the two-point boundary value problem involves the introduction of a new adjoint vector $\bar{\gamma}$ and a new angular washout vector $\bar{n}$ that are related to $\bar{p}_\lambda$ and $\bar{u}$ by

$$\bar{\gamma} = [F'(\bar{\lambda}_c)]^{-1} \bar{p}_\lambda \tag{2.64}$$

$$\bar{n} = F(\bar{\lambda}_c)\,\bar{u} \tag{2.65}$$

Multiplying both sides of (2.64) by $F'(\bar{\lambda}_c)$ and differentiating with respect to time, we have

$$\dot{\bar{p}}_\lambda = F'(\bar{\lambda}_c)\dot{\bar{\gamma}} + \bar{u}_c' \frac{\partial F'(\bar{\lambda}_c)}{\partial \bar{\lambda}_c} \bar{\gamma} \tag{2.66}$$

Equate (2.66) to the last equation in (2.63), gives

$$\dot{\bar{\gamma}} = [F'(\bar{\lambda}_c)]^{-1} \vec{a}_c' \frac{\partial C'(\bar{\lambda}_c)}{\partial \bar{\lambda}} C(\bar{\lambda}_c)\bar{p}_v \tag{2.67}$$

After performing the sequence of matrix multiplications in (2.67), the differential equation for the new adjoint vector simplifies to

$$\begin{aligned}\dot{\bar{\gamma}} &= -\vec{\alpha}_c \times C(\bar{\lambda}_c)\bar{p}_v \\ &= -C(\bar{\lambda}_c)[\vec{a}_c \times \bar{p}_v]\end{aligned} \tag{2.68}$$

where the symbol "x" denotes the "cross product" of two vectors. For mathematical convenience, (2.68) can be rewritten as (see Appendix I)

$$\dot{\bar{\gamma}} = -\vec{\alpha}_c \times \bar{\eta} \tag{2.69}$$

where

$$\bar{\eta} = -\frac{1}{\beta_A^2}\left\{\left(1 - \frac{K_\beta}{K_\beta - \sqrt{\beta_A^2 p_v^2 + 2K_\beta \vec{\beta}' C(\lambda_c)\bar{p}_v + K_\beta^2}}\right)\vec{\alpha}_A + K_\beta \vec{\beta}_A\right\} \tag{2.70}$$

The two-point boundary value problem given by (2. 62) and (2. 63), is next rewritten in terms of the new variables to give

$$\begin{aligned}
&\dot{\vec{r}} = \vec{v} && \vec{r}(t) = \vec{r}_A(t) \\
&\dot{\vec{v}} = \vec{a} && \vec{v}(t) = \vec{v}_A(t) \\
&\dot{\bar{\lambda}} = F^{-1}(\bar{\lambda}_c)\bar{n} && \bar{\lambda}(t) = 0
\end{aligned} \qquad (2.71)$$

$$\begin{aligned}
&\dot{\bar{p}}_r = \epsilon \frac{\partial L(\vec{r}_c)}{\partial \vec{r}} && \bar{p}_r(t+T) = 0 \\
&\dot{\bar{p}}_v = -\bar{p}_r && \bar{p}_v(t+T) = 0 \\
&\dot{\bar{\gamma}} = -C(\bar{\lambda}_c)[\vec{a}_c \times \bar{p}_v] && \bar{\gamma}(t+T) = 0
\end{aligned} \qquad (2.72)$$

where the translational control $\vec{a}$ is shown in (2. 53) and the transformed angular control $\bar{n}$ is rewritten from (2. 54) as

$$\bar{n} = \left[1 - \frac{K_\omega}{\sqrt{\omega_A^2 \gamma^2/k^2 + 2K_\omega \vec{\omega}_A' \bar{\gamma}/k + K_\omega^2}}\right] \left[\omega_A^2 \bar{\gamma}/k + K_\omega \vec{\omega}_A\right] + \vec{\omega}_A - F(\bar{\lambda}_c)\bar{u}_A \qquad (2.73)$$

2.5.2 Physical Implication of the Mathematical Formulation

As a result of the theoretical developments in the preceeding subsection, the optimal control problem was reduced to a problem of solving a set of differential equations given by (2. 71) and (2. 72) for the adjoint vectors $\bar{p}_r$, $\bar{p}_v$ and $\bar{\gamma}$ in the terms of the state vectors $\vec{r}$, $\vec{v}$ and $\bar{\lambda}$. Before proceeding further with the theoretical solution of the problem, we will pause at this point to examine the physical implications of the equations (2. 71) and (2. 72).

First, for reasons of simplicity, we will consider the "linear" case in which no "phase" penalty is imposed, i.e. $K_\beta = K_\omega = 0$. For this case, it follows from (2.53), (2.70) and (2.73), that the system equations given by (2.71) and (2.72) reduce to

$$\dot{\vec{r}} = \vec{v}$$

$$\dot{\vec{v}} = \beta_A^2 \bar{p}_v + C'(\bar{\lambda}_c)\vec{\alpha}_A - \vec{a}_A \qquad (2.74)$$

$$\dot{\bar{\lambda}} = \frac{\omega_A^2}{k} F^{-1}(\bar{\lambda}_c)\bar{\gamma} + F^{-1}(\bar{\lambda}_c)\vec{\omega}_A - \bar{u}_A$$

$$\dot{\bar{p}}_r = \epsilon \frac{\partial L(\vec{r})}{\partial \vec{r}}$$

$$\dot{\bar{p}}_v = -\bar{p}_r \qquad (2.75)$$

$$\dot{\bar{\gamma}} = \frac{1}{\beta_A^2}(\vec{\alpha}_c \times \vec{\alpha}_A)$$

Also from the linearity assumption, the closed-loop cab dynamics (2.17) reduces to

$$\ddot{\vec{r}}_c = \beta_A^2 \bar{p}_v + C'(\bar{\lambda}_c)\vec{\alpha}_A + \vec{g} \qquad (2.76)$$

$$\dot{\bar{\lambda}}_c = F^{-1}(\bar{\lambda}_c)\left[\frac{\omega_A^2}{k}\bar{\gamma} + \vec{\omega}_A\right] \qquad (2.77)$$

in which the adjoint variables $\bar{p}_v$ and $\bar{\gamma}$ are obtained from the solution of (2.74) and (2.75).

As noted previously, the parameter k is designed to account for the relative importance between the angular and the translational motion errors. Thus, it is of interest to see how the cab motion would behave for extreme values of k.

(i) $k \to \infty$:

This case heavily weights errors in angular motion which for the limiting situation gives that the angular motion of the cab will be identical to the aircraft. This is indeed the case, since for $k = \infty$, (2.77) reduces to

$$\dot{\bar{\lambda}}_c = F^{-1}(\bar{\lambda}_c)\,\vec{\omega}_A$$

which, upon substitution of the assumed initial condition $\bar{\lambda}_c(t) = \bar{\lambda}_A(t)$, further reduces to

$$\dot{\bar{\lambda}}_c = F^{-1}(\bar{\lambda}_A)\,\bar{\omega}_A = \dot{\bar{\lambda}}_A \qquad (2.78)$$

The translational motion equation (2.76), with $\bar{\lambda}_c = \bar{\lambda}_A$, can be written as

$$\begin{aligned} \ddot{\vec{r}}_c &= \beta_A^2\,\bar{p}_v + C'(\bar{\lambda}_A)\,\vec{\alpha}_A + \vec{g} \qquad (2.79) \\ &= \beta_A^2\,\bar{p}_v + \vec{a}_A + \vec{g} \\ &= \beta_A^2\,\bar{p}_v + \ddot{\vec{r}}_A \end{aligned}$$

which shows that the cab acceleration differs from the aircraft acceleration by the amount $\beta_A^2\,\bar{p}_v$. The wash-out signal $\beta_A^2\,\bar{p}_v$ which can be obtained from (2.75) is dependent on the excursion penalty $L(\vec{r}_c)$ and its adjustable weighting ϵ.

(ii) $k \to 0$:

Direct visualization of the effect of $k = 0$ is not obvious from the closed-loop equations since the terms involving k tend to ∞ as $k \to 0$. Referring to the performance index, given by (2.44), it is intuitively obvious that, since no penalty is imposed on the angular motion error for $k = 0$, the cab should assume whatever angular motion is necessary to minimize the translational motion error. It is derived in the Appendix III that this is indeed the case. In fact, as $k \to 0$, the optimal trajectory tends to approach a "singular" subarc for which the adjoint variable $\tilde{\gamma} = 0$ and for which

$$\vec{\alpha}_c \times \vec{\alpha}_A = C(\bar{\lambda}_c)\,\vec{a}_c \times \vec{\alpha}_A \equiv 0 \qquad (2.80)$$

The implication of (2.80) is that along the singular trajectory the cab attitude $\bar{\lambda}_c$ should be so maintained to keep the sensed translational accelerations $\vec{\alpha}_c$ and $\vec{\alpha}_A$ co-linear for any specific force $\vec{a}_c$ being exerted on the cab. The fact that the two vectors are co-linear provides that the cab motion is either completely in phase, or completely out of phase relative to the aircraft. The possibility of the motion being completely out of phase arises because K_β was set to zero and no phase error penalty was imposed.

Substitution of $\bar{\lambda}_c$, obtained from the solution of (2.80), into (2.76) yields the corresponding translational motion for the cab.

Thus, for intermediate values of k, the cab motion will always have some translational and angular motion errors, and it is a subject of experimental study to determine what particular values of k will give an acceptable compromise between the two extremes.

2.5.3 Quasi-Optimum Solution of the Two-Point Boundary Value Problem

Simplified Control:

In applying the quasi-optimum control technique, the system is first approximated by a simpler model for which the exact optimum solution can be expressed in closed form. This simplified control law is then corrected to account for the difference between the original system and its simplified model. A convenient simplified system in the present application is obtained for $\epsilon = 0$, i.e. by ignoring the physical constraint. For $\epsilon = 0$, the two-point boundary value problem, given by (2.71) and (2.72) reduces to

$$\dot{\vec{r}}_s = \vec{v}_s \qquad \dot{\vec{r}}_s(t) = \vec{r}_A(t) \qquad (2.81)$$

$$\dot{\vec{v}}_s = \vec{a}_s \qquad \dot{\vec{v}}_s(t) = \vec{v}_A(t)$$

$$\dot{\bar{\lambda}}_s = F^{-1}(\bar{\lambda}_{cs})\bar{n}_s \qquad \bar{\lambda}_s(t) = 0$$

$$\dot{\bar{p}}_{rs} = 0 \qquad \bar{p}_{rs}(t+T) = 0 \qquad (2.82)$$

$$\dot{\bar{p}}_{vs} = -\bar{p}_{rs} \qquad \bar{p}_{vs}(t+T) = 0$$

$$\dot{\bar{\gamma}} = -\vec{\alpha}_{cs} \times C(\bar{\lambda}_{cs})\bar{p}_{vs} \qquad \bar{\gamma}_s(t+T) = 0$$

where the subscript "s" has been added to signify the simplified system.

Solution of (2.82) immediately yields

$$\bar{p}_{rs} = 0 \qquad (2.83)$$

$$\bar{p}_{vs} = 0$$

$$\bar{\gamma}_s = 0$$

Consequently, from (2.53) and (2.73), the simplified controls are

$$\vec{a}_s = C'(\bar{\lambda}_{cs})\vec{\alpha}_A - \vec{a}_A \qquad (2.84)$$

$$\bar{n}_s = \vec{\omega}_A - F(\lambda_{cs})\bar{u}_A$$

Substitution of (2.84) into (2.81) and noting that $\bar{\lambda}_{cs} = \bar{\lambda}_s + \bar{\lambda}_A$, we get the closed-loop error state equations

$$\dot{\vec{r}}_s = \vec{v}_s \qquad (2.85)$$

$$\dot{\vec{v}}_s = C'(\bar{\lambda}_s + \bar{\lambda}_A)\vec{\alpha}_A - \vec{a}_A$$

$$\dot{\bar{\lambda}}_s = F^{-1}(\bar{\lambda}_s + \bar{\lambda}_A)\vec{\omega}_A - \bar{u}_A$$

It is noteworthy to observe that the simplified controls in (2.84) and the corresponding error states in (2.85) are not zero, even though no excursion limits are imposed on the cab motion. However, the "sensed" errors are zero which can be seen by substituting (2.84) into the definitions of $\vec{\beta}$ and $\vec{\omega}$ given by (2.8).

$$\vec{\beta} = \vec{\alpha}_{cs} - \vec{\alpha}_A = C(\bar{\lambda}_{cs})(\vec{a}_s + \vec{a}_A) - \vec{\alpha}_A = 0$$

$$\vec{\omega} = \vec{\omega}_{cs} - \vec{\omega}_A = F(\bar{\lambda}_{cs})(\bar{v}_s + \bar{v}_A) - \vec{\omega}_A = 0$$

An examination of the error state equations (2.85) reveals that the nonzero simplified controls and the nonzero error states are a consequence of a nonzero initial attitude error $\bar{\lambda}_s$. If it happens that $\bar{\lambda}_s$ is initially zero, then the solution of the last equation in (2.85) yields $\bar{\lambda}_s(\tau) \equiv 0$ which upon substitution into the remaining equations in (2.85) and in (2.84) results in the errors and the controls being zero.

In summary, when no boundary limitations are considered (simplified control problem), a one-to-one simulation, i.e. $\vec{\beta} = \vec{\omega} = 0$, can be achieved for arbitrary initial conditions by using the wash-out controls in (2.84).

The solution of the simplified problem is required to calculate the quasi-optimum control law to be derived in the next section. Unfortunately, there are two major difficulties that arise when attempting to obtain analytical solutions to the simplified problem:

(A) The transformation matrices C and F, as defined in (2.2) and (2.6) are nonlinear.

(B) In order to solve the two-point boundary value problem, the quantities $\vec{\alpha}_A$, $\vec{a}_A$, $\vec{\omega}_A$ and $\bar{\lambda}_A$ describing the aircraft motion must not only be known for the current time t but for time in the future of t.

To overcome these difficulties it will be assumed that the attitude error $\bar{\lambda}_s$ between the cab and the aircraft is sufficiently small to permit the approximation

$$C'(\bar{\lambda}_{cs})\vec{\alpha}_A - \vec{a}_A \cong C'(\bar{\lambda}_A)\vec{\alpha}_A - \vec{a}_A = 0$$
$$F^{-1}(\bar{\lambda}_{cs})\vec{\omega}_A - \dot{\bar{\lambda}}_A \cong F^{-1}(\bar{\lambda}_A)\vec{\omega}_A - \bar{u}_A = 0 \qquad (2.86)$$

Such an approximation is not unreasonable since, with no excursion limits imposed on the simplified system the attitude error will tend to decrease from its initial value. If the initial attitude error is zero, then it will remain at zero.

From (2. 86), (2.85) can easily be solved to give

$$\vec{r}_s(\tau) = \vec{r}_s(t) + \vec{v}_s(t)(\tau - t)$$
$$\vec{v}_s(\tau) = \vec{v}_s(t) \qquad (2.87)$$
$$\bar{\lambda}_s(\tau) = \bar{\lambda}_s(t)$$

Quasi-Optimum Control:

The quasi-optimum controls are obtained by first deriving the correction factors $\bar{\psi}_r$, $\bar{\psi}_v$ and $\bar{\psi}_\gamma$ so that the adjoint variables $\bar{p}_r$, $\bar{p}_v$ and $\bar{\gamma}$ of the original system can be approximated by

$$\bar{p}_r \cong \bar{p}_{rs} + \bar{\psi}_r = \bar{\psi}_r$$
$$\bar{p}_v \cong \bar{p}_{vs} + \bar{\psi}_v = \bar{\psi}_v \qquad (2.88)$$
$$\bar{\gamma} \cong \bar{\gamma}_s + \bar{\psi}_\gamma = \bar{\psi}_\gamma$$

Next, $\bar{p}_v$ and $\bar{\gamma}$ are substituted into the control laws for $\vec{a}$ and $\bar{n}$ given by (2. 53) and (2. 73), respectively.

It is shown in Appendix II that the quasi-optimum solutions for the costate variables $\bar{p}_v$ and $\bar{\gamma}$ are given by

$$\bar{p}_v \cong -\epsilon \left[T \int_t^{t+T} \frac{\partial L}{\partial \vec{r}} \, d\lambda - \int_t^{t+T} \int_t^{\tau} \frac{\partial L}{\partial \vec{r}} \, d\lambda \, d\tau \right] \qquad (2.89)$$

$$\bar{\gamma} \cong \bar{\gamma}(t) - \int_t^{t+T} (\vec{\alpha}_c \times \bar{\eta}) \, d\tau \qquad (2.90)$$

In order to evaluate the integral in (2.89), where the analytical expression for the function $L(\vec{r})$ is given in (2.42), knowledge of aircraft's position $\vec{r}_A(\tau)$ for time τ in the future of the current time $t(\tau \geq t)$ is required. To resolve this problem, a weighted Taylor's series expansion of $\vec{r}_A(\tau)$ is used to extrapolate the future position of the aircraft from its current value $\vec{r}_A(t)$. The resulting expansion is

$$\vec{r}_A(\tau) = \vec{r}_A(t) + (\tau - t)\,\dot{\vec{r}}_A(t) + \frac{(\tau - t)^2}{2\beta_{A\ max}^2}\,\ddot{\vec{r}}_A(t) \qquad (2.91)$$

where

$\beta_{A\ max}$ is the maximum value of β_A that must be determined (approximately) a priori. Utilizing (2.91), gives

$$\begin{aligned}
\left.\frac{\partial L}{\partial \vec{r}}\right|_{\epsilon = 0} &= D\,\vec{r}_c \Big|_{\epsilon = 0} \\
&= D(\vec{r} + \vec{r}_A) \Big|_{\epsilon = 0} \\
&= D(\vec{r}_s + \vec{r}_A) \\
&= D\left[\vec{r}_s(t) + (\tau - t)\,\dot{\vec{r}}_s(t) + \vec{r}_A(t) + (\tau - t)\,\dot{\vec{r}}_A(t) + \frac{(\tau - t)^2}{2\beta_{A\ max}^2}\,\ddot{\vec{r}}_A(t)\right] \\
&= D\left[\vec{r}_{cs}(t) + (\tau - t)\,\dot{\vec{r}}_{cs}(t) + \frac{(\tau - t)^2}{2\beta_{A\ max}^2}\,\ddot{\vec{r}}_A(t)\right] \qquad (2.92)
\end{aligned}$$

Therefore, dropping the subscript "s" we have from (2. 89)

$$\bar{p}_v = -\epsilon D\left[\frac{T^2}{2}\vec{r}_c + \frac{T^3}{3}\dot{\vec{r}}_c + \frac{T^4}{8\beta_{A\,max}^2}\ddot{\vec{r}}_A\right] \qquad (2.93\ )$$

The evaluation of (2. 90) will be done numerically during the simulation because of the complicated expression for the integrand.

2.6 Summary and System Implementation

In this section the simulator control system designed previously using the quasi-optimum control technique is summarized and its implementation is discussed. A block diagram showing how the required computations can be implemented during an actual flight simulation is given. A FORTRAN IV subroutine which performs the computations shown in the block diagram is also described.

2.6.1 Summary of the Simulator Control System Design

Recalling from Figure 2-2, the complete six degree-of-freedom simulator consists of the simulator cab, aircraft computer simulation, simulator control system, and cab drive system. The flight commands resulting from the pilot's manipulation of the cab controls are fed into the computer simulation of the aircraft. The computed aircraft motion, in particular, the translational acceleration $\ddot{\vec{r}}_A$ and the angular velocity $\dot{\bar{\lambda}}_A$ are the inputs to the simulator control system which in turn generates the drive command signals used to control the motion of the cab. In the problem formulation it was assumed that the cab drive system consists of perfect servos so that the outputs from the simulator control system are the cab position $\vec{r}_c$ and the cab attitude $\bar{\lambda}_c$. The basic input-output equations for the simulator control system are

$$\ddot{\vec{r}}_c = \ddot{\vec{r}}_A + \vec{a} \qquad \text{"translation"} \qquad (2.94)$$

$$\dot{\bar{\lambda}}_c = \dot{\bar{\lambda}}_A + \bar{u} \qquad \text{"rotation"} \qquad (2.95)$$

where

$$\vec{r}_i' = [x_i \ , \ y_i \ , \ z_i]$$

$$\bar{\lambda}_i' = [\Phi_i \ , \ \theta_i \ , \ \psi_i]$$

$$i = c, A$$

as illustrated in Figure 2-4. Thus, the simulator control system has a total of 6 inputs and 6 outputs.

The washout signals $\vec{a}$ and $\bar{u}$ are included in (2.94) and (2.95), respectively, in order to compensate for the limits on the cab excursions. The purpose of this study is to design the control laws for computing $\vec{a}$ and $\bar{u}$. The performance index used in section 2.5 for determining $\vec{a}$ and $\bar{u}$ was

$$S = \int_{t}^{t+T} (M_{\beta} + kM_{\omega} + \epsilon L) d\tau \qquad (2.96)$$

where $M_{\beta} = \beta^2 / 2\beta_A^2 + K_{\beta}(\beta/\beta_A - \vec{\beta}'_A \vec{\beta} / \beta_A^2)$

$$M_{\omega} = \omega^2 / 2\omega_A^2 + K_{\omega}(\omega/\omega_A - \vec{\omega}'_A \vec{\omega} / \omega_A^2)$$

$$L = \frac{1}{2} \vec{r}'_c D \vec{r}_c$$

$$D = \text{Diag}\{1/d_x^2, 1/d_y^2, 1/d_z^2\}$$

This performance index minimizes the sensed motion errors while penalizing large cab excursions. This performance index gives rise to 8 scaler parameters $T, k, \epsilon, K_{\beta}, K_{\omega}, d_x, d_y, d_z$. A large portion of the computer simulation study described subsequently is concerned with an investigation of the effects of using different values of these adjustable parameters in order to arrive at a range of values that may optimize the performance of the moving base simulator.

In Section 2.5, the quasi-optimum technique was used to design a washout system that minimizes the performance index in (2.96). The resulting equations for computing $\vec{a}$ and $\bar{u}$ are summarized below.

Translational Washout Signals:

$$\vec{a} = (1 - K_{\beta}\beta_A/\xi)\bar{\xi} + C'(\bar{\lambda}_c)\vec{\alpha}_A - \vec{a}_A$$

$$\bar{\xi} = \beta_A^2 \bar{P}_v + K_{\beta} C'(\bar{\lambda}_c)\vec{\beta}_A \qquad (2.97)$$

Rotational Washout Signals:

$$\bar{u} = F^{-1}(\bar{\lambda}_c)\bar{n}$$

$$\bar{n} = (1 - K_\omega \omega_A / \Omega)\bar{\Omega} + \vec{\omega}_A - F(\bar{\lambda}_c)\dot{\bar{\lambda}}_A \qquad (2.98)$$

$$\bar{\Omega} = (\omega_A^2 / K)\bar{\gamma} + K_\omega \vec{\omega}_A$$

Adjoint Variables

$$\bar{p}_v = -\epsilon D[(T^2/2)\vec{r}_c + (T^3/3)\dot{\vec{r}}_c + (T^4/8\beta^2_{A\,max})\ddot{\vec{r}}_c]$$

$$\dot{\bar{\gamma}} = -\vec{\alpha}_c \times \bar{\eta} \qquad (2.99)$$

$$\bar{\eta} = [1/(1 - K_\beta \beta_A / \xi)\beta_A^2]\vec{\alpha}_A + (K_\beta / \beta_A^2)\vec{\beta}_A$$

Sensed Motion Variables

$$\vec{a}_A = \ddot{\vec{r}} - \vec{g} \qquad \vec{a}_c = \ddot{\vec{r}}_c - \vec{g}$$

$$\vec{\alpha}_A = C(\bar{\lambda}_A)\vec{a}_A \qquad \vec{\alpha}_c = C(\bar{\lambda}_c)\vec{a}_c \qquad (2.100)$$

$$\vec{\beta}_A = \vec{\alpha}_A + \vec{g} \qquad \vec{\omega}_A = F(\bar{\lambda}_A)\dot{\bar{\lambda}}_A$$

$$\vec{g}' = [0, 0, g] \quad (g = 32.2 \text{ ft/sec}^2 = 9.81 \text{ m/sec}^2)$$

Transformation Matrices

$$C(\bar{\lambda}) = \begin{bmatrix} \cos\psi\cos\theta & \sin\psi & -\cos\psi\sin\theta \\ \sin\Phi\sin\theta - \sin\psi\cos\Phi\cos\theta & \cos\Phi\cos\psi & \sin\Phi\cos\theta + \cos\Phi\sin\psi\sin\theta \\ \cos\Phi\sin\theta + \sin\Phi\sin\psi\cos\theta & -\sin\Phi\cos\psi & \cos\Phi\cos\theta - \sin\Phi\sin\psi\sin\theta \end{bmatrix} \qquad (2.101)$$

$$F(\bar{\lambda}) = \begin{bmatrix} 1 & \sin\psi & 0 \\ 0 & \cos\Phi\cos\psi & \sin\Phi \\ 0 & -\sin\Phi\cos\psi & \cos\Phi \end{bmatrix}, \quad F^{-1}(\bar{\lambda}) = \begin{bmatrix} 1 & -\tan\psi\cos\Phi & \tan\psi\sin\Phi \\ 0 & \cos\Phi\sec\psi & -\sin\Phi\sec\psi \\ 0 & \sin\Phi & \cos\Phi \end{bmatrix}$$

$$\bar{\lambda}' = [\Phi, \theta, \psi]$$

A block diagram of the simulator control system showing the implementation of (2.94), (2.95), and (2.97) - (2.101) is given in Figure 2-19. Each arrow or path in the block diagram corresponds to a 3-component vector quantity. A total of $3 \times 5 = 15$ integrators are required to realize the simulator control system. The boxes in the block diagram represent gains multiplying the various vector quantities with the one exception of a single vector cross product indicated by a bold face X . The gains are composed of both scaler and matrix multiplication of the vector inputs to the boxes. The boldface letters C, D, and F indicate matrix operations. The matrix D is a constant, diagonal matrix (see (2.96)). The matrices C and F denote coordinate transformations which are a function of either $\bar{\lambda}_A$ or $\bar{\lambda}_c$; the particular choice is indicated in the block diagram. Thus, the matrices C and F are nonlinear gains which must be computed continuously. To simplify the block diagram, arrows connecting the integrator outputs $\bar{\lambda}_A$ and $\bar{\lambda}_c$ to the corresponding boxes containing C and F are not shown.

Of the scaler gains, some are linear, constant gains while the others are nonlinear, time-varying gains which must be computed at each iteration. The nonlinear gains require computation of β_A , ω_A , ξ , Ω which are the magnitudes of the vectors $\vec{\beta}_A$, $\vec{\omega}_A$, $\bar{\xi}$, $\bar{\Omega}$, respectively. These magnitudes are obtained by computing at each iteration the square root of the vector dot product. Again for simplicity purposes, the computation of these magnitudes is not explicitly shown in the block diagram.

In summary, the block diagram shows that the washout signals $\vec{a}$ and $\bar{u}$ are a function of

$$\vec{a} = \vec{a}(\ddot{\vec{r}}_A, \dot{\bar{\lambda}}_A, \bar{\lambda}_A, \dot{\vec{r}}_c, \vec{r}_c, \bar{\lambda}_c, \bar{\gamma})$$

$$\bar{u} = \bar{u}(\ddot{\vec{r}}_A, \dot{\bar{\lambda}}_A, \bar{\lambda}_A, \dot{\vec{r}}_c, \vec{r}, \bar{\lambda}_c, \bar{\gamma})$$

where

$\bar{\lambda}_A, \dot{\vec{r}}_c, \vec{r}_c, \bar{\lambda}_c, \bar{\gamma}$: state variables of the simulator control system (outputs of the integrators).

$\ddot{\vec{r}}_A, \dot{\bar{\lambda}}_A$: inputs to the simulator control system.

$\vec{r}_c , \bar{\lambda}_c$: outputs from the simulator control system.

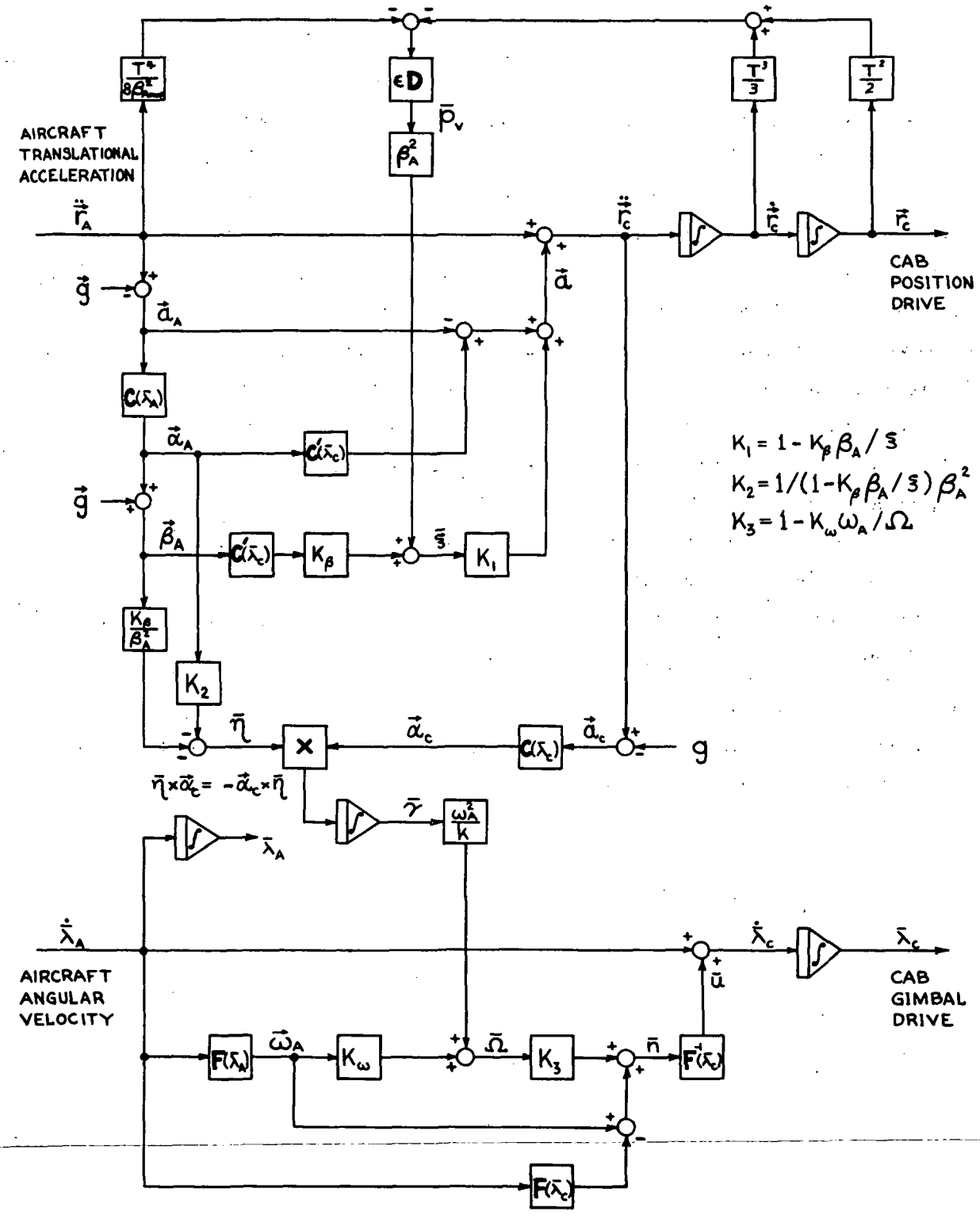

Figure 2-19

Block Diagram of the Simulator Control System

2.6.2 Analysis of the Linear Design Case

The general characteristics of the simulator control system shown in Figure 2-19 are of interest and would be valuable in selecting the optimum values of the parameters. Unfortunately, a detailed analytical analysis is very difficult to perform because of the nonlinear cross-coupling between the six degrees-of-freedom. Consequently, the selection of the parameters must be performed by computer simulation. However, for the special case of the quadratic performance index to be discussed below, it is possible analytically to gain some insight into the characteristics of the simulator control system.

If $K_\beta = K_\omega = 0$ in the performance index shown in (2.96) then the equations for the simulator control system given by (2.94), (2.95), (2.97) - (2.101) can be simplified. In this case it can be shown that the equations for computing $\vec{r}_c$ and $\bar{\lambda}_c$ from $\vec{r}_A$ and $\dot{\bar{\lambda}}_A$ are

$$\ddot{\vec{r}}_c + A_1\dot{\vec{r}}_c + A_2\vec{r}_c = (I - A_3)\ddot{\vec{r}}_A + [C'(\bar{\lambda}_c)C(\bar{\lambda}_A) - I]\vec{a}_A \qquad (2.102)$$

$$\dot{\bar{\lambda}}_c = F^{-1}(\bar{\lambda}_c)\left[F(\bar{\lambda}_A)\dot{\bar{\lambda}}_A - \frac{\omega_A^2}{k}\int_o^t \frac{\vec{\alpha}_c \times \vec{\alpha}_A}{\beta_A^2}\, d\tau\right] \qquad (2.103)$$

where matrix coefficients in the first equation describing the translational motion of the cab are given by

$$A_1 = \frac{1}{6}\epsilon T^3 \beta_A^2 D$$

$$A_2 = \frac{1}{4}\epsilon T^2 \beta_A^2 D$$

$$A_3 = \frac{1}{16}\epsilon T^4 \beta_A^2 D / \beta_{A\,max}^2$$

The second equation (2.103) for the angular motion of the cab can be rewritten as

$$\vec{\omega} = \vec{\omega}_c - \vec{\omega}_A = -\frac{\omega_A^2}{K}\int_0^t \frac{\vec{\alpha}_c \times \vec{\alpha}_A}{\beta_A^2}\, d\tau \qquad (2.104)$$

If $\epsilon = 0$ then $A_1 = A_2 = A_3 = 0$ and from (2.100) it can be shown that (2.102) reduces to $\vec{\alpha}_c \equiv \vec{\alpha}_A$ or $\vec{\alpha} \equiv 0$. Substituting $\vec{\alpha}_c \equiv \vec{\alpha}_A$ into (2.104) immediately gives that $\vec{\omega}_c \equiv \vec{\omega}_A$ or $\vec{\omega} \equiv 0$. In other words, if no penalty is imposed on the cab excursions then the simulator control system will cause the cab to move so that there is no error in the sensed motion. For $\epsilon > 0$ there will be errors in the sensed motion.

An examination of (2.102) shows that the translation motion of the cab is governed by a second order system with two forcing terms $\ddot{\vec{r}}_A$ and $\vec{a}_A = \ddot{\vec{r}}_A + g$. The second forcing term on the right hand side of (2.102) makes adjustments in the translational cab motion due to differences in the cab and aircraft attitudes. If $\bar{\lambda}_c = \bar{\lambda}_A$ then the second forcing term vanishes. The second forcing term occurs because the objective is to minimize the sensed errors rather than the actual motion errors.

Ignoring the second forcing term in (2.102), the computation of $\vec{r}_c$ from $\ddot{\vec{r}}_A$ is almost a second order linear system with constant coefficients; it would be a time-invariant, linear system except for the β_A^2 term in the matrix coefficients A_1, A_2, A_3. Assuming for the sake of argument that β_A is a constant, then the transfer function from $\vec{r}_A$ to $\vec{r}_c$ is a high pass filter. To illustrate, suppose the characteristic equation of the left hand side of (2.102) has real roots ω_1 and ω_2 then the Bode plot of the frequency response would appear as shown in Figure 2-20.

Figure 2-20

High Pass Filtering Characteristics of the Simulator Control System

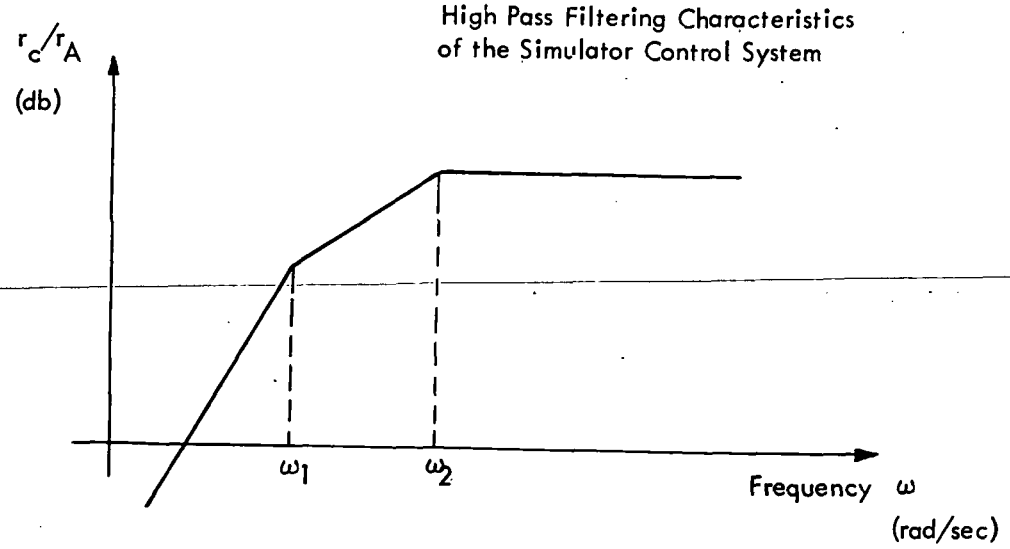

The high pass filtering characteristics that evolved from minimizing the performance index are intuitively reasonable since one of the common approaches is to attenuate the low frequency portion of the aircraft motion while passing the high frequencies. Another feature incorporated in the translational equation (2.102) is the presence of the scaling factor $(I-A_3)$ multiplying the aircraft acceleration. Equation (2.102) shows that the magnitude of the cab position will tend to vary linearly with difference between I and A_3. Thus, the adjustment of the constant parameter ϵ, T, D and $\beta^2_{A\,max}$, that affect the values of A_1, A_2 and A_3, in turn amounts to the trade-off between the high pass characteristics and the degree of scaling.

The rotational motion of cab governed by (2.103) or (2.104) encompasses the idea of residual tilt. An examination of (2.104) shows that as long as the sensed translational motion vectors for the cab and aircraft remain colinear (i.e., $\vec{\alpha}_c \times \vec{\alpha}_A = 0$) then the cab attitude identically follows the aircraft attitude. As the phase error between $\vec{\alpha}_c$ and $\vec{\alpha}_A$ deviates from zero, (2.104) induces an angular error in order to help reduce the error $\vec{\beta}$ and $\vec{\alpha}$ in the sensed translational motion. The trade off between angular and translational errors in the sensed motion is governed by the parameter k. As k increases, the level of angular error decreases according to (2.104).

2.6.3 Computer Simulation Program

In order to study the performance of the simulator control system design, a FORTRAN computer program was developed to simulate the complete six degree-of-freedom motion simulator. The simulated time histories shown in Section 3 were obtained by use of this program. The computations required to implement the simulator control system design shown in Figure 2-19 were performed in a subroutine entitled WASHFL.

The inputs to the WASHFL subroutine consists of the aircraft motion given by $\bar{\lambda}_A$, $\vec{\omega}_A$, and $\ddot{\vec{r}}_A$, the integration step size Δt, and an index variable governing the mode of operation. The outputs from WASHFL are the cab motion command signals given by $\vec{r}_c$ and $\bar{\lambda}_c$. The adjustable parameters in the performance index may be entered as input data to the program or stored internally in the subroutine in DATA statements. The latter storage option permits WASHFL to be used on the NASA AMES computer facility in order to generate the drive commands during an actual flight simulation.

A more detailed description of the WASHFL subroutine, including a program listing and description of all computer variables, is given in Appendix IV. Two other subroutines required by WASHFL to perform the numerical integration of the state variables are also given in Appendix IV.

3. PERFORMANCE SIMULATION

3.1 Description of the Reference Aircraft Motions

To have a realistic assessment of the performance of the washout circuit designed in the preceding sections it ultimately would be necessary to conduct a full-fledged pilot simulation using the simulation facilities at the Ames Research Center. As a preliminary step toward such a simulation, digital computer simulation studies were conducted to evaluate possible performance of the quasi-optimum washout circuit and to determine suitable ranges of the values for the adjustable parameters in the washout circuit.

The first phase of the computer simulation study was to generate examples of the aircraft motion that result in several distinctive "tasks", which the simulator cab attempts to duplicate, during typical operations of the motion simulator. The second phase, discussed in the next section, was to examine the cab motion resulting from the application of the washout circuit for the reference aircraft motion generated in the first phase.

The dynamics used to compute the reference aircraft motion are for a medium sized twin jet transport whose aerodynamic characteristics are summarized in Table 3.1.

To generate the reference aircraft motion, a general six degree-of-freedom aircraft motion simulation program (SIXDOF) was used. This program was developed at the Kearfott Research Center and has been used extensively for a variety of studies. The SIXDOF program incorporates an autopilot, also developed by the Kearfott Research Center as part of an automatic landing study. This autopilot was used to simulate the behavior of a human pilot. To use the SIXDOF program, a nominal trajectory for a given typical flight task is first defined in the manner required by the program. The autopilot then computes the aircraft control-surface deflections required to minimize the difference between the actual aircraft flight path and that of the defined nominal trajectory at each instant after the inception of simulation run. From the control-surface deflections, the reference aircraft motion is generated by the model of the aircraft dynamics.

The three flight tasks considered in this study are the following:

Task 1 Tracking Maneuver - This task was created for the purpose of simulating such flight operations as mid-air refueling, formation flying, etc. It is also a useful task for evaluation of quantitative pilot followup error. The reference trajectory of the aircraft and the time histories of 24 dynamic variables of the aircraft are shown in Fig. 3-1 for 30 seconds

of flight time. These variables are:

x, y, z = inertial x, y, z excursions

$\dot{x}, \dot{y}, \dot{z}$ = inertial x, y, z velocities

$\ddot{x}, \ddot{y}, \ddot{z}$ = inertial x, y, z accelerations

$\alpha_x, \alpha_y, \alpha_z$ = sensed x, y, z specific forces

ϕ, θ, ψ = Euler angles

$\dot{\phi}, \dot{\theta}, \dot{\psi}$ = Euler angle rates

p, q, r = angular rates

$\delta_e, \delta_a, \delta_r$ = elevator, aileron and rudder deflections

It is seen from these trajectories that the flight is quite hectic. This is intentional and designed to give the washout circuit a good workout.

Task 2 Approach Landing Maneuver - Aircraft landing operation is another typical example of simulator application. To generate a reference aircraft motion, it is assumed that during a landing approach, at about 50 seconds before touchdown, the pilot "suddenly" realizes that the aircraft is 200 ft (61 m) and to the right of a prespecified nominal landing trajectory and that, instead of aborting the landing as he would normally do under these circumstances, he tries to complete the landing. In view of the relatively large course error, just 50 seconds prior to touchdown, a rather severe maneuver is called for. The autopilot that simulates the pilot performance completes the desired landing successfully 55 seconds after the maneuver is initiated.

Figure 3-2 shows the resulting reference aircraft trajectory for those dynamic variables listed in the preceding section.

Task 3 Emergency Pull-up Maneuver - The last simulation mission selected was an emergency pull-up maneuver during a final landing approach. In this mission the aircraft was assumed to be initially flying the ILS beam. At an altitude of about 50 ft (15.2m) above the runway the pilot decided to abort the landing and excuted the pull-up maneuver, in which the aircraft pitched up sharply while simultaneously turning away to the right side of the runway.

A particular feature of this flight operation is the large yaw and pitch angles it induces, and, as a consequence, the large deviation in forward (x) acceleration. Figure 3-3 shows the resulting trajectories.

TABLE 3.1

CHARACTERISTICS OF SIMULATED AIRCRAFT

(a) Physical Properties

$\bar{c}$	11.08 ft (3.377 m)	I_x	125000.slug · ft^2 (169477. kg·m^2)
b	71.2 ft (21.70 m)	I_y	120312.slug · ft^2 (163121. kg·m^2)
s	690. ft (210. m)	I_z	234375.slug · ft^2 (317770. kg·m^2)
m	777.5 slug (11347. kg)	I_{xz}	8125.slug · ft^2 (11016. kg·m^2)
v	236.4 ft/sec (72.05 m/sec)	Pilot's Seat	30 ft (9.14 m) ahead of vehicle CG

(b) Stability Derivatives

C_{D_o}	.098	$C_{\ell_r}\ (\alpha = 0)$	.2
C_{D_α}	.377	$\partial C_{\ell_r}/\partial\alpha$	.76
$\partial C_D/\partial\alpha_\alpha$	1.82	$C_{n_p}\ (\alpha = 0)$	-.025
$C_{\ell_\beta}\ (\alpha = 0)$	-.1722	$\partial C_{n_p}/\partial\alpha$	-.93
$\partial C_{\ell_\beta}/\partial\alpha$	-.506	$C_{L_o}\ (\alpha = 0)$	.375
C_{ℓ_p}	-.22	C_{L_α}	5.35
$C_{\ell_{\delta_a}}$	-.1722	$C_{L_{\delta_e}}$	.302
$C_{\ell_{\delta_r}}$	.021	C_{m_q}	-12.3
C_{m_α}	-1.022	$C_{m_{\dot{\alpha}}}$	-4.01
$C_{m_{\delta_e}}$	-.923	C_{n_β}	.1
$C_{n_{\delta_r}}$	-.1	C_{n_r}	-.32
C_{Y_β}	-.8		

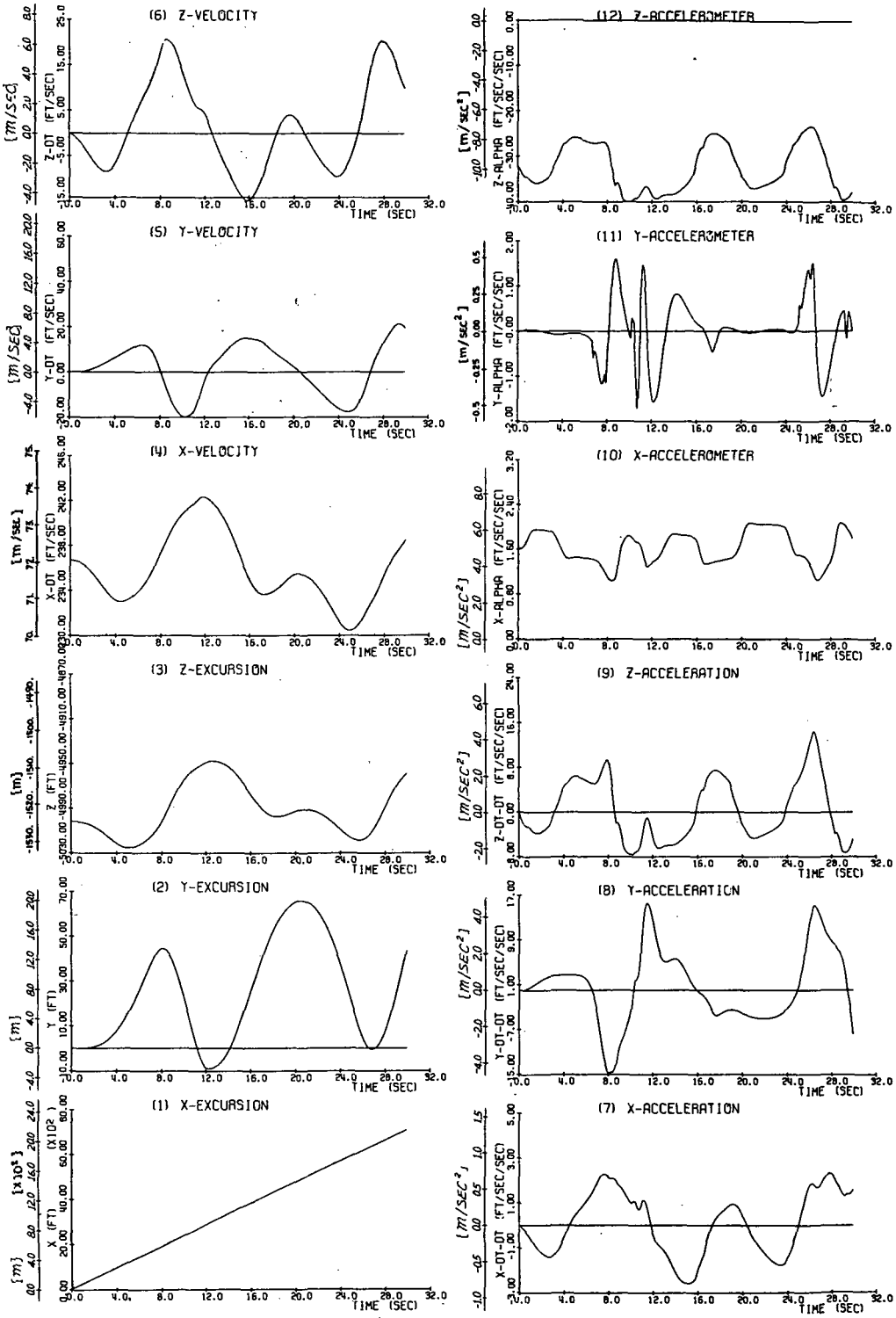

Figure 3-1

Reference Aircraft Trajectory - Tracking Maneuver

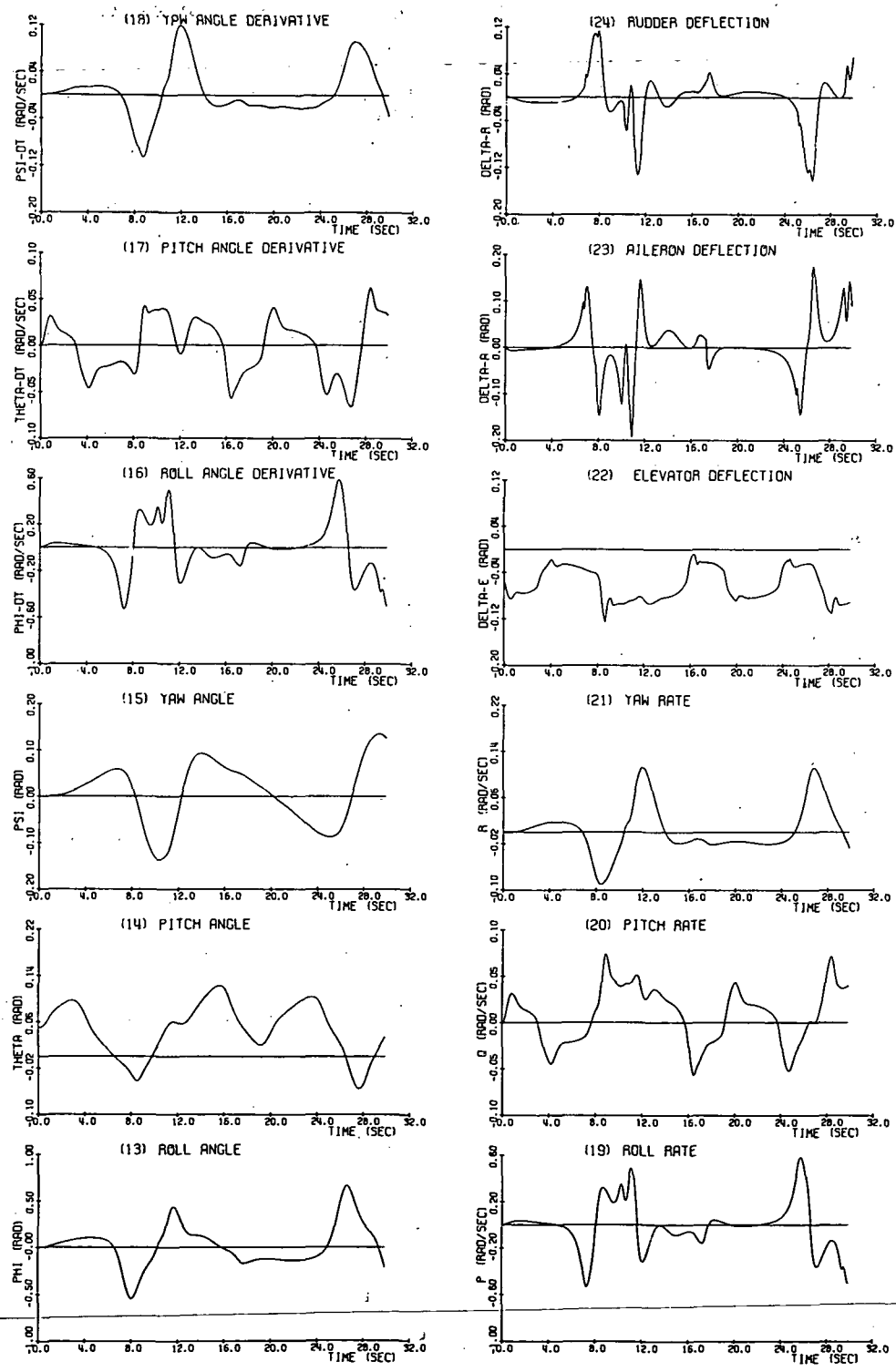

Figure 3-1

(Continued)

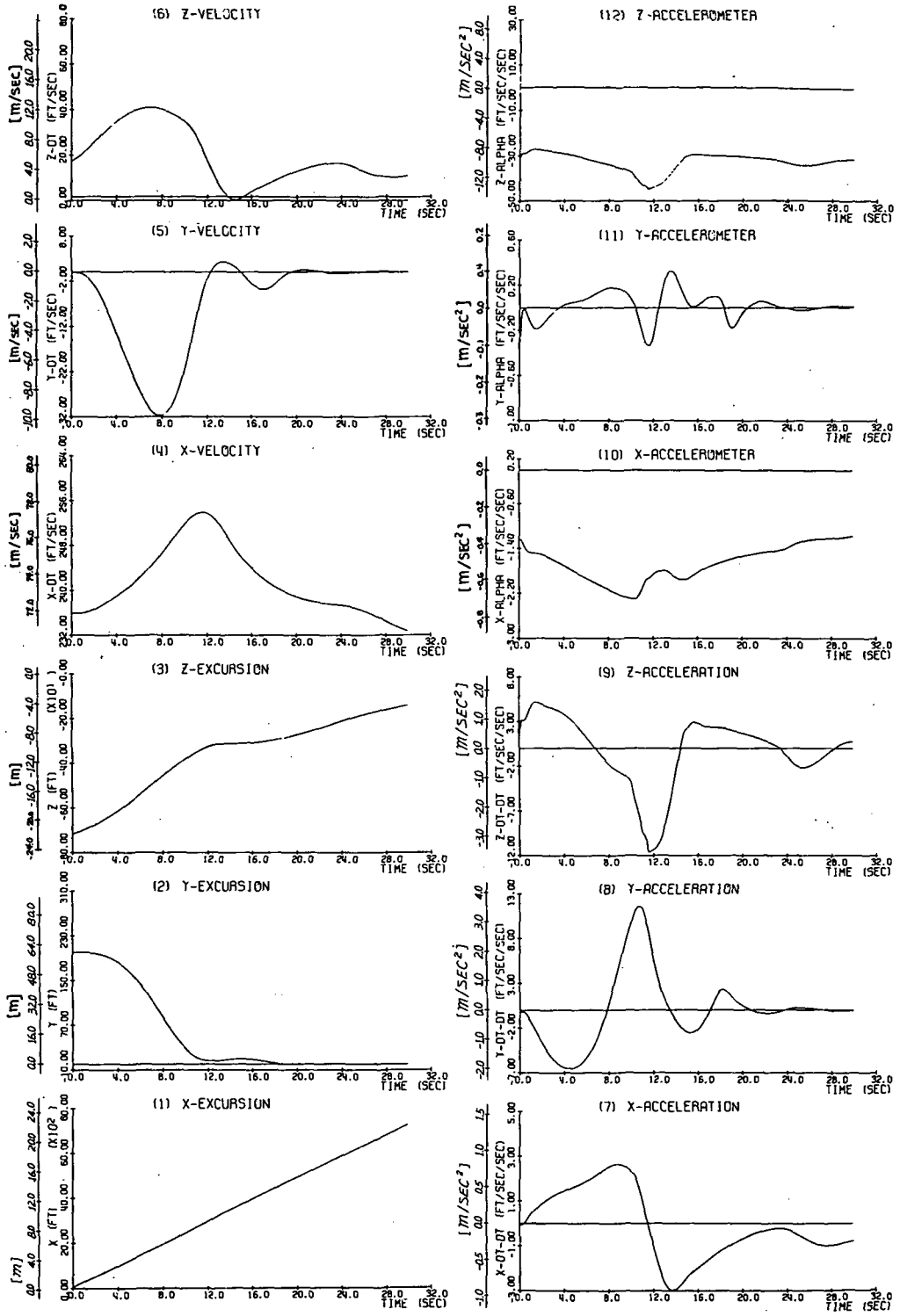

Figure 3-2

Reference Aircraft Trajectory - Approach Landing Maneuver

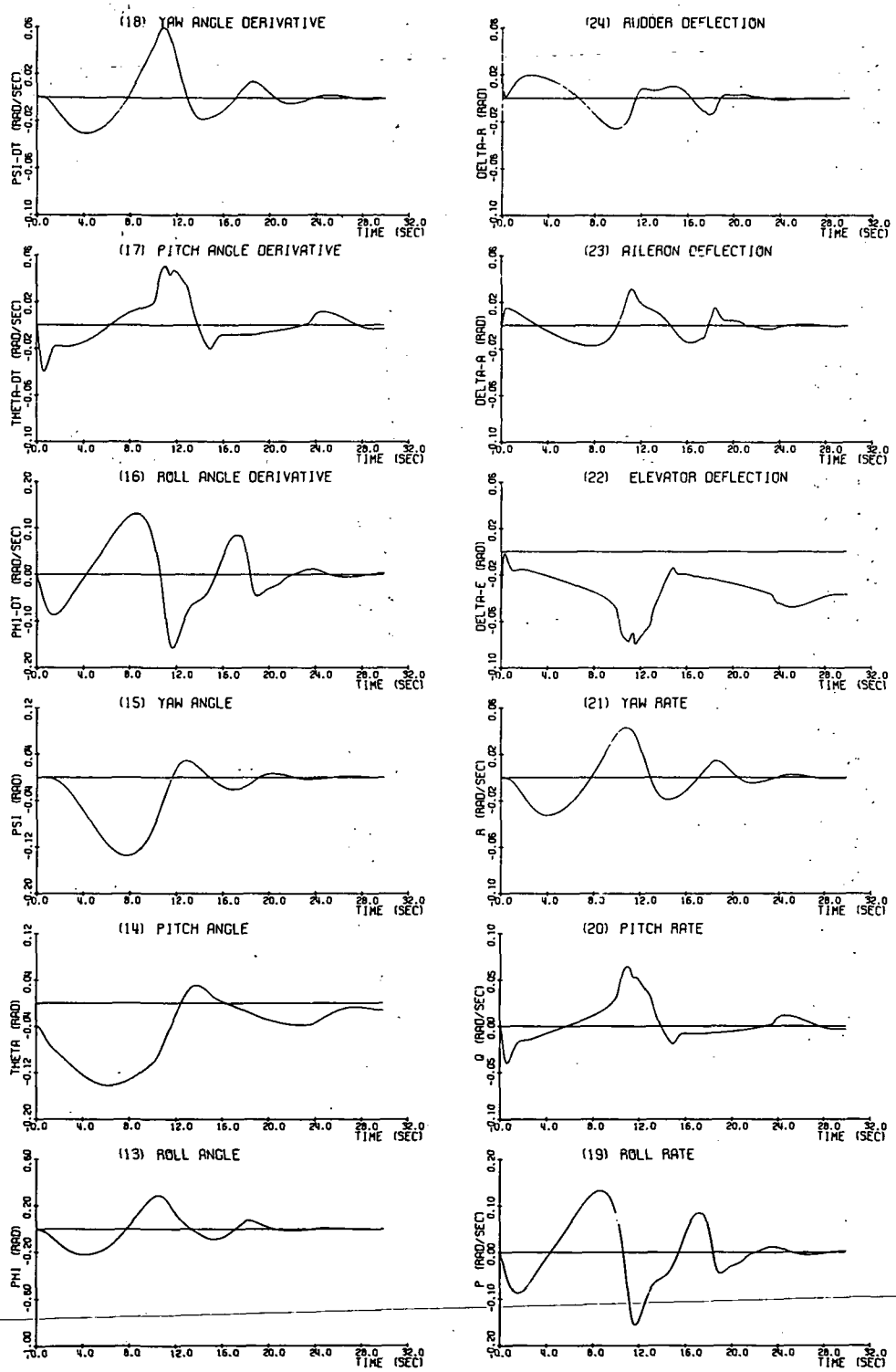

Figure 3-2

(Continued)

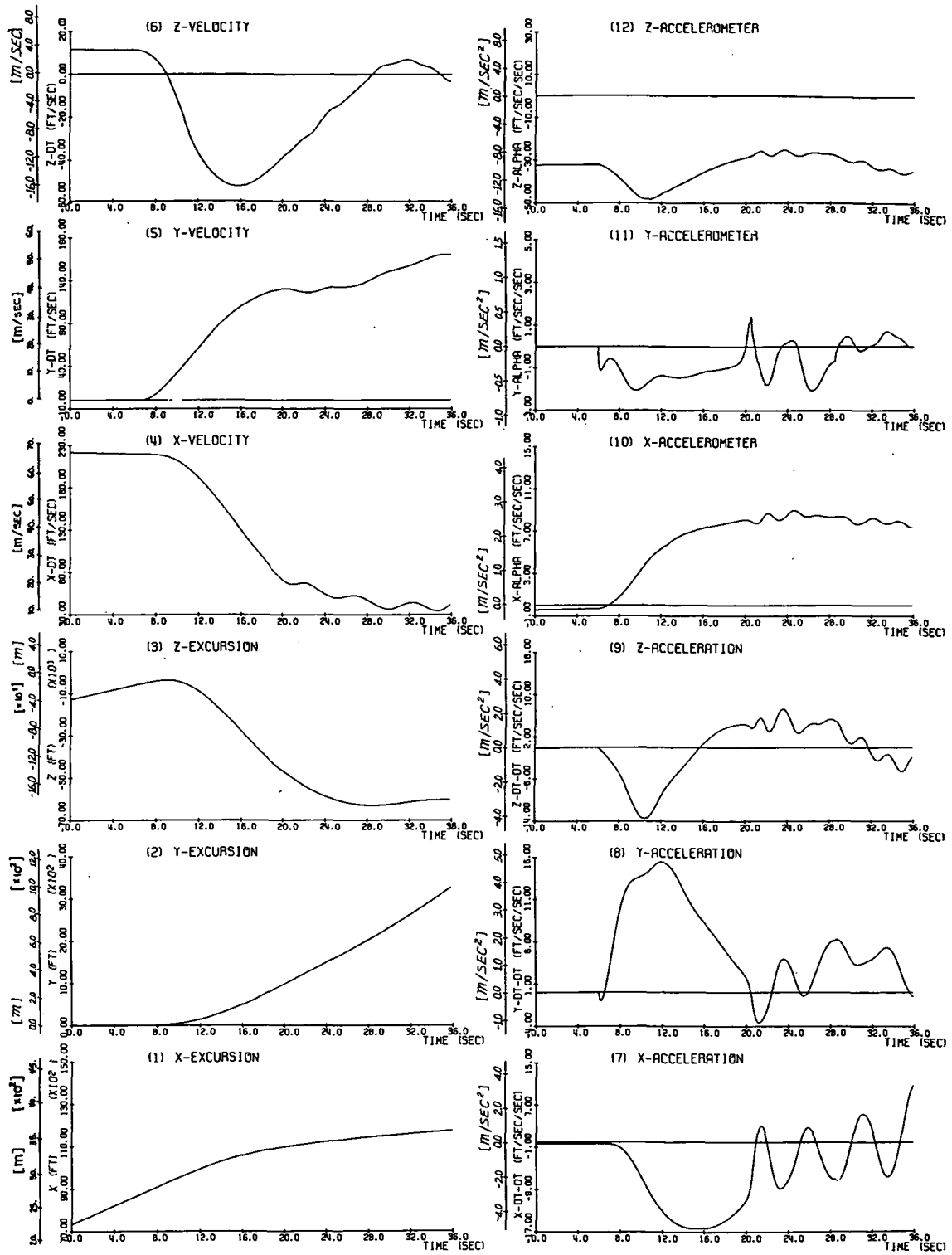

Figure 3-3

Reference Aircraft Trajectory - Emergency Pull-up Maneuver

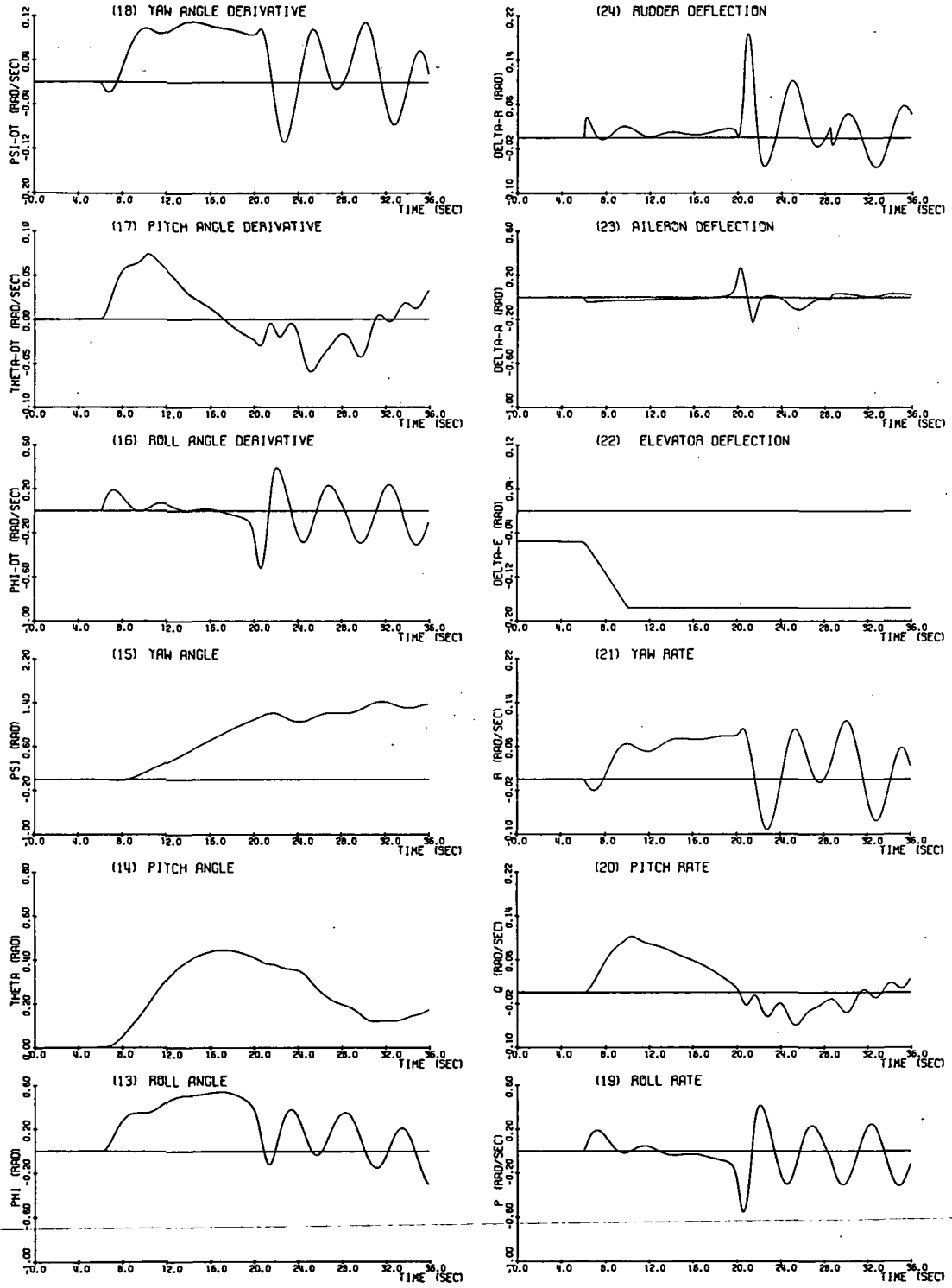

Figure 3-3
(Continued)

3.2 Simulated Time Histories of Cab Motion

The washout control law as summarized in (2.97) - (2.101) contains nine adjustable parameters, namely:

ϵ - adjust the amount of linear translational magnitude washout

k - adjust the amount of linear angular magnitude washout

K_β - adjust the amount of nonlinear translational phase washout

K_ω - adjust the amount of nonlinear angular phase washout

T - adjust the "filtering" characteristics between high-cut-off-and-low-scaling and low-cut-off-and-high-scaling

d_x, d_y, d_z - adjust the weighting of ϵ in x, y, z directions

$\beta^2_{A\ max}$ - limits the maximum scaling

The task of choosing a suitable combination of these parameters is highly complicated in view of the multidimensional performance requirements and the interrelationship between these parameters and performance. For the purpose of facilitating a systematic determination of the performance and the adjustable parameters, the following sequence of cases were considered during the course of simulation study,

Case 1 Linear translational washout only ($K_\beta = K_\omega = 0,\ k \to \infty$)

Case 2 Linear translational and angular washout ($K_\beta = K_\omega = 0$)

Case 3 Nonlinear translational and linear angular washout ($K_\omega = 0$)

Case 4 Nonlinear translational and angular washout

It should be noted that these cases were studied in consecutive order and a parameter which was found suitable for a previous case was not altered for the following case unless it was necessary to maintain the cab excursions to stay within confinement. In other words, the simulation is not exhaustive for every case due to limitation in available computer time. It is conceivable that better results than those shown in this section may be achieved by a more exhaustive simulation.

Of the three tasks considered, the tracking and landing maneuvers received a fairly thorough investigation but only Case 1 and Case 2 were considered for the emergency pull-up

maneuver. Typical time histories of the cab motion and that of corresponding aircraft motion for these tasks and cases are shown in the following pages and their corresponding values of the parameters and figure numbers are tabulated in Tables 3.2-3.4.

In the Figures 3-4-3-29, the cab motion is represented by solid lines and the corresponding aircraft motion, by solid lines with circles. The dynamic quantities shown in these figures are

x, y, z = inertial x, y, z excursions

$\beta_x, \beta_y, \beta_z$ = "unbiased" x, y, z sensed specific forces

φ, θ, ψ = gimbal angles

p, q, r = angular rates

The cab excursions shown in these figures are all confined to within ± 10.0 ft. (3.05 m) and aircraft excursions, which are in the order of 1000 ft (300 m), were purposely "trimmed" down from the actual values shown in Figs. 3-1-3-3 in order to permit plotting both cab and aircraft excursions by the same scale. Let $x_{fig}, y_{fig}, z_{fig}$ be the aircraft excursions shown in Fig. 3-4-3-29 and $x_{act}, y_{act}, z_{act}$ be the actual aircraft excursions as shown in Fig. 3-1-3-3, then for

Tracking task:

$$x_{act} = x_{fig} + 30.0 + 236.7t \text{ (ft)} \quad [x_{fig} + 9.14 + 72.15t \text{ (m)}]$$

$$y_{act} = y_{fig}$$

$$z_{act} = z_{fig} - 5001.5 \text{ (ft)} \quad [z_{fig} - 1524.5 \text{ (m)}]$$

Landing task:

$$x_{act} = x_{fig} + 30.0 + 243.0t \text{ (ft)} \quad [x_{fig} + 9.14 + 74.0t \text{ (m)}]$$

$$y_{act} = y_{fig} + 200.0 \text{ (ft)} \quad [y_{fig} + 61.96 \text{ (m)}]$$

$$z_{act} = z_{fig} - 718.8 \text{ (ft)} \quad [z_{fig} - 219.1 \text{ (m)}]$$

Pull-up task:

$$x_{act} = x_{fig} + 7320.5 + 120.0t \text{ (ft)} \quad [x_{fig} + 2231.3 + 36.58t \text{ (m)}]$$

$$y_{act} = y_{fig} + 90.0t \text{ (ft)} \quad [y_{fig} + 27.43 \text{ (m)}]$$

$$z_{act} = z_{fig} - 127.2 - 13.5t \text{ (ft)} \quad [z_{fig} - 38.77 - 4.11t \text{ (m)}]$$

Case No.	T	ϵ	K	K_β	K_ω	$\beta^2_{A\,max}$	d_x	d_y	d_z	Fig. No.
1	500.0	0.000000074	10000000.0	0	0	350.0	10.0	10.0	10.0	3.4
1	40.0	0.00027	10000000.0	↑	↑	↑	↑	↑	↑	3.5
1	2.0	2.3	10000000.0							3.6
2	500.0	0.000000076	90.0							3.7
2	40.0	0.00027	60.0	↓						3.8
2	2.0	1.8	40.0	0						3.9
3	500.0	0.00000035	150.0	1.0						3.10
3	40.0	0.001	90.0	1.0	↓					3.11
3	2.0	3.5	40.0	1.0	0					3.12
4	500.0	0.00000035	150.0	1.0	10.0					3.13
4	40.0	0.001	90.0	1.0	10.0	↓	↓	↓	↓	3.14
4	2.0	3.5	40.0	1.0	10.0	350.0	10.0	10.0	10.0	3.15

Table 3.2

Values of Adjustable Parameters for the Tracking Task

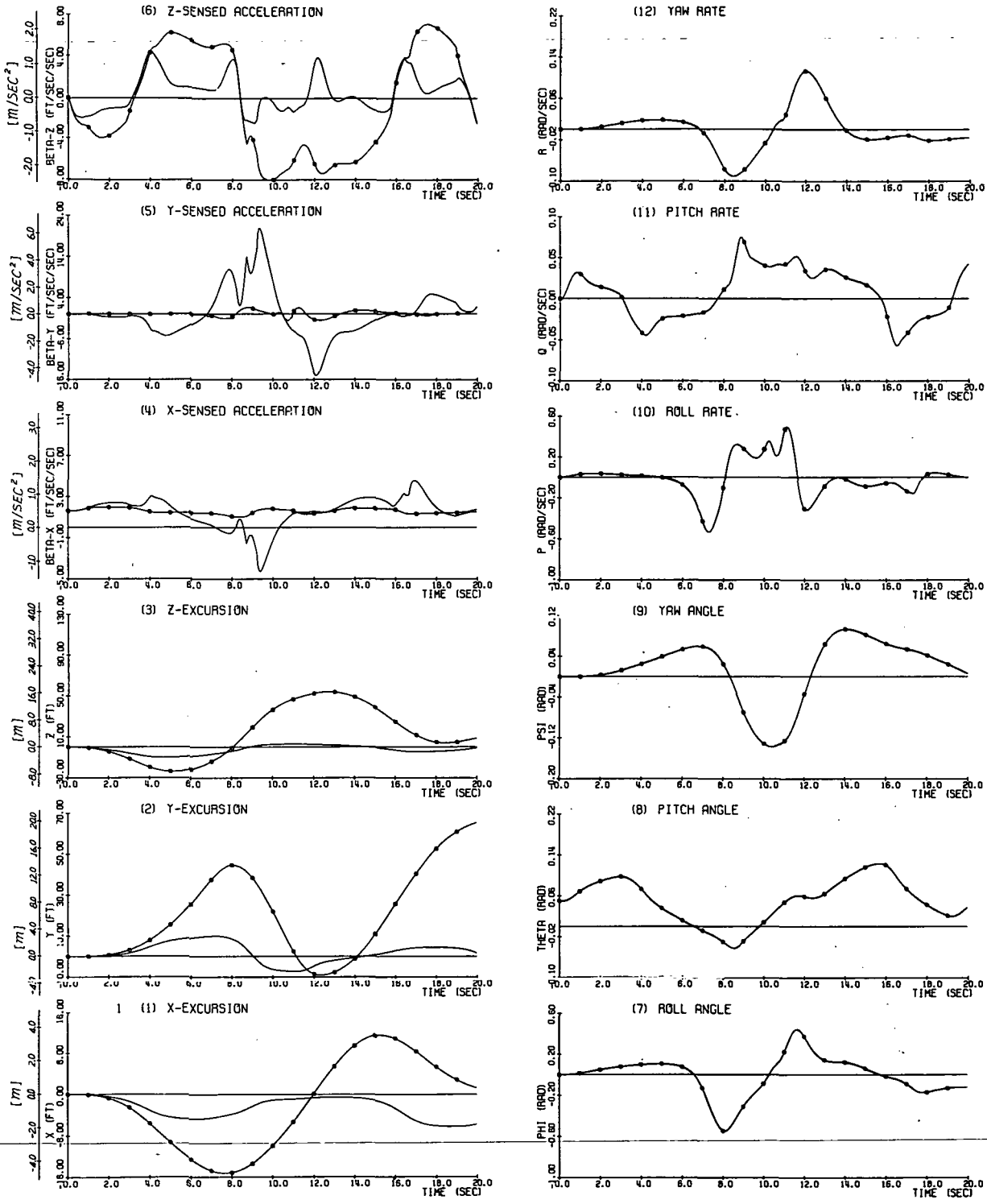

Figure 3-4

Relative Motions of the Aircraft and the Cab - Tracking Maneuver - Case 1 (linear translational washout only). - T = 500.0

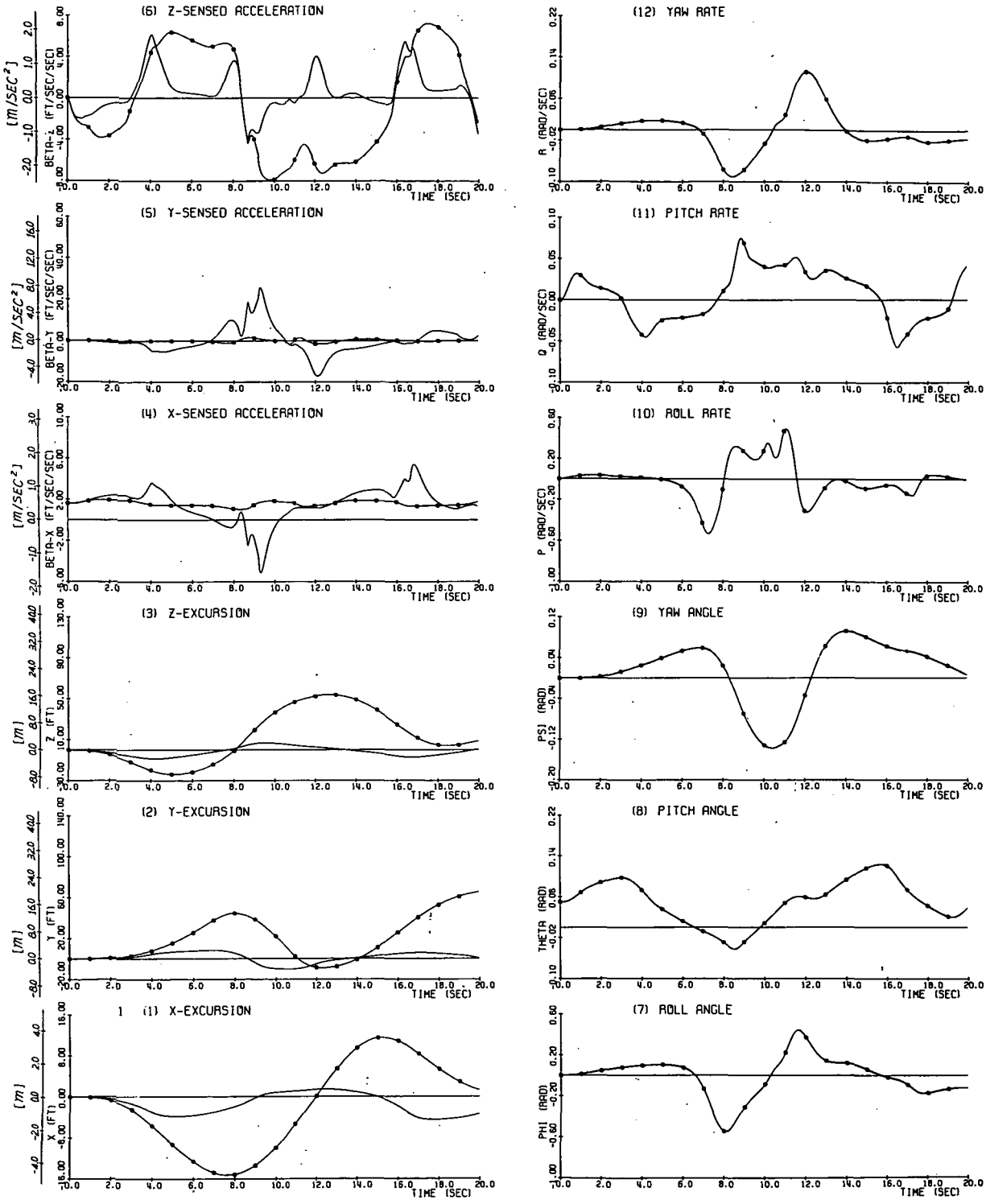

Figure 3-5

Relative Motions of the Aircraft and the Cab - Tracking Maneuver - Case 1 (linear translational washout only). - T = 40.0

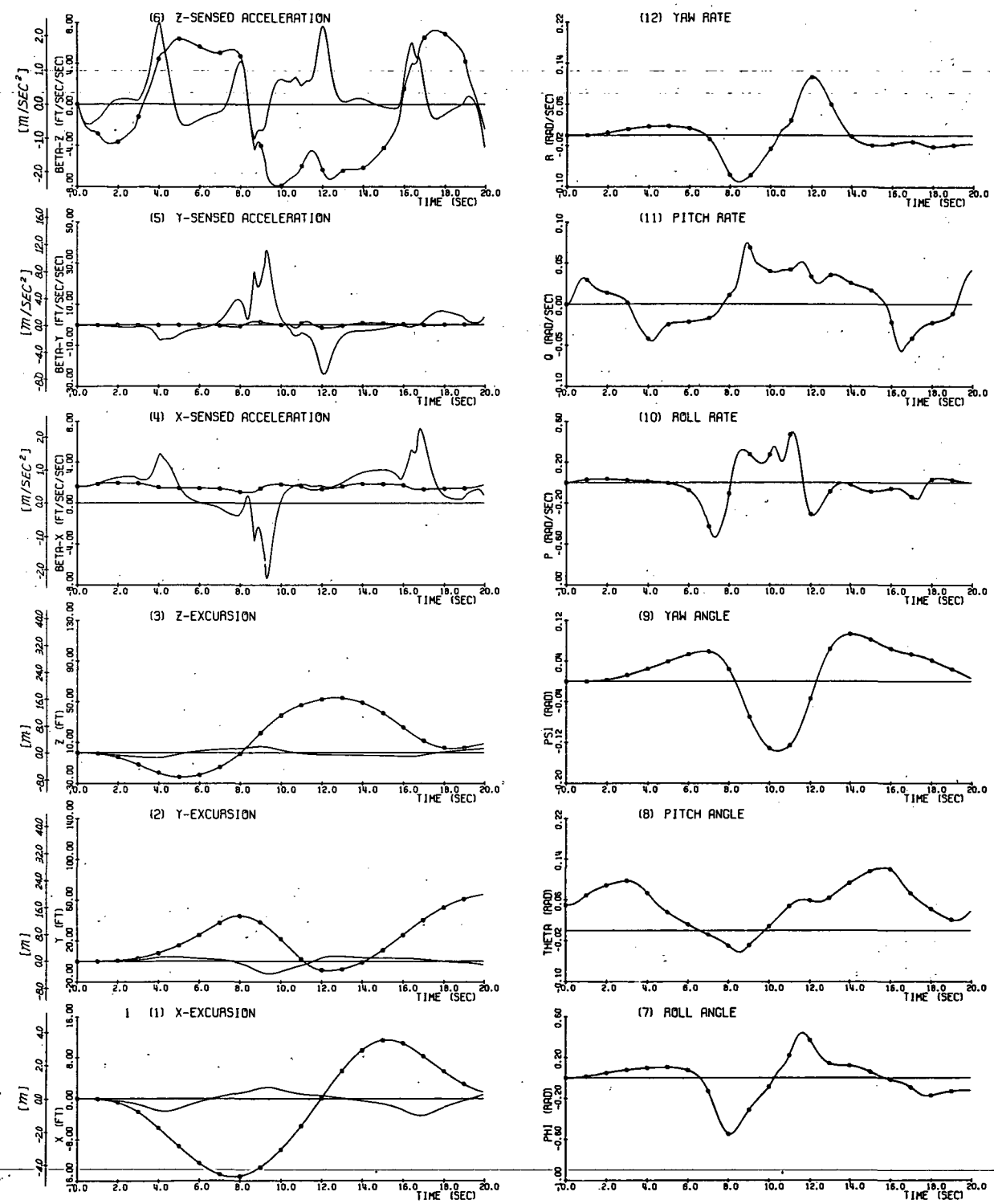

Figure 3-6

Relative Motions of the Aircraft and the Cab - Tracking Maneuver - Case 1 (linear translational washout only). - T = 2.0

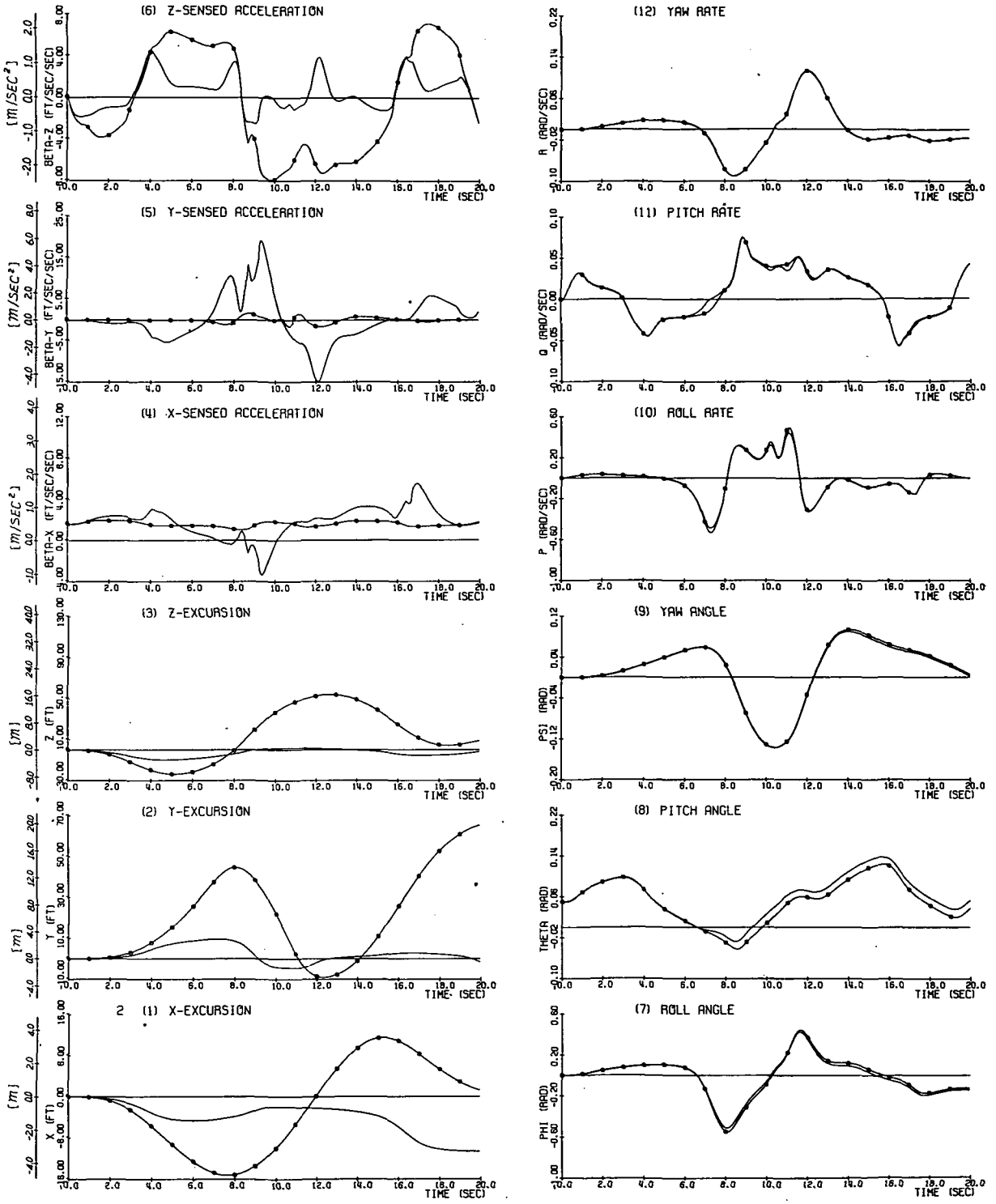

Figure 3-7

Relative Motions of the Aircraft and the Cab - Tracking Maneuver - Case 2 (linear translational and angular washout). - T = 500.0

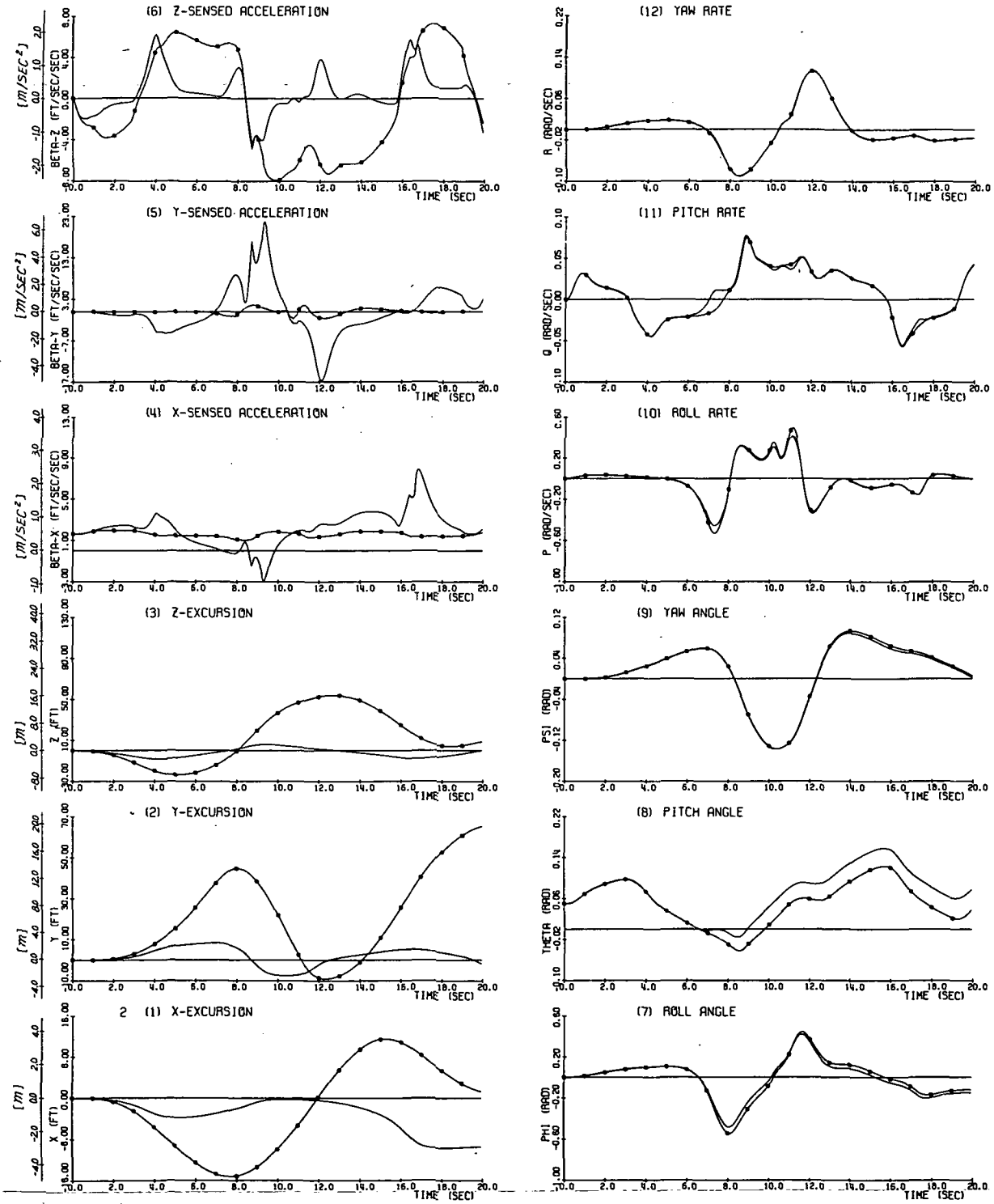

Figure 3-8

Relative Motions of the Aircraft and the Cab - Tracking Maneuver - Case 2 (linear translational and angular washout). - T = 40.0

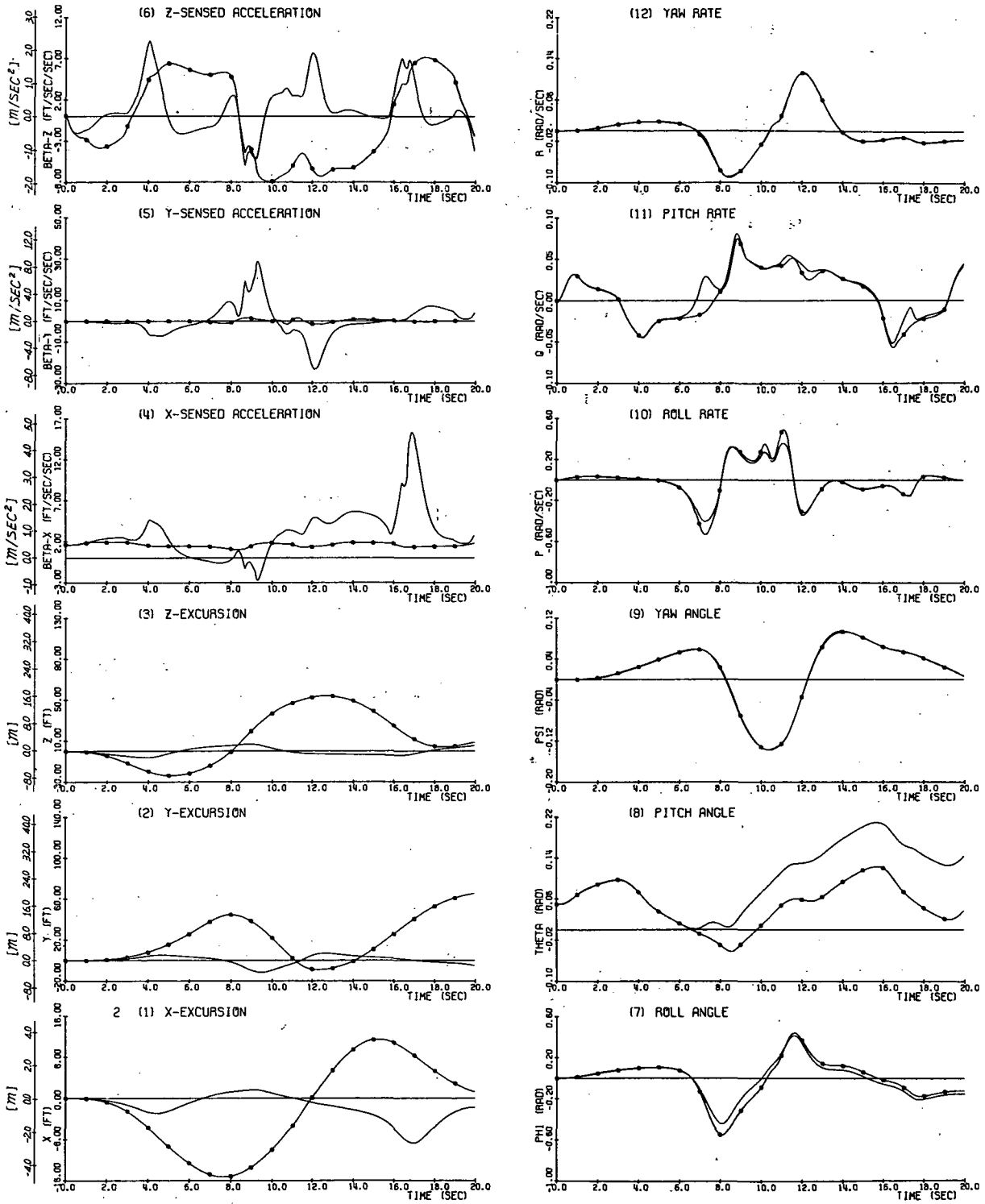

Figure 3-9

Relative Motions of the Aircraft and the Cab - Tracking Maneuver - Case 2 (linear translational and angular washout). - T = 2.0

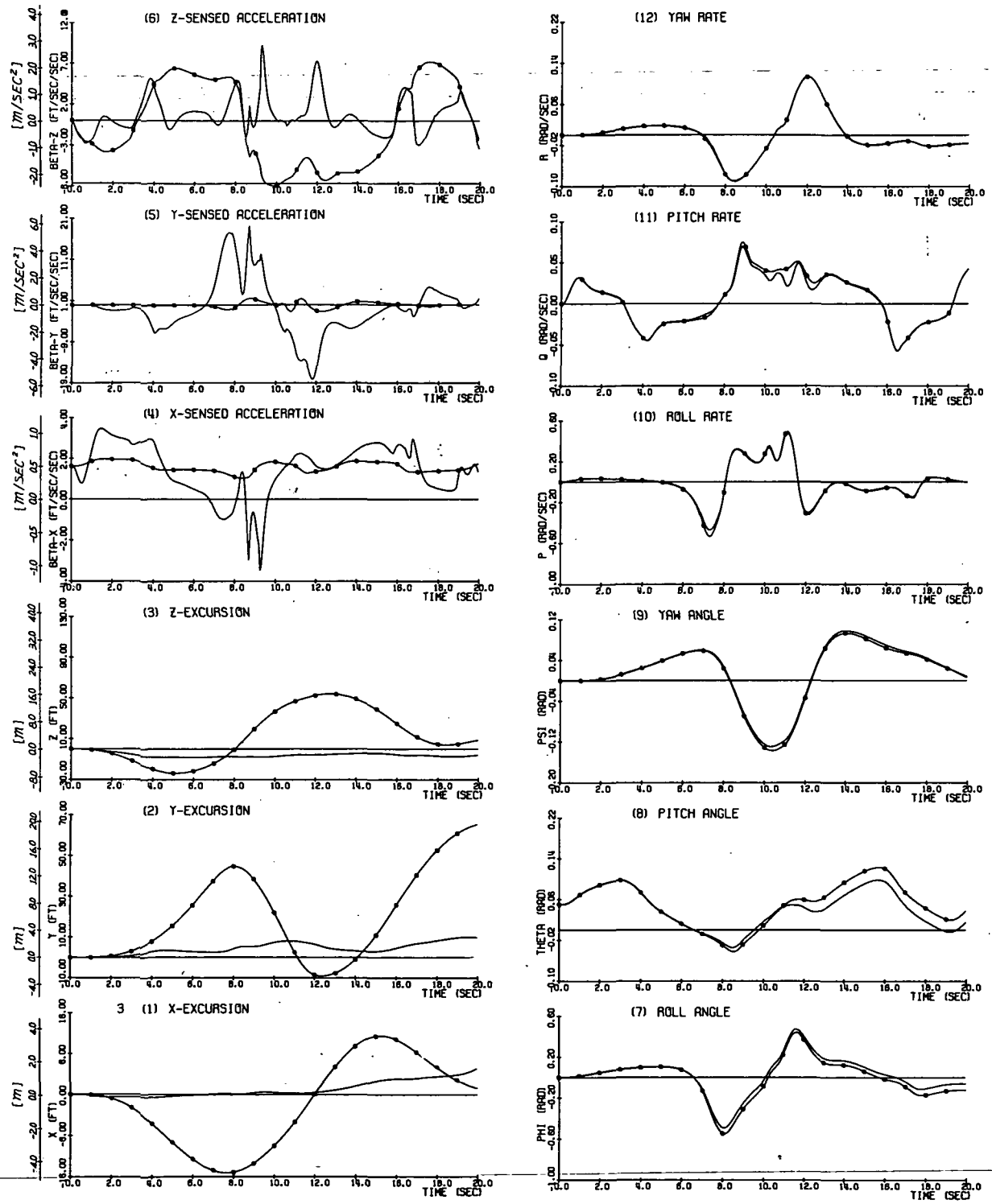

Figure 3-10

Relative Motions of the Aircraft and the Cab - Tracking Maneuver - Case 3 (nonlinear translational and linear angular washout). - T = 500.0

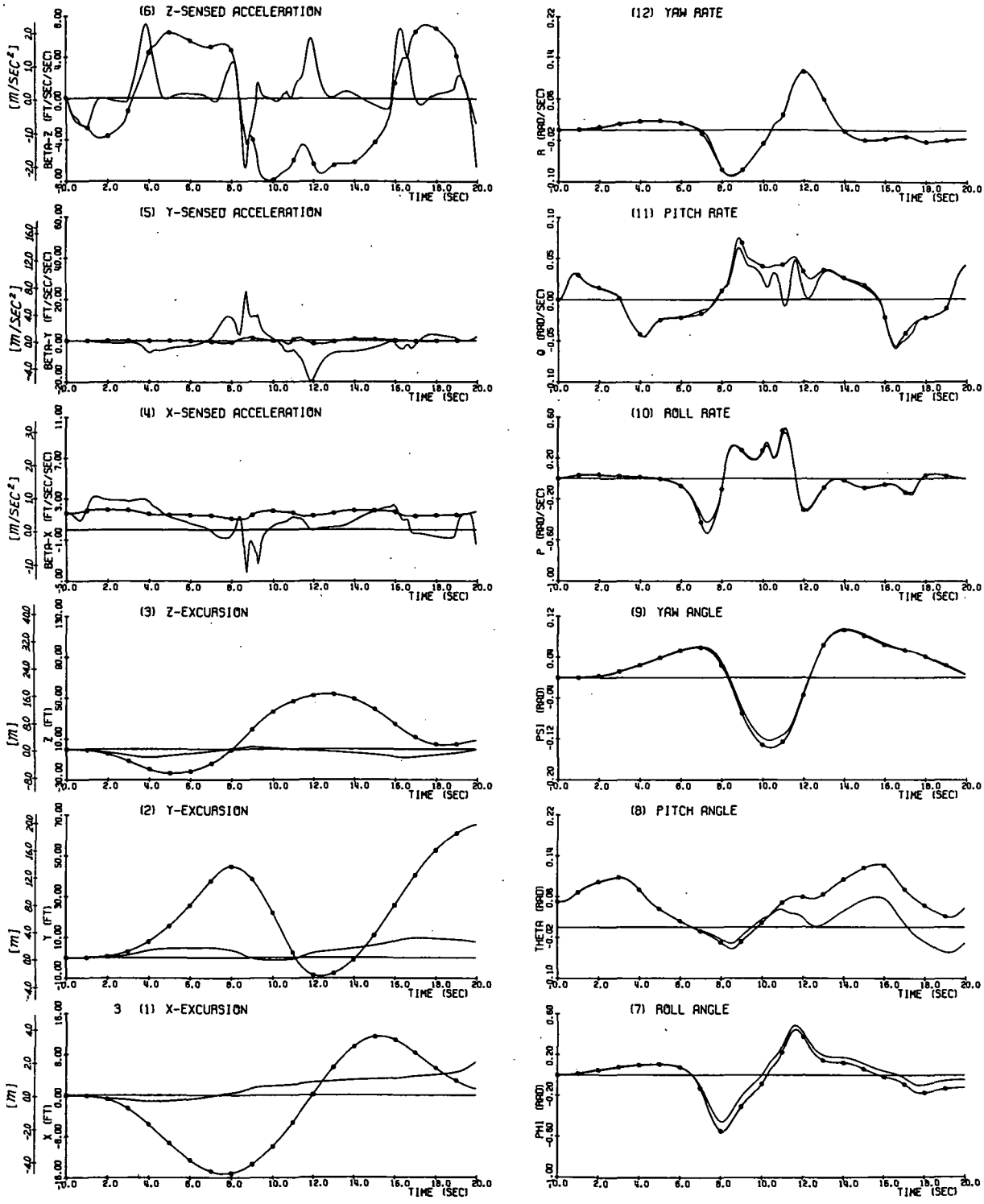

Figure 3-11

Relative Motions of the Aircraft and the Cab - Tracking Maneuver - Case 3 (nonlinear translational and linear angular washout). - T = 40.0

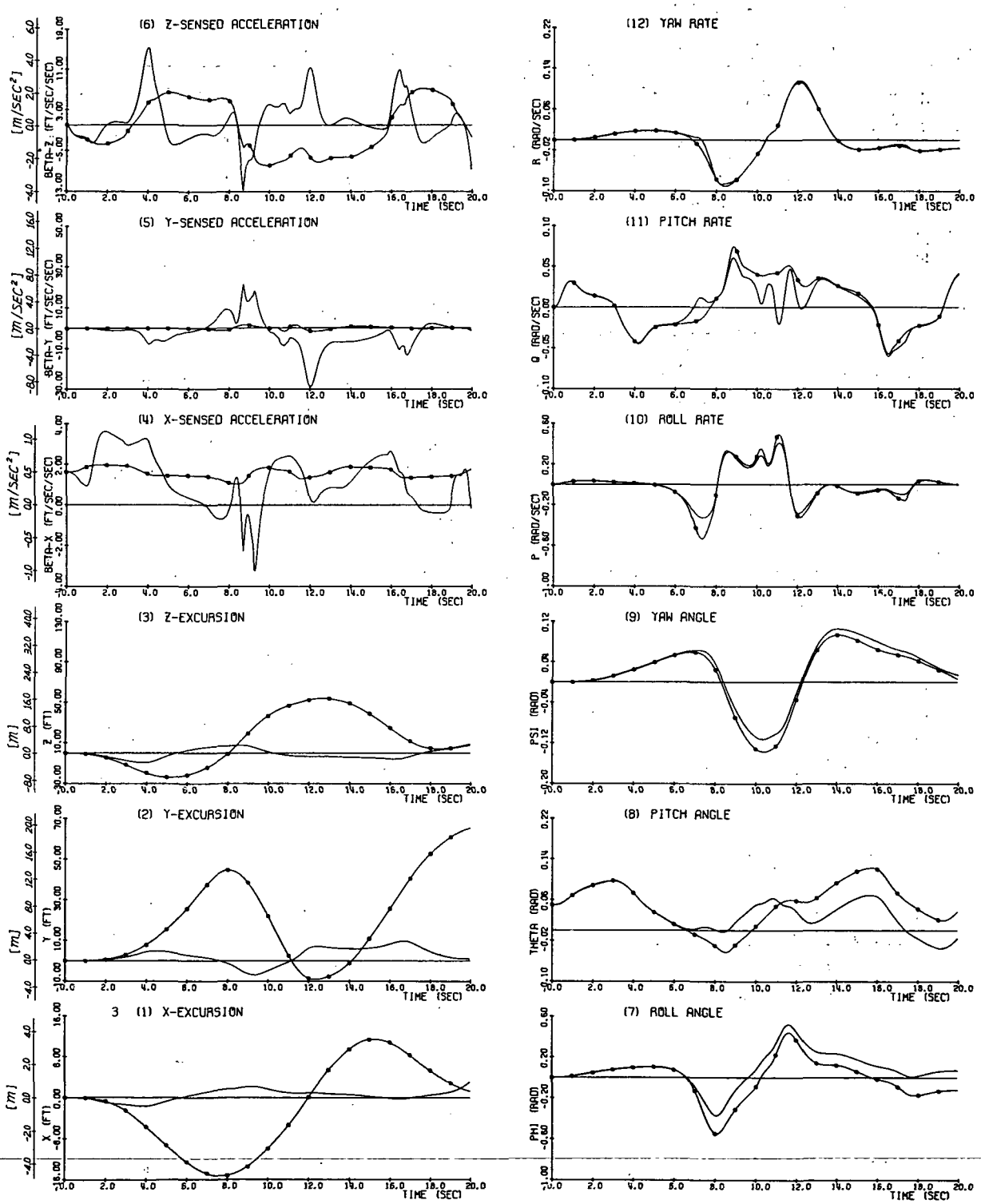

Figure 3-12

Relative Motions of the Aircraft and the Cab - Tracking Maneuver - Case 3 (nonlinear translational and linear angular washout). - T = 2.0

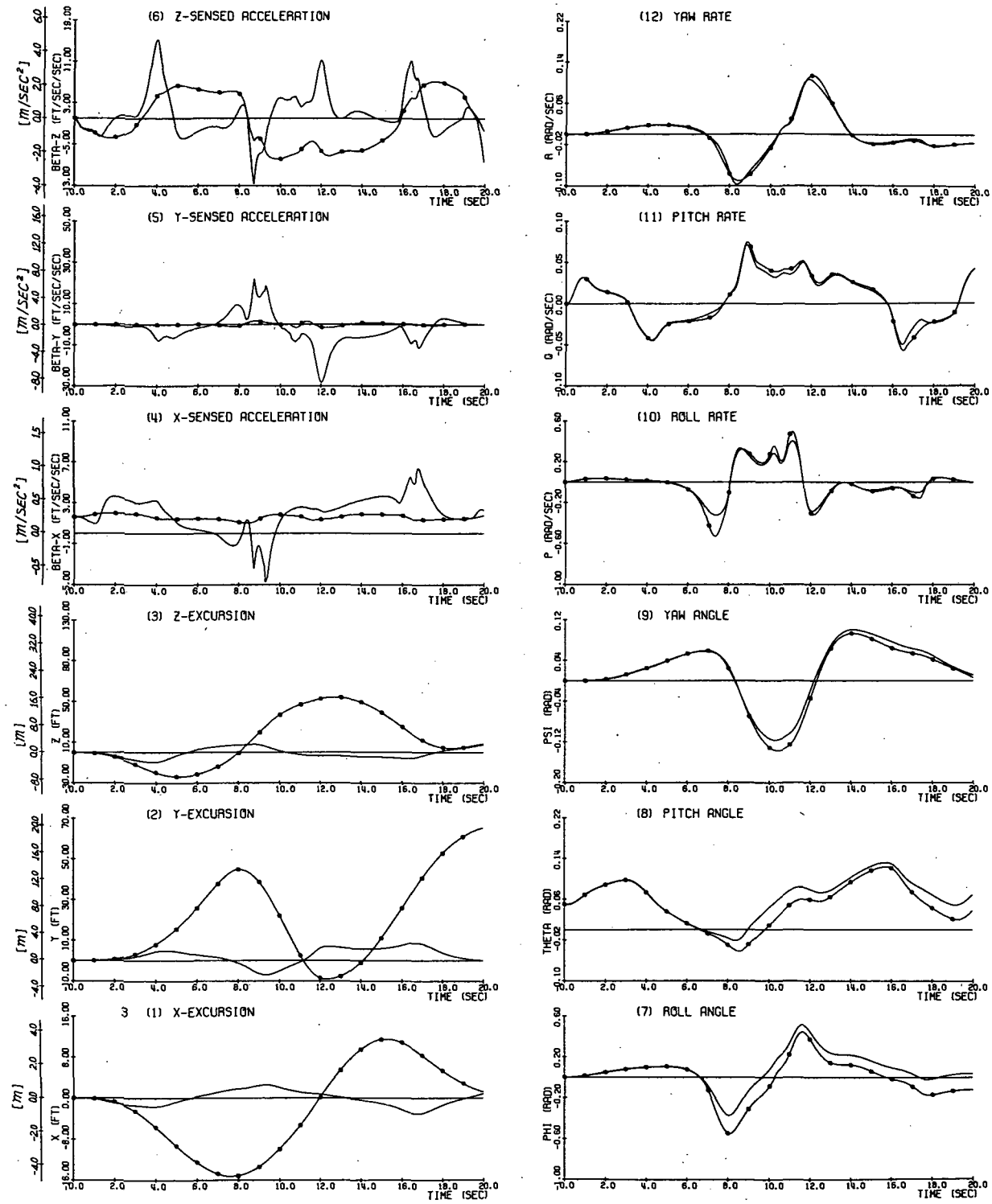

Figure 3-13

Relative Motions of the Aircraft and the Cab - Tracking Maneuver - Case 4 (nonlinear translational and angular washout). T = 500.0

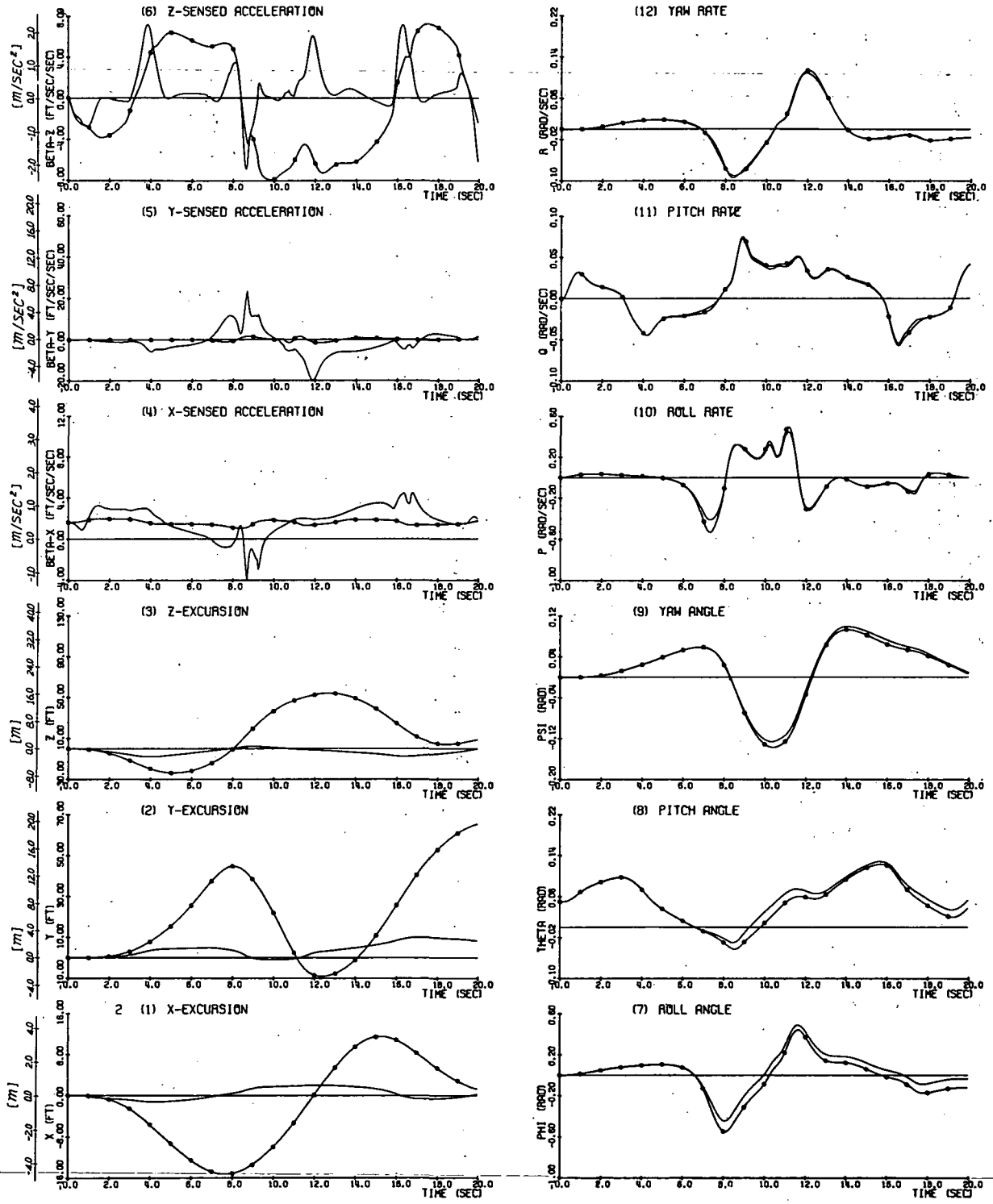

Figure 3-14

Relative Motions of the Aircraft and the Cab - Tracking Maneuver - Case 4 (nonlinear translational and angular washout). T = 40.0

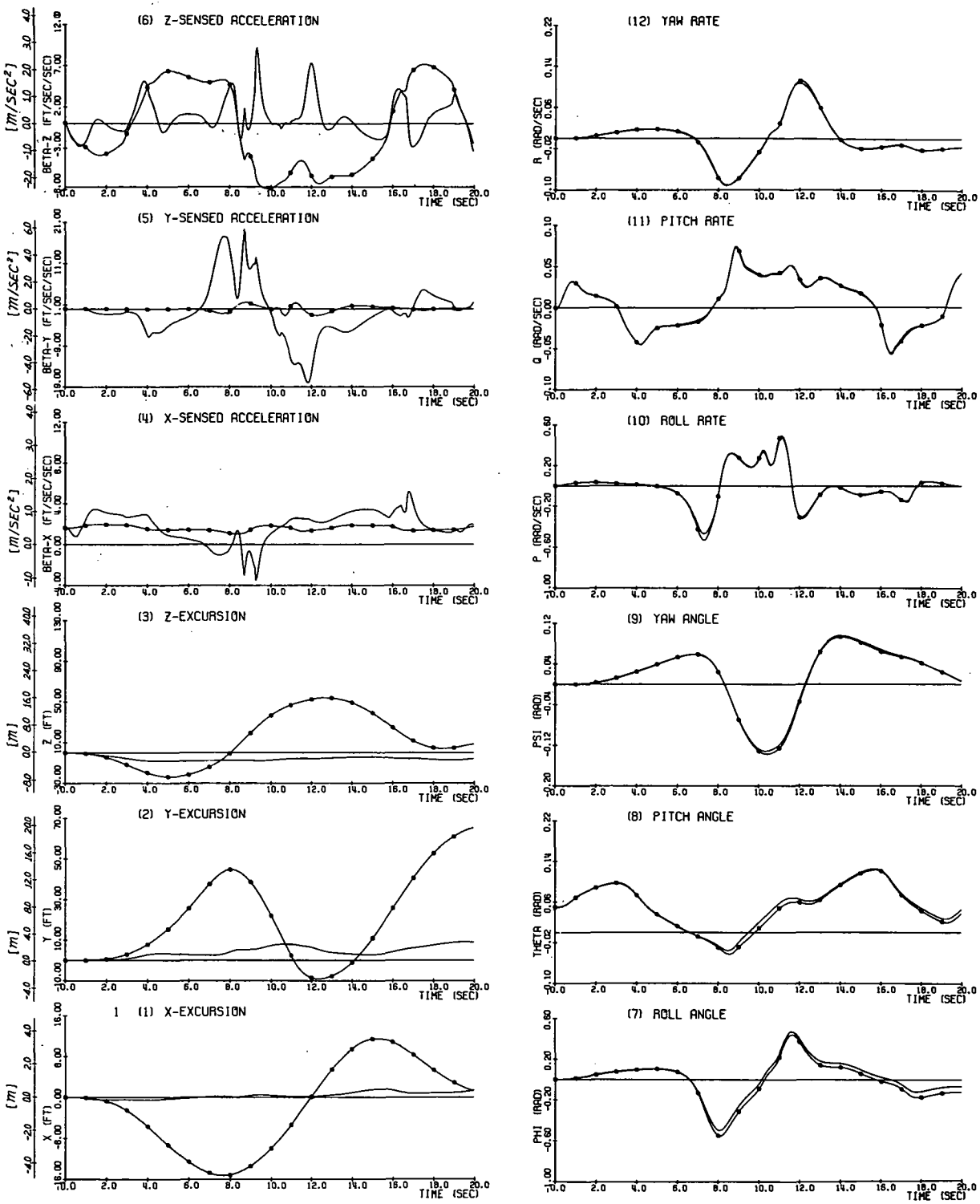

Figure 3-15

Relative Motions of the Aircraft and the Cab - Tracking Maneuver - Case 4 (nonlinear translational and angular washout). T = 2.0

Case No	T	ϵ	K	K_β	K_ω	$\beta^2_{A\,max}$	d_x	d_y	d_z	Fig. No.
1	30.0	0.004	100000000.0	0	0	350.0	15.0	10.0	15.0	3.16
1	10.0	0.085	100000000.0	↑	↑	↑	↑	↑	↑	3.17
1	2.0	5.2	100000000.0	↑	↑	↑	↑	↑	↑	3.18
2	30.0	0.004	140.0	↓	↑	↑	↑	↑	↑	3.19
2	10.0	0.085	130.0	↓	↑	↑	↑	↑	↑	3.20
2	2.0	5.2	120.0	0	↑	↑	↑	↑	↑	3.21
3	30.0	0.009	140.0	1.0	↑	↑	↑	↑	↑	3.22
3	10.0	0.18	130.0	1.0	↑	↑	↑	↑	↑	3.23
3	2.0	11.0	120.0	1.0	0	↑	↑	↑	↑	3.24
4	30.0	0.009	140.0	1.0	10.0	↓	↓	↓	↓	3.25
4	10.0	0.18	130.0	1.0	10.0	↓	↓	↓	↓	3.26
4	2.0	11.0	120.0	1.0	10.0	350.0	15.0	10.0	15.0	3.27

Table 3.3

Values of Adjustable Parameters for the Landing Task

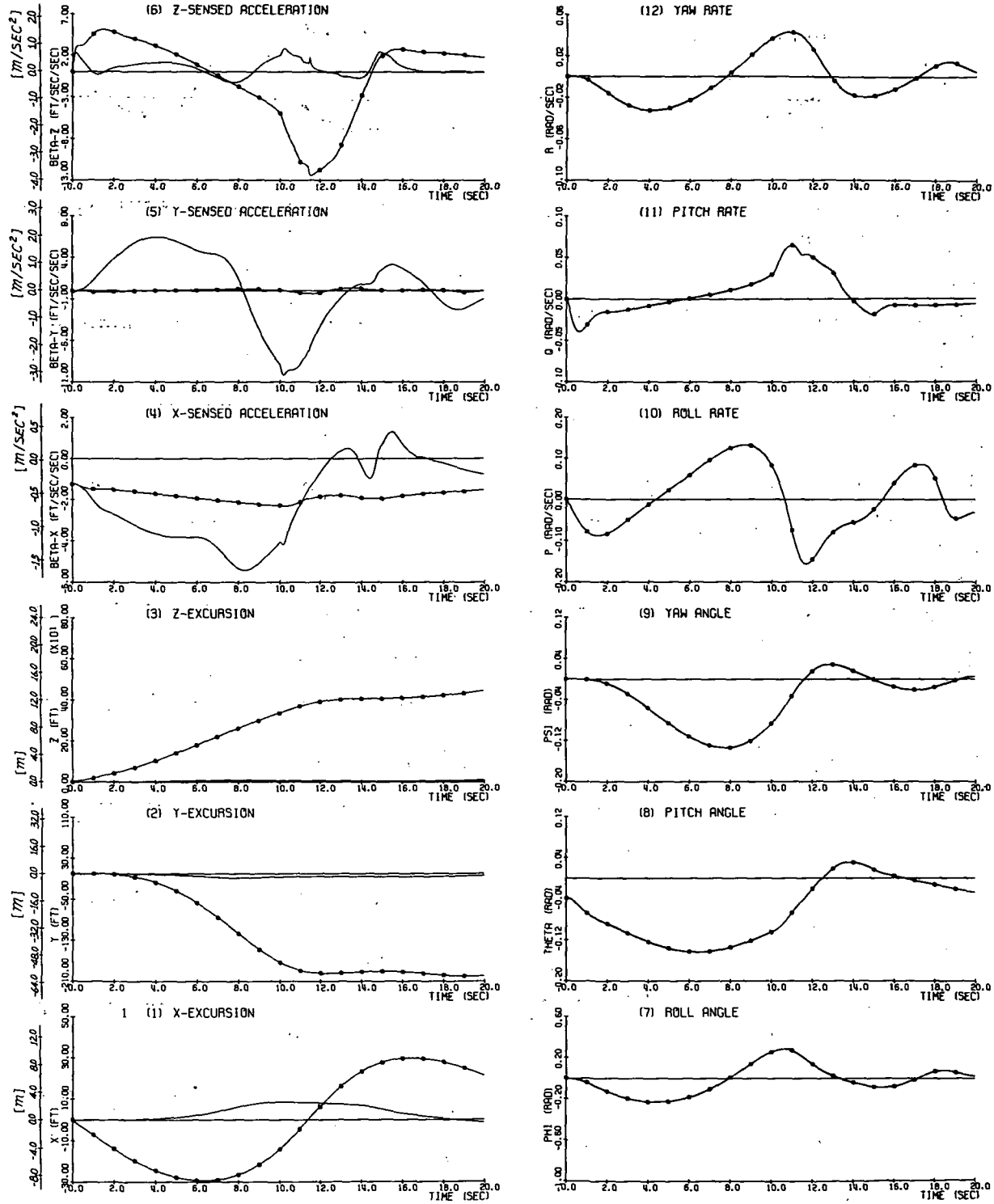

Figure 3-16

Relative Motions of the Aircraft and the Cab - Landing Maneuver - Case 1 (linear translational washout only). T = 30.0

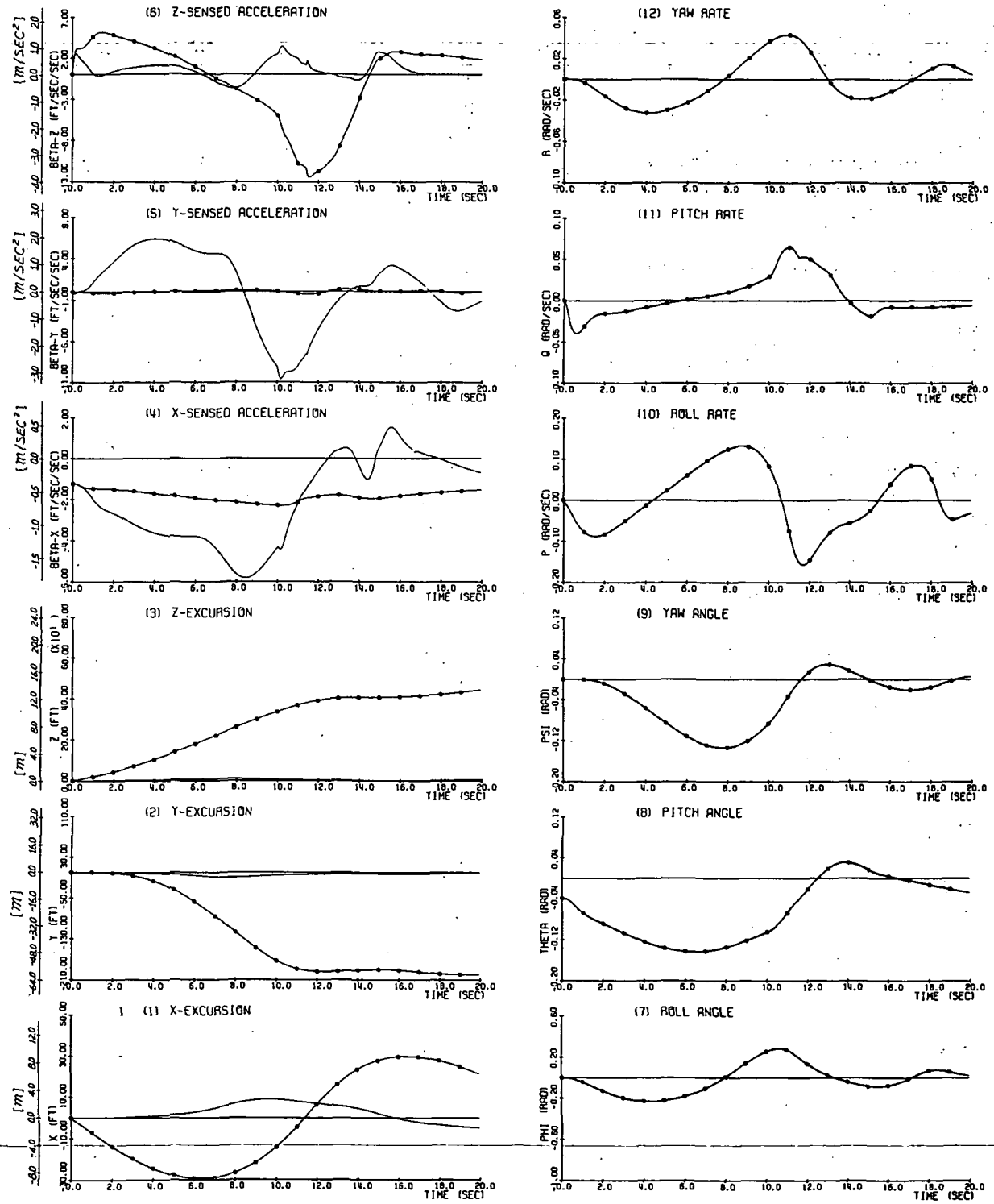

Figure 3-17

Relative Motions of the Aircraft and the Cab - Landing Maneuver - Case 1 (linear translational washout only). T = 10.0

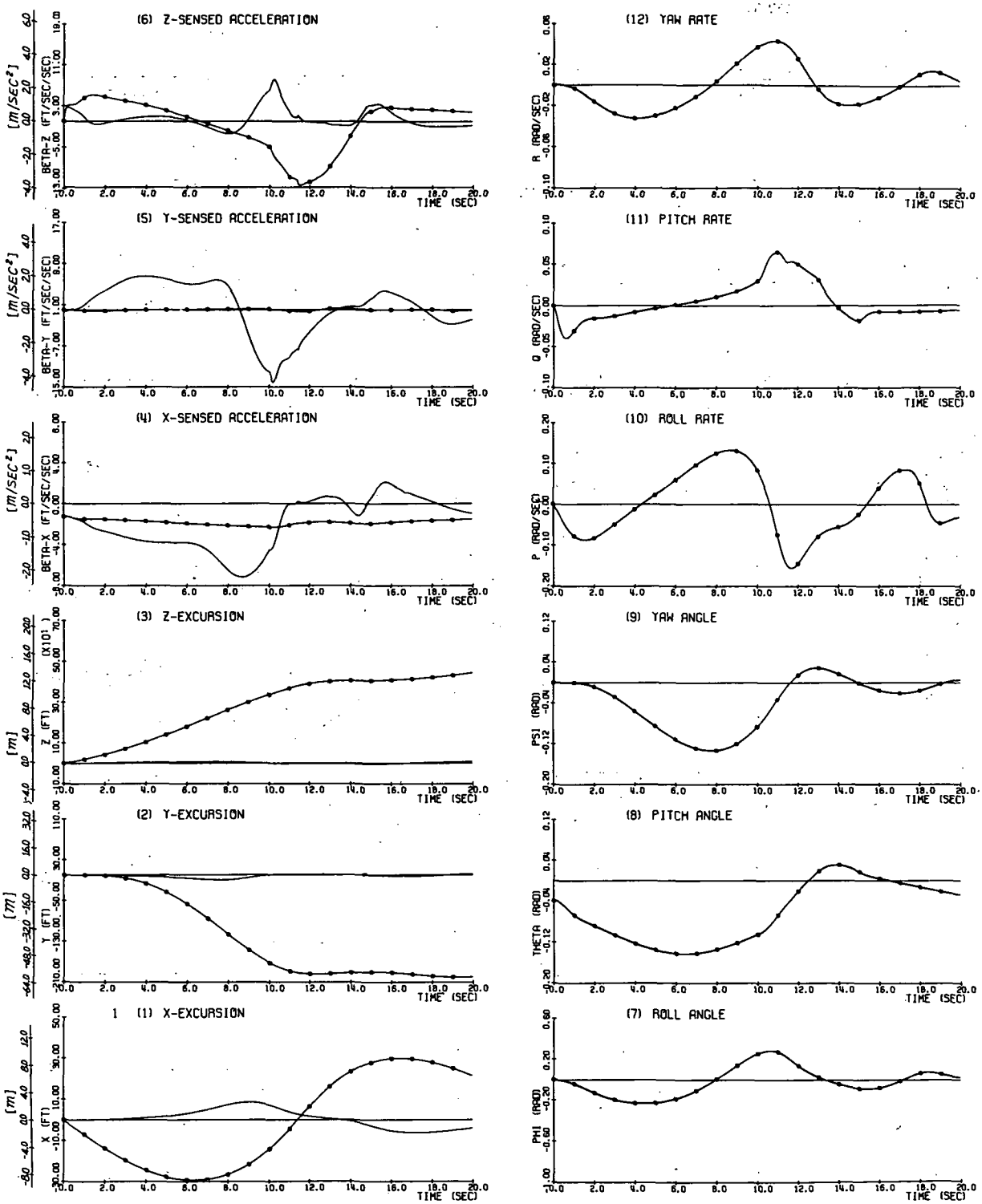

Figure 3-18

Relative Motions of the Aircraft and the Cab - Landing Maneuver - Case 1 (linear translational washout only). T = 2.0

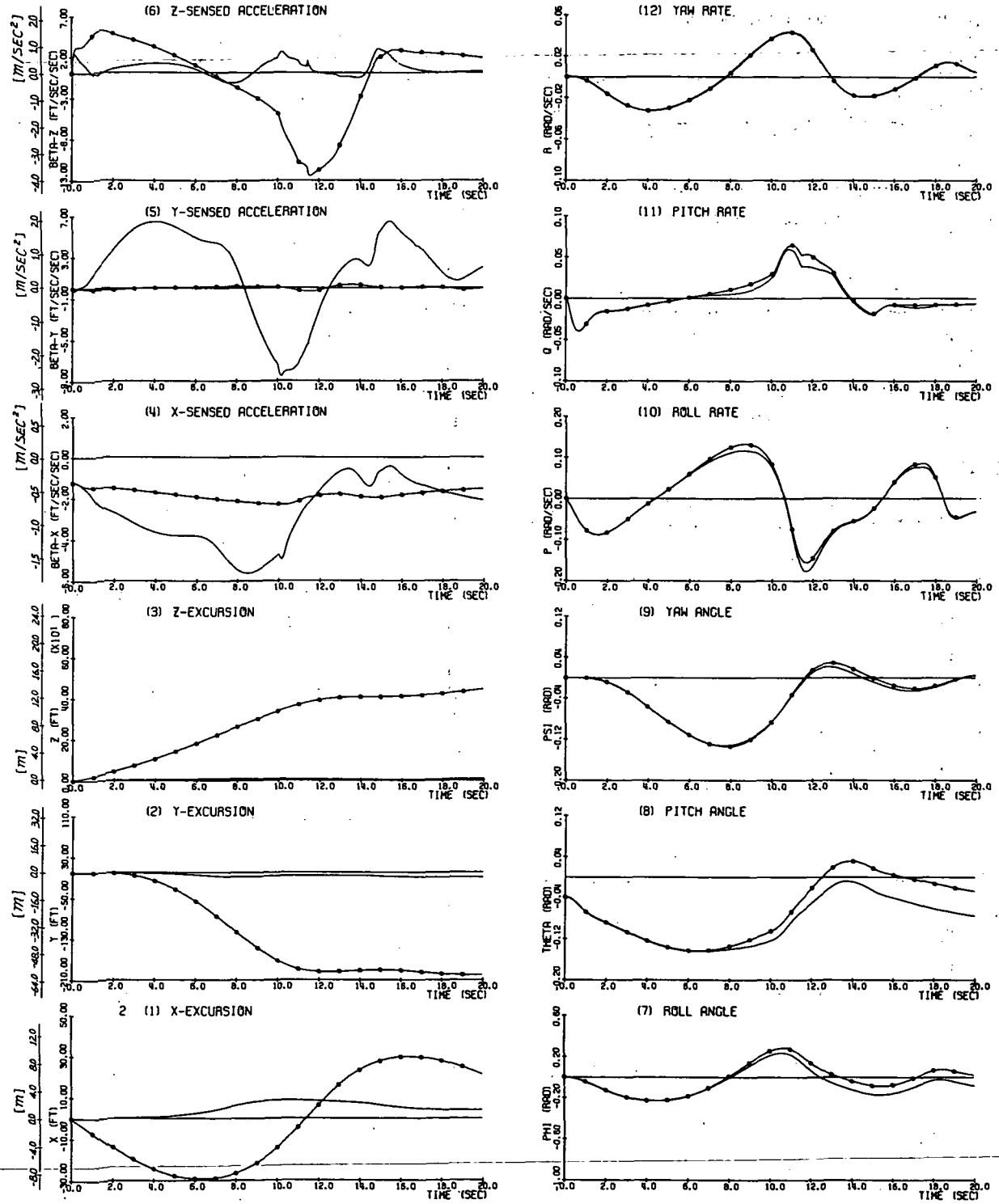

Figure 3-19

Relative Motions of the Aircraft and the Cab. - Landing Maneuver - Case 2 (linear translational and angular washout). T = 30.0

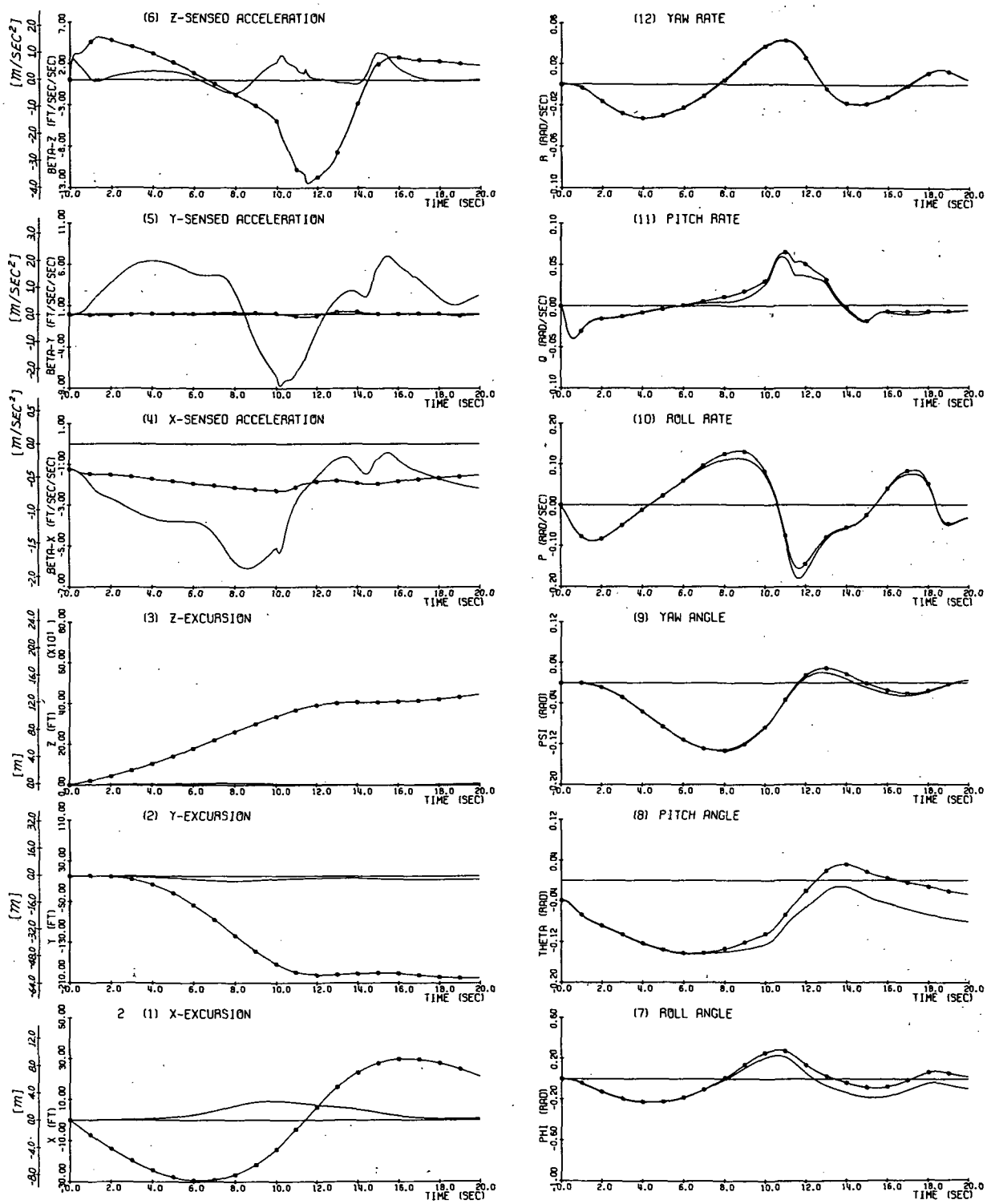

Figure 3-20

Relative Motions of the Aircraft and the Cab - Landing Maneuver - Case 2 (linear translational and angular washout). T = 10.0

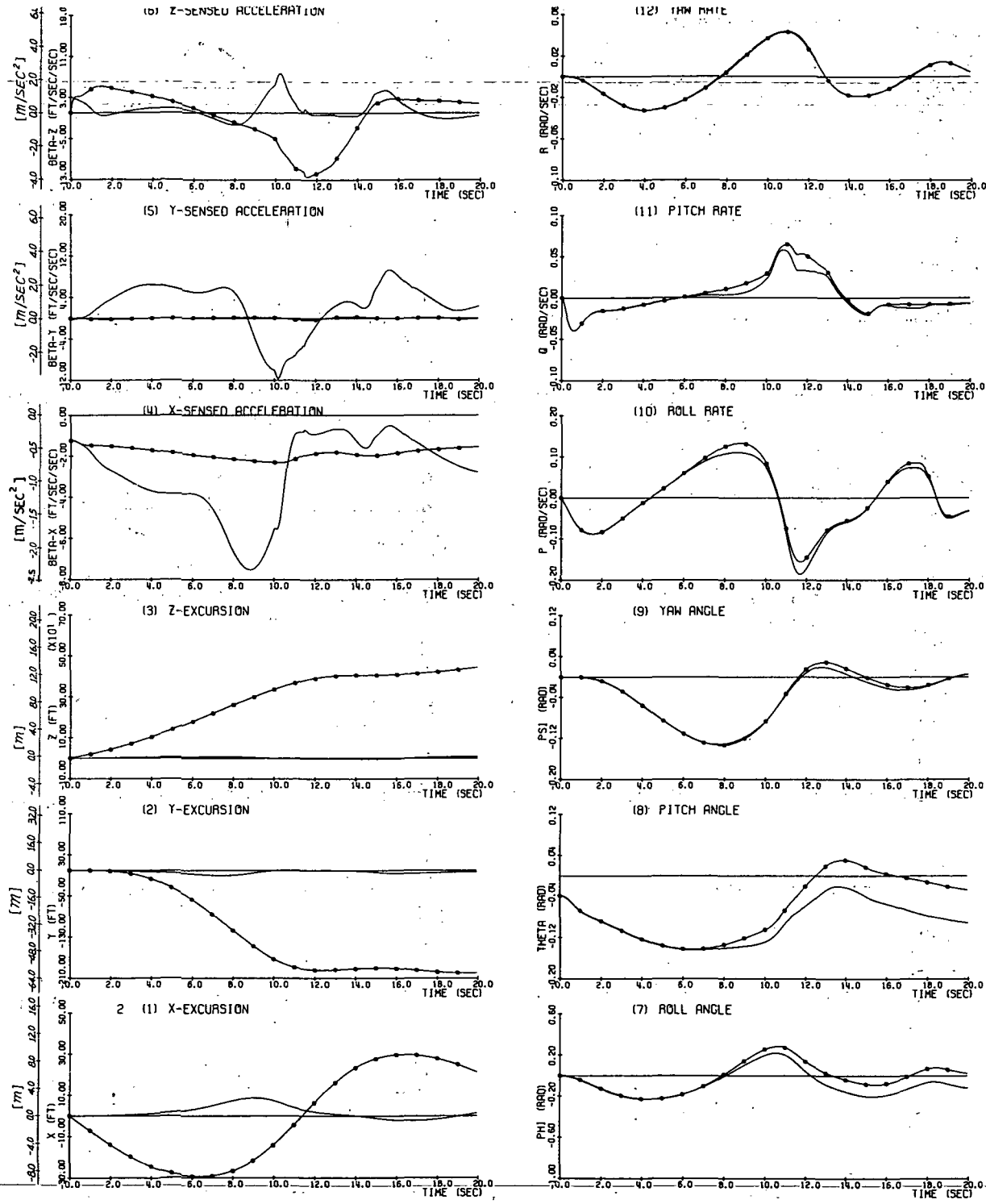

Figure 3-21

Relative Motions of the Aircraft and the Cab - Landing Maneuver - Case 2 (linear translational and angular washout). T = 2.0

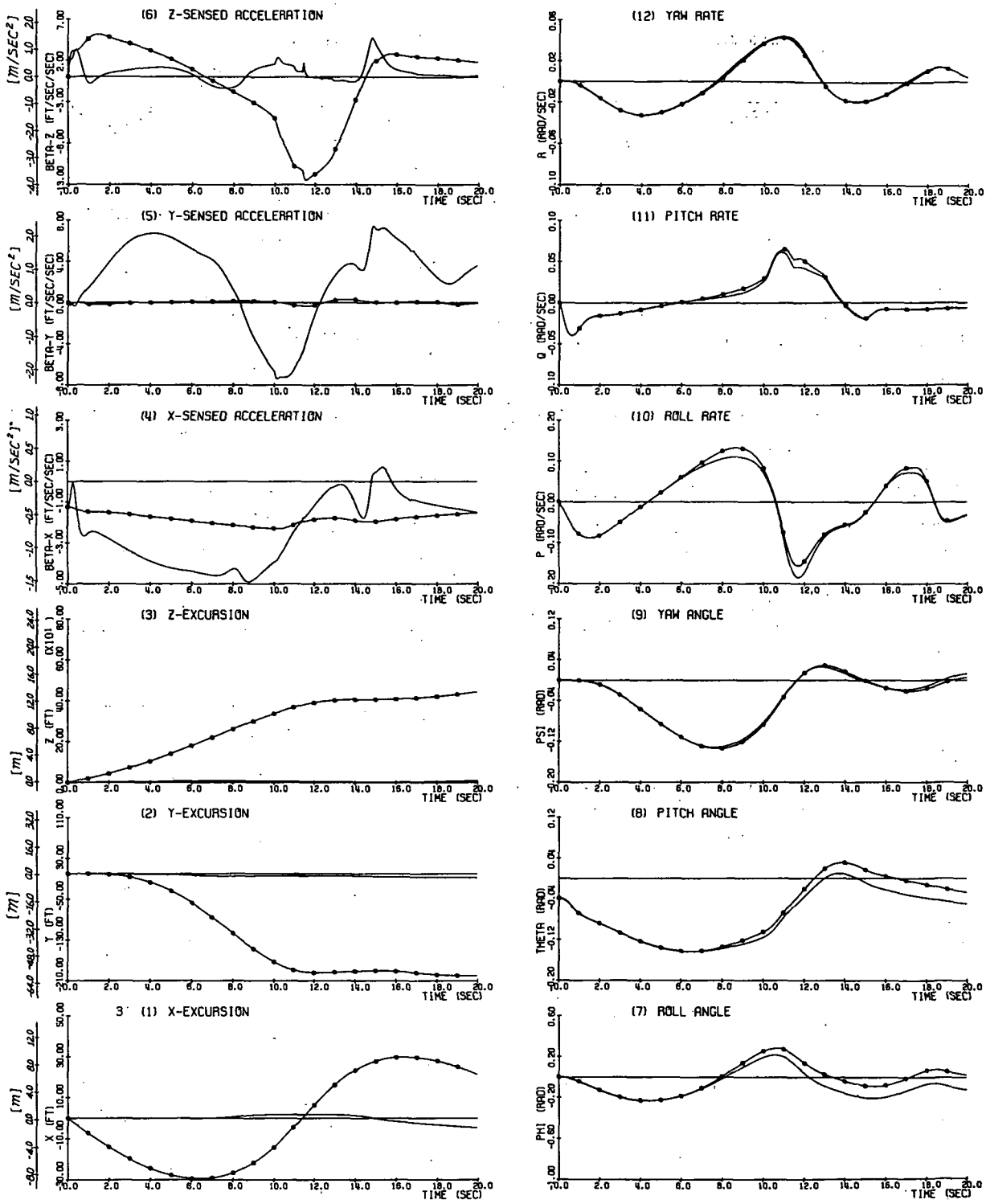

Figure 3-22

Relative Motions of the Aircraft and the Cab - Landing Maneuver - Case 3 (nonlinear translational and linear angular washout). T = 30.0

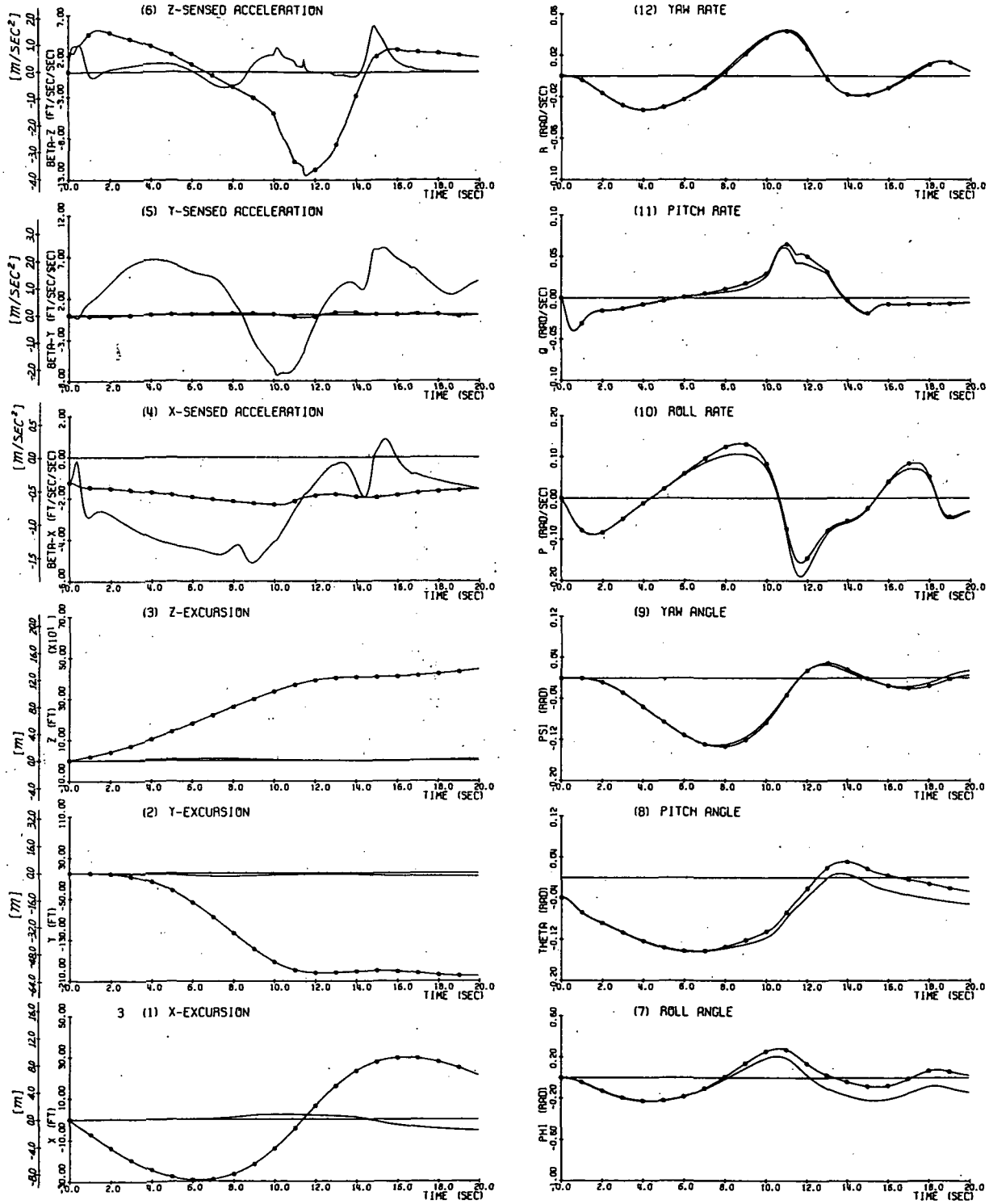

Figure 3-23

Relative Motions of the Aircraft and the Cab - Landing Maneuver - Case 3 (nonlinear translational and linear angular washout). T = 10.0

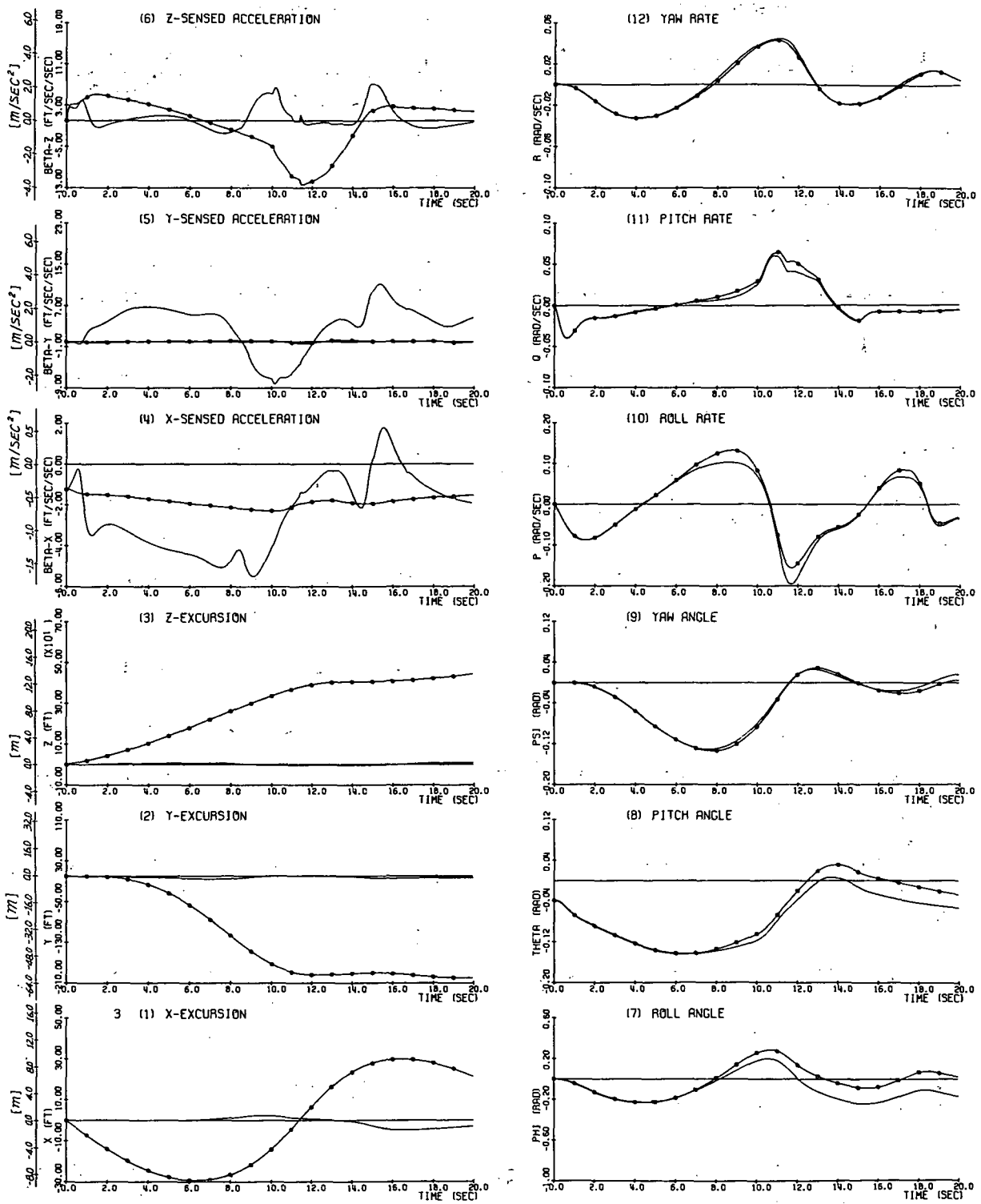

Figure 3-24

Relative Motions of the Aircraft and the Cab - Landing Maneuver - Case 3 (nonlinear translational and linear angular washout). T = 2.0

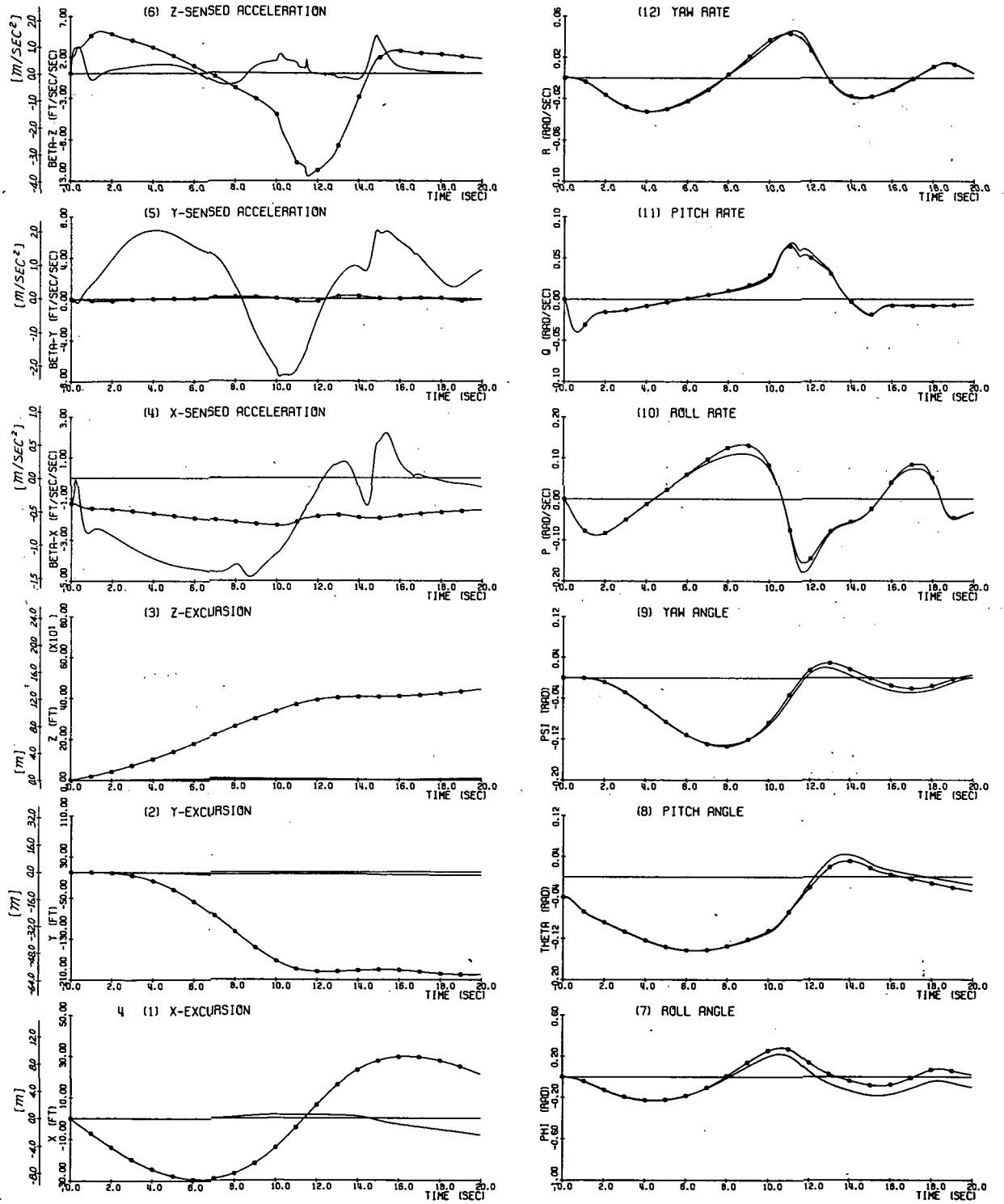

Figure 3-25

Relative Motions of the Aircraft and the Cab - Landing Maneuver - Case 4 (nonlinear translational and angular washout). T = 30.0

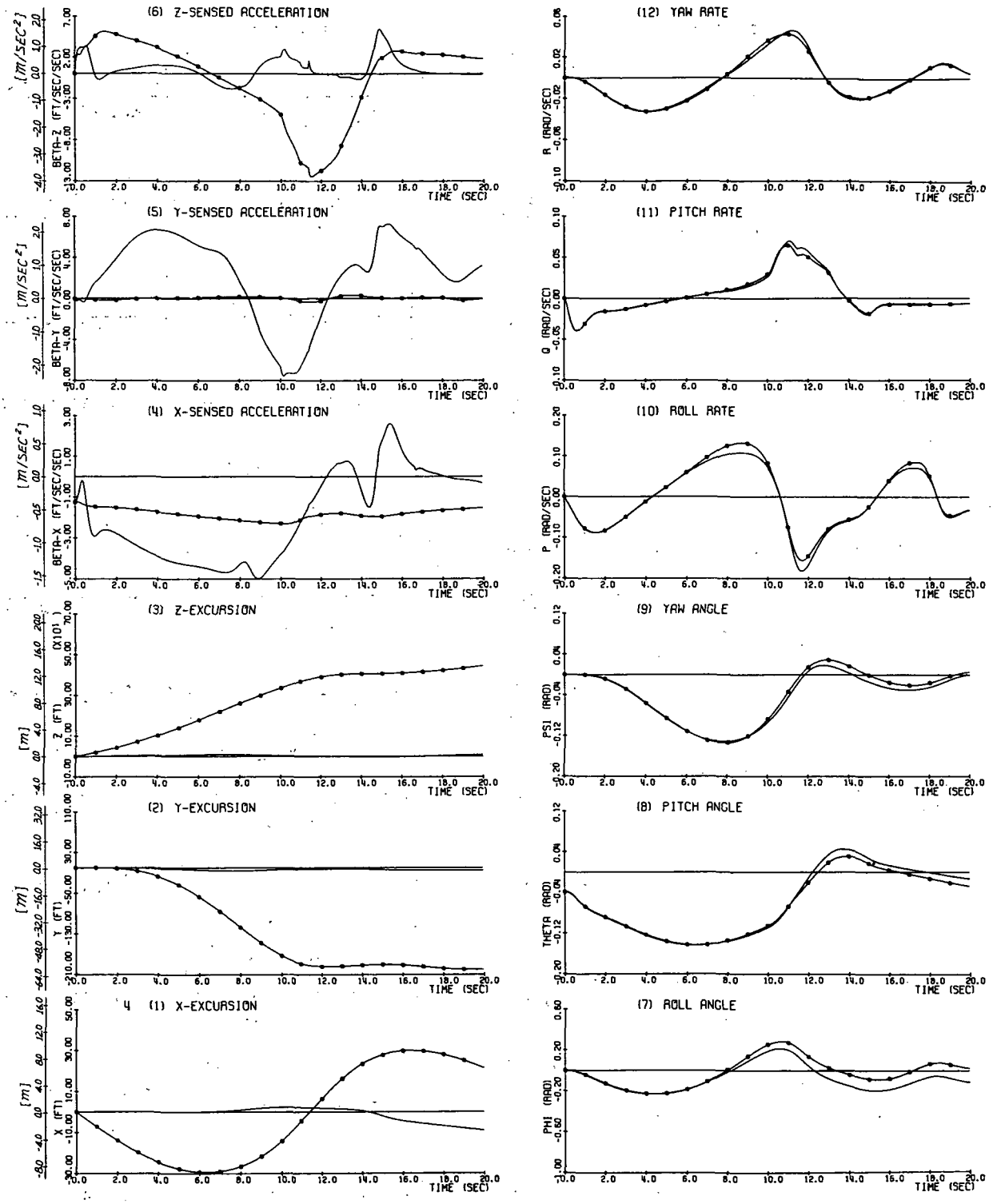

Figure 3-26

Relative Motions of the Aircraft and the Cab. - Landing Maneuver - Case 4 (nonlinear translational and angular washout). T = 10.0

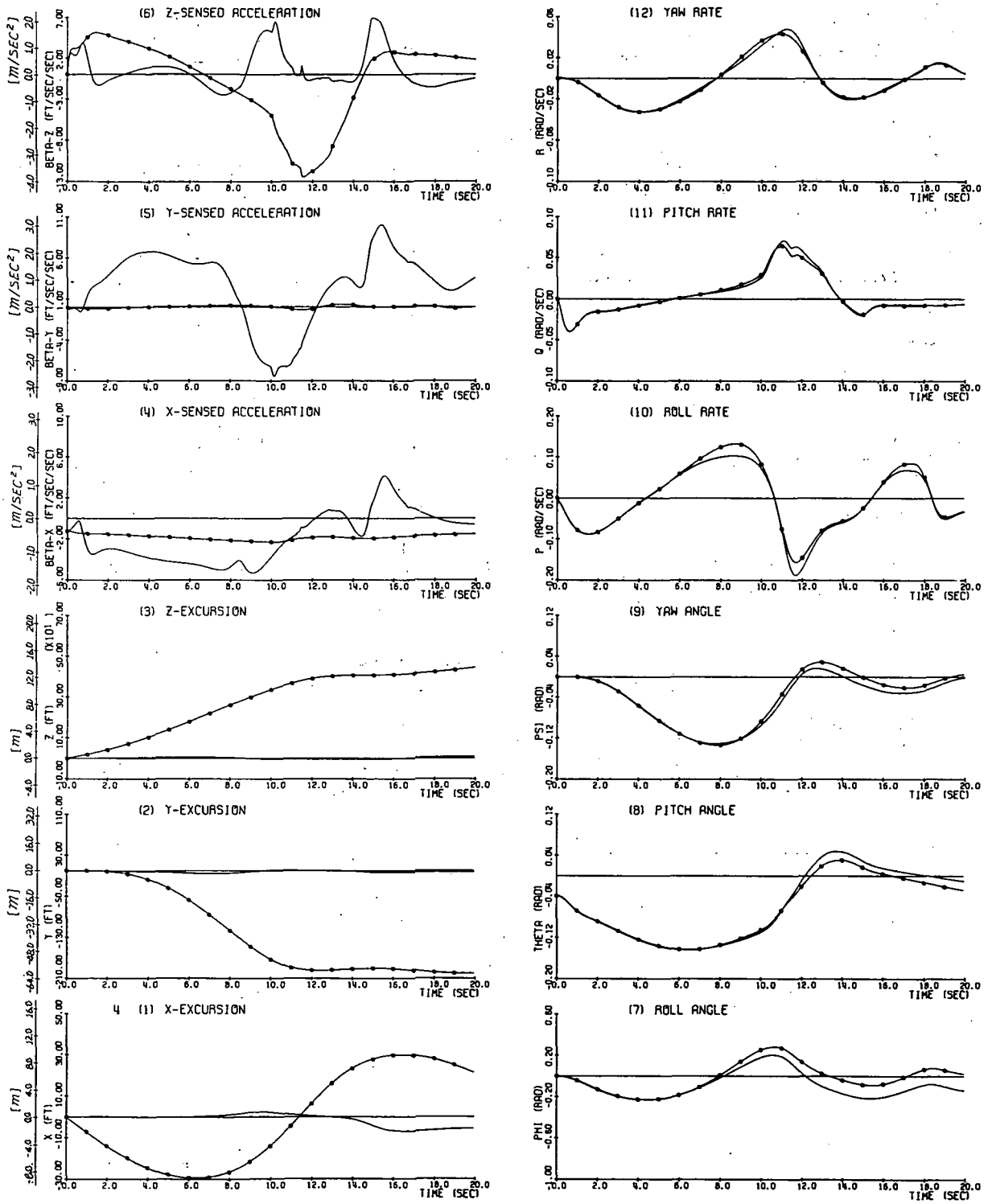

Figure 3-27

Relative Motions of the Aircraft and the Cab - Landing Maneuver - Case 4 (nonlinear translational and angular washout). T = 2.0

Case No.	T	ϵ	K	K_β	K_ω	$\beta^2_{A\,max}$	d_x	d_y	d_z	Fig. No.
1	10.0	0.028	100000000.0	0	0	350.0	10.0	13.0	16.0	3.28
2	10.0	0.028	500.0	0	0	350.0	10.0	13.0	16.0	3.29

Table 3.4

Values of Adjustable Parameters for the Pull-up Task

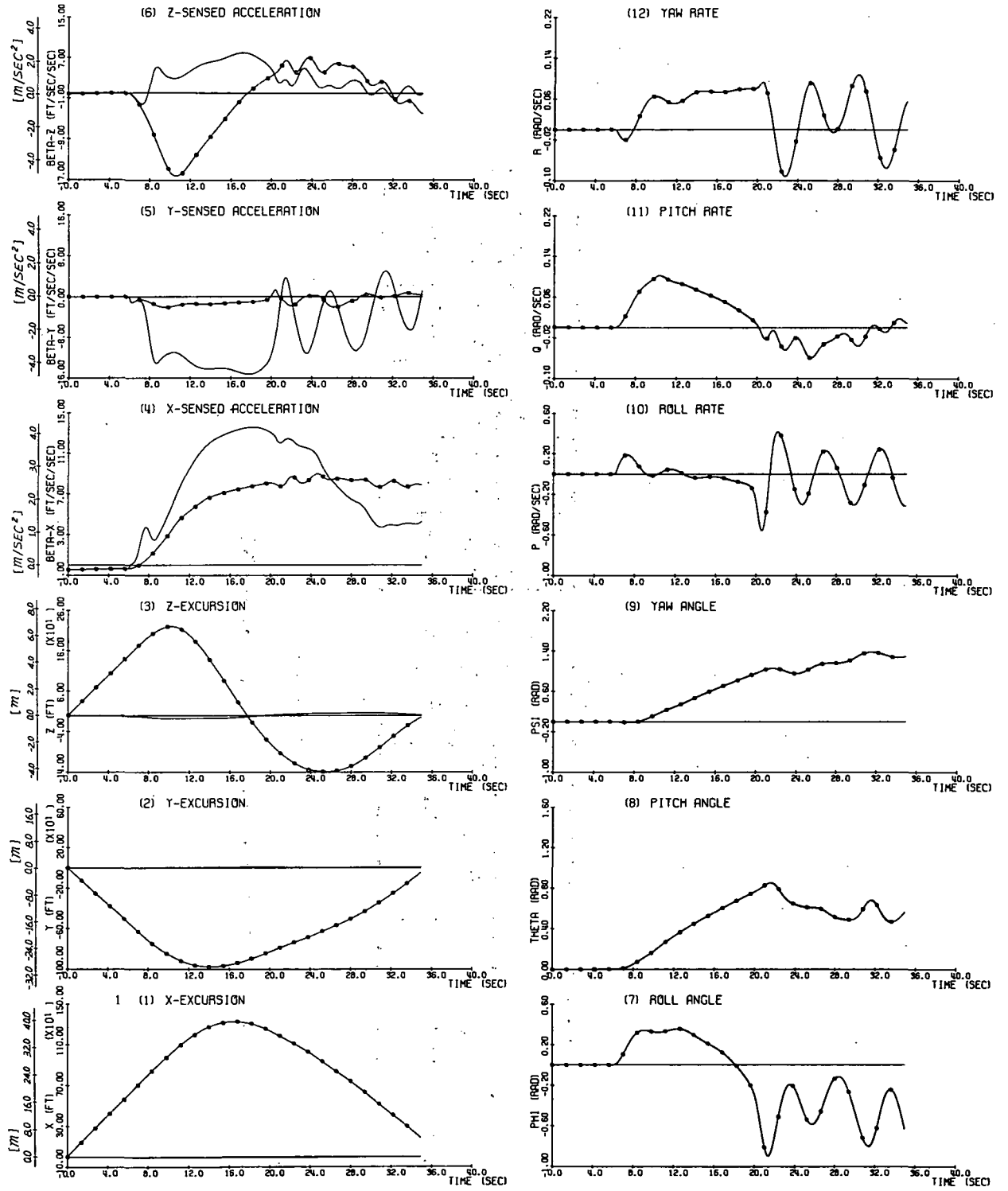

Figure 3-28

Relative Motions of the Aircraft and the Cab - Pull-up Maneuver - Case 1 (linear translational washout only). T = 10.0

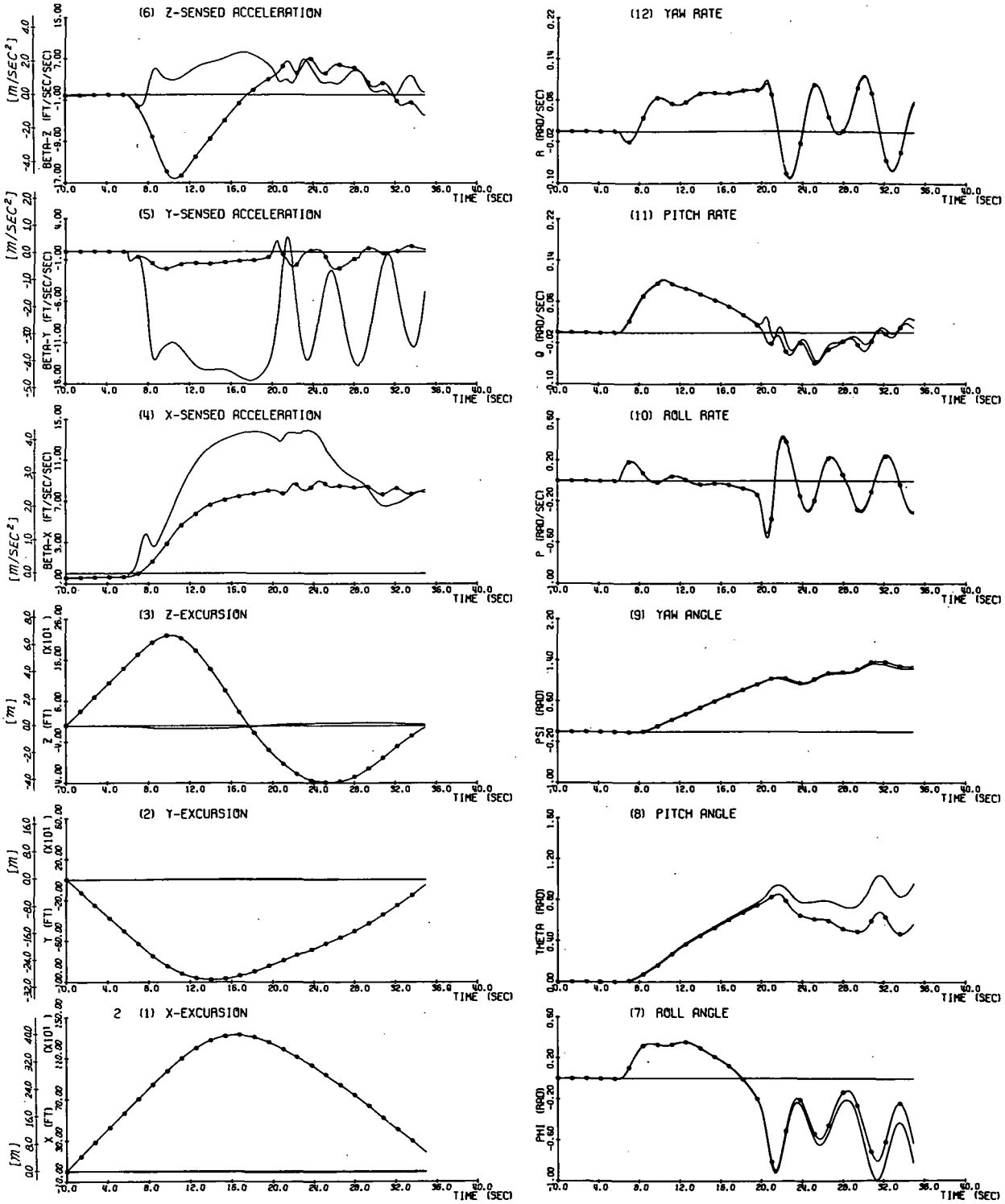

Figure 3-29

Relative Motions of the Aircraft and the Cab - Pull-up Maneuver - Case 2 (linear translational and angular washout). T = 10.0

3.3 Summary and Discussion of Simulation Results

Of the nine adjustable parameters ϵ, k, K_β, K_ω, T, d_x, d_y, d_z and $\beta^2_{A\,max}$, the three parameters k, K_β, K_ω were used to define the four cases in Section 3.2, the parameters ϵ, d_x, d_y, d_z were used as direct control of the cab excursions, $\beta^2_{A\,max}$, which limits the the magnitude of maximum scaling, were kept constant throughout the simulation study after initial trial runs, whereas the remaining parameter T was used to alter the nonlinear filtering characteristics of washout circuit for the translational motion.

It is noted from Section 2.6.2 that for large T, the system tends to behave as a high-pass filter with low cut-off frequency and high scaling of the input aircraft accelerations, while for small T, the system is more like a high-pass filter with higher cut-off frequency and low scaling effect. In general, the low-cut-off-and-high-scaling effect is reflected in the sensed cab motion with good phase and poor amplitude relations with that of sensed aircraft motion. On the other hand, the high-cut-off-and-low-scaling effect tends to give poor phase but with better amplitude relations. These effects are visibly evident for all the tasks and cases considered in the present study as will be pointed out in the sequel.

Another important property for assessing performance is the "onset" characteristic, i.e., the ability of the cab to follow the initial aircraft translational acceleration. The onset motion generally occurs in the vertical (z) direction since the turns are normally well coordinated and forward speed variation is more often kept at low level. A glance at the part (6) of the Figs 3-4-3-29 reveals excellent onset following characteristics of the washout system for all tasks.

As for the angular motion, it is generally agreed that the deviation between the sensed angular motion (i.e., angular rates) of the cab and the aircraft should be preferably kept small since the human motion sensor tends to be more sensitive to the deviation in the angular motion than to the deviation in the translational motion. In the present washout system, the amount of angular motion deviation is controlled by the adjustment of parameter k, which has been kept at a value that keeps angular motion error small.

Thus, the major effort in the simulation study is to obtain a range of the adjustable parameters to provide suitable choice of translational motion with limited motion deviation.

In the discussion that follows, attention will be directed to the response of the sensed translational motion β_x, β_y, and β_z in part (4), (5) and (6), respectively, of Fig. 3-4-3-29.

Tracking Task:

Three values of the parameter T were considered in each case to illustrate the trade-off between th e good-phase-poor-amplitude and poor-phase-good-amplitude responses. Take Case I (Figs. 3-4, 3-5 and 3-6) for example: at the initiation of the simulation, all cases show excellent onset following; after I sec, however, small T (Fig. 3-6 (6)) is seen to cause the sensed cab motion β_{cz} to go in an opposite direction to that of sensed aircraft motion β_{Az} (phase error) while for large T (Fig. 3-4 (6)), β_{cz} remains at the same direction as that of β_{Az}. On the other hand, at about 4 seconds, large T causes β_{cz} to reach a magnitude of 8 ft/sec/sec whereas, for small T, the peak β_{cz} reaches only 4 ft/sec/sec. Again during the following period of 4 sec, large T provides better amplitude response with the cost of phase error while small T provides better phase relation with the cost of larger amplitude attenuation. An intermediate value of T (Fig. 3-5 (6)) results in a compromise between the two extremes.

The reduced peak amplitude response caused by large T, which may not be favorable in z-direction, is definitely favorable in y and x-directions. Because of well coordinated turns, the aircraft has a small lateral sensed acceleration β_{Ay}, but the cab motion which cannot be coordinated within the available maneuvering region shows some spurious lateral acceleration β_{cy}. It is seen that the peak β_{cy} for large T (Fig. 3-4 (5)) is significantly smaller than that for small T (Fig. 3-6 (5)). The same effect is also true for the forward acceleration β_{cx} as can be seen from Fig. 3-4 (4), 3-5 (4), and 3-6 (4).

The effect of the adjustment of T on the cab motion discussed above for Case 1 (Figs. 3-4, 3-5, 3-6) can be extended to cover Case 2 (Figs. 3-7, 3-8, 3-9), Case 3 (Figs. 3-10, 3-11, 3-12), and Case 4 (3-13, 3-14, 3-15).

The introduction of angular washout by the adjustment of k in Case 2 is designed to utilize the residual tilt for the purpose of improving translational motion. This effect can be visualized by comparing the corresponding time-histories for Case 1 (Figs. 3-4, 3-5, 3-6) and Case 2 (Figs. 3-7, 3-8, 3-9). For the limited amount of washout provided, a general

improvement in x and y directions are visible from the figures.

In Case 3 (Figs. 3-10, 3-11, 3-12) an additional nonlinear washout signal was provided for the purpose of improving phase relations in the translational motion. The effect is relatively moderate for the combination of parameters used in the simulation, however, the nonlinear washout does provide an alternative to the linear cases.

In addition to the translational nonlinear washout in Case 3, a nonlinear angular washout signal was utilized in Case 4 (Figs. 3-13, 3-14, 3-15) for the purpose of improving angular phase relations. Since the angular phase relations are nearly perfect in all cases, no significant improvement can be expected from the nonlinear signal. The figures are presented here for the sake of completeness.

Landing Task:

The response characteristics of the washout system discussed in the foregoing paragraphs for the tracking task also applies to this task in general. A major difference between the tracking task and the landing task is that the former has a relatively symmetric vertical acceleration whereas the latter is asymmetric as can be seen from part 6 of the figures. For a motion with asymmetric acceleration profile, the high-cut-off, low-scaling characteristics of the filter can be utilized more advantageously to eliminate the d-c component of the acceleration. Thus, substantially smaller values of T can be used in the present task than had to be used in the previous task.

Another consideration in the determination of suitable combinations of the adjustable parameters is that because of the larger vertical excursion than the lateral excursion in the landing task, the weighting on the amount of translational washout (d_x, d_y, d_z) need not be equal in all three directions as was the case in the tracking task. In a direction in which large excursion occurs a larger weighting is needed to restrain the cab from moving beyond the physical boundary, and in a direction with small aircraft excursion the weighting can be smaller to permit the cab to move in a larger volume.

Again, three values of T were considered in each of the four cases and its effect to the cab response is similar to that in the tracking task as can be observed by comparing the three figures in each case: Figs. 3-16. 3-17, 3-18 for Case 1, Figs. 3-19, 3-20, 3-21 for

Case 2, Figs. 3-22, 3-23, 3-24 for Case 3 and Figs 3-25, 3-26, 3-27 for Case 4. Good vertical onset following and improved lateral and forward performance are visible in all cases.

Pull-up Task:

Substantially different aircraft motion, reflected in the presense of large forward acceleration variation, in this task from the preceding tasks provides a good test of the adaptability of the washout system. Only Case 1 and Case 2 were considered and only one value of T was simulated for both cases.

Referring to Figs. 3-28 and 3-29, a perfect following of the aircraft motion by the cab for the first 6 sec, in which the aircraft was descending at a trim condition, is as expected. After the commencement of the pull-up maneuver, the sensed cab accelerations display a good onset following before subsequent deviation from that of aircraft motion. The effect of high-pass characteristics is most visible after 20 sec: the high frequency component of the aircraft vertical acceleration was faithfully preserved by the cab motion, while d-c component of the acceleration was effectively removed. The effect of residual tilt can be seen by comparing Figs. 3-28 and 3-29. A general improvement in cab acceleration is visible in Fig. 3-29 particularly during the period beyond 20 sec.

4. CONCLUSION AND RECOMMENDATION

This investigation is concerned with the design of a six degree-of-freedom motion simulator control system. The problem considered herein is a generalization of the problem considered in an earlier study [1] in which control systems for a two degree-of-freedom motion simulator were designed by applying the quasi-optimum control technique described in [2.3]. Although the same general method was employed in the present investigation, the mathematical formulation of the physical problem here is substantially more general and more convenient, in that, (a) the reference aircraft dynamic was not necessary in the formulation, (b) the effects of residual tilt and phase error were incorporated in the nonlinear performance index.

The results of this investigation may be interpreted as demonstrating that:

- The quasi-optimum washout control system can be effectively used for a wide variety of flight simulation tasks,
- For each simulation task, the cab excursions can be readily confined to within any specified value and the characteristics of motion sensation can be varied by adjustment of constant parameters.

It is believed, however, that the adaptability of the washout system has not been fully explored in the simulation study reported here. The general presence of spurious lateral sensed acceleration β_{cy} throughout the simulations, for instance, may be an inherent limitation of motion simulation in a finite volume and may have to be present irrespective of the manner in which the washout signals are generated. On the other hand, the possibility of improvement through better combination of adjustable parameters cannot be discounted. Another option, which is logically promising but has not been simulated in this study, is the employment of different filtering charactistics of the washout system in each direction. It was pointed out in Section 3.3 that, to achieve an appropriate washout effect, the filtering characteristics embodied in the washout system should be altered by adjustment of parameters from task to task. But for any one task, the filtering characteristics were maintained the same in all x, y, and z directions despite the fact that the acceleration profiles are significantly different in each direction. Thus it is conceivable that tailoring the filtering characteristics in each direction in accordance with each acceleration component may ultimately provide improved performance.

Based on a comparison of the results obtained in the present study and those achieved for the two degree-of-freedom case which has received favorable comments from pilots who made actual flight tests, it is not unreasonable to conclude that we have achieved a design which may be preferable to those achieved by use of conventional washout techniques.

In view of these results the following further effort can be recommended:

- More exhaustive simulation study of the washout system design reported here.
- Experimental assessment of the washout system by means of actual flight simulation at the Ames Research Center.
- Extension of present design approach to include the consideration of human kinesthetic sensor models.

The importance of experimental evaluation with actual pilots cannot be minimized. It is possible to scrutinize an unending number of time histories without knowing for certain whether one design is better than another, because the characteristics that are being sought in the time-history have not been pinpointed. Thus, actual pilot experiments are ultimately indispensible for complete evaluation of washout system performance.

REFERENCES

1. Friedland, B., Ling, C. K., "Quasi-Optimum Design of Control Systems for Moving-Base Simulators", NASA CR 1613, October 1970.

2. Friedland, B., Thau, F.E., Cohen, V. D., and Ellis, J., "Study of Quasi-Optimum Feedback Control Techniques", NASA CR-527, August 1966.

3. Friedland, B., Thau, F.E., Welt, S., Ling, C. K. and Schilder, M, "Additional Studies of Quasi-Optimum Feedback Control Techniques", NASA CR-1099, July 1968.

APPENDIX I

Derivation of Optimum Controls $\vec{a}$, $\bar{u}$

In this Appendix, analytical expressions for the optimum controls $\vec{a}$ and $\bar{u}$ will be obtained from (2.51) and (2.52), respectively,

$$\frac{\partial M_\beta}{\partial \bar{a}} = \bar{p}_v \tag{I-1}$$

$$\frac{\partial M_\omega}{\partial \bar{u}} = \bar{p}_\lambda / k \tag{I-2}$$

for the penalty functions in (2.40) and (2.41),

$$M_\beta(\vec{\beta}(\vec{a}, \bar{\lambda}), \vec{\beta}_A(\tau)) = \frac{\beta^2}{2\beta_A^2} + K_\beta \left(\frac{\beta}{\beta_A} - \frac{\vec{\beta}_A' \vec{\beta}}{\beta_A^2} \right) \tag{I-3}$$

$$M_\omega(\vec{\omega}(\bar{u}, \bar{\lambda}), \vec{\omega}_A(\tau)) = \frac{\omega^2}{2\omega_A^2} + K_\omega \left(\frac{\omega}{\omega_A} - \frac{\vec{\omega}_A' \vec{\omega}}{\omega_A^2} \right) \tag{I-4}$$

Since the solution of $\bar{u}$ from (I-2) and (I-4) is essentially the same as the solution of $\vec{a}$ from (I-1) and (I-3), we will first solve (I-1) and (I-3) for $\vec{a}$.

Applying chain rule to (I-1), we have

$$\frac{\partial M_\beta}{\partial \bar{a}} = \left(\frac{\partial \vec{\beta}}{\partial \bar{a}} \right)' \frac{\partial M_\beta}{\partial \vec{\beta}}$$

$$= C'(\bar{\lambda}_c) \left\{ \frac{\vec{\beta}}{\beta_A^2} + K_\beta \left(\frac{\vec{\beta}}{\beta_A \beta} - \frac{\vec{\beta}_A}{\beta_A^2} \right) \right\} \tag{I-5}$$

where use of the following relation was made

$$\vec{\beta} = C(\bar{\lambda}_c) \left\{ \vec{a} + [\vec{a}_A - C'(\bar{\lambda}_c)\vec{\alpha}_A] \right\} \tag{I-6}$$

Equating the right hand sides of (I-1) and (I-5) gives

$$\frac{\vec{\beta}}{\beta_A^2} + K_\beta \left(\frac{\vec{\beta}}{\beta_A \beta} - \frac{\vec{\beta}_A}{\beta_A^2} \right) = C(\bar{\lambda}_c)\, \bar{p}_v \qquad \text{(I-7)}$$

Next substituting (I-6) into (I-7) and solving for $\vec{a}$, yields

$$\vec{a} = \frac{\beta_A \beta}{\beta_A \beta + K_\beta \beta_A^2} \left[\beta_A^2\, \bar{p}_v + K_\beta\, C'(\bar{\lambda}_c)\vec{\beta}_A \right] + C'(\bar{\lambda}_c)\vec{\alpha}_A - \vec{a}_A \qquad \text{(I-8)}$$

To eliminate the β term in (I-8), (I-7) is rewritten as

$$\left(\frac{1}{\beta_A^2} + \frac{K_\beta}{\beta_A \beta} \right) \vec{\beta} = \frac{K_\beta}{\beta_A^2}\, \vec{\beta}_A + C(\bar{\lambda}_c)\, \bar{p}_v \qquad \text{(I-9)}$$

Next, compute the inner products of the vectors on either side of equal sign in (I-9); the resulting scaler equation may then be solved for β to obtain

$$\beta = \beta_A \left\{ -K_\beta + \sqrt{\beta_A^2\, p_v^2 + 2\, K_\beta\, \vec{\beta}_A'\, C(\bar{\lambda}_c)\, \bar{p}_v + K_\beta^2} \right\} \qquad \text{(I-10)}$$

Substitution of (I-10) into (I-8) gives the desired result

$$\vec{a} = \left[1 - \frac{K_\beta}{\sqrt{\beta_A^2\, p_v^2 + 2\, K_\beta\, \vec{\beta}_A'\, C(\bar{\lambda}_c)\, \bar{p}_v + K_\beta^2}} \right] \left(\beta_A^2\, \bar{p}_v + K_\beta\, C'(\bar{\lambda}_c)\vec{\beta}_A \right) + C'(\bar{\lambda}_c)\vec{\alpha}_A - \vec{a}_A \qquad \text{(I-11)}$$

Following the same procedure results in a similar expression for the angular wash-out, given below

$$\bar{u} = \left\{ 1 - \frac{K_\omega}{\sqrt{\omega_A^2\, \bar{p}_\lambda'\, F^{-1}(\bar{\lambda}_c)[F'(\bar{\lambda}_c)]^{-1}\, \bar{p}_\lambda / k^2 + 2K_\omega\, \vec{\omega}_A'\, [F'(\bar{\lambda}_c)]^{-1}\, \bar{p}_\lambda / k + K_\omega^2}} \right\} \cdot$$

$$\left\{ \omega_A^2\, F^{-1}(\bar{\lambda}_c)\, [F'(\bar{\lambda}_c)]^{-1}\, \bar{p}_\lambda / k + K_\omega F^{-1}(\bar{\lambda}_c)\, \vec{\omega}_A \right\} + F^{-1}(\bar{\lambda}_c)\, \vec{\omega}_A - \dot{\bar{u}}_A$$

APPENDIX II

Derivation of Quasi-Optimum Correction Factors

The optimum control problem defined in (2. 94) — (2. 97) is summarized below:

$$
\begin{aligned}
&\dot{r}_0 = M_\beta + k M_\omega + \epsilon L && ; \quad r_0(t) = 0 \quad , && r_0(t+T) = \text{free} \\
&\dot{\vec{r}} = \vec{v} && ; \quad \vec{r}(t) = \vec{r}_A(t) , && \vec{r}(t+T) = \text{free} \\
&\dot{\vec{v}} = \vec{a} && ; \quad \vec{v}(t) = \vec{v}_A(t) , && \vec{v}(t+T) = \text{free} \\
&\dot{\bar{\lambda}} = \bar{u} && ; \quad \bar{\lambda}(t) = 0 \quad , && \bar{\lambda}(t+T) = \text{free} \\
&\dot{\tau} = 1 && ; \quad \tau(t) = t \quad , && \tau(t+T) = t+T \\
&\dot{\epsilon} = 0 && ; \quad \epsilon(t) = \epsilon \quad , && \epsilon(t+T) = \text{free}
\end{aligned}
\tag{II-1}
$$

$$
h = p_0 (M_\beta + K M_\omega + \epsilon L) + \bar{p}_r' \vec{v} + \bar{p}_v' \vec{a} + \bar{p}_\lambda' \bar{u} + p_\tau \tag{II-2}
$$

$$
\begin{aligned}
&\dot{p}_0 = 0 && ; \ p_0(t+T) = -1 \\
&\dot{\bar{p}}_r = -\epsilon p_0 \frac{\partial L}{\partial \vec{r}} && ; \ p_r(t+T) = 0 \\
&\dot{\bar{p}}_v = -\bar{p}_r && ; \ p_v(t+T) = 0 \\
&\dot{\bar{p}}_\lambda = \bar{u}_c' \left[\frac{\partial F}{\partial \bar{\lambda}}\right]' [F']^{-1} \bar{p}_\lambda + \vec{a}_c' \left[\frac{\partial C}{\partial \bar{\lambda}}\right]' C \bar{p}_v && ; \ p_\lambda(t+T) = 0 \\
&\dot{p}_\tau = -p_0 \left(\frac{\partial M_\beta}{\partial \tau} + k \frac{\partial M_\omega}{\partial \tau} + \epsilon \frac{\partial L}{\partial \tau}\right) && ; \ p_\tau(t+T) = \text{free} \\
&\dot{p}_\epsilon = -p_0 L && ; \ p_\epsilon(t+T) = 0
\end{aligned}
\tag{II-3}
$$

Let the vectors $\bar{x}$ and $\bar{p}$ represent all the state variables and the corresponding adjoint variables, respectively,

$$\bar{x} = \begin{bmatrix} r_0 \\ \vec{r} \\ \vec{v} \\ \bar{\lambda} \\ \tau \\ \epsilon \end{bmatrix} \qquad \bar{p} = \begin{bmatrix} p_0 \\ \bar{p}_r \\ \bar{p}_v \\ \bar{p}_\lambda \\ p_\tau \\ \bar{p}_\epsilon \end{bmatrix} \tag{II-4}$$

The corresponding quantities for the "simplified" problem ($\epsilon = 0$) are denoted by the subscript "s":

$$\bar{x}_s = \begin{bmatrix} r_{0s} \\ \bar{r}_s \\ \bar{v}_s \\ \bar{\lambda}_s \\ \tau_s \\ 0 \end{bmatrix} \qquad \bar{p}_s = \begin{bmatrix} p_{0s} \\ \bar{p}_{rs} \\ \bar{p}_{vs} \\ \bar{p}_{\lambda s} \\ p_{\tau s} \\ 0 \end{bmatrix} \tag{II-5}$$

In this appendix, we will derive a correction matrix $\bar{M}$ so that the original adjoint vector $\bar{p}$ is given by

$$\begin{aligned} \bar{p} &= \bar{p}_s + \bar{\psi} \\ &= \bar{p}_s + \bar{M}\,\bar{\xi} \end{aligned} \tag{II-6}$$

where $\bar{\psi}$ is the correction to adjoint vector $\bar{p}$ and $\bar{\xi}$ is the correction to state vector $\bar{x}$.

$$\bar{x} = \bar{x}_s + \bar{\xi} \tag{II-7}$$

The matrix $\bar{M}$ is conveniently partitioned as follows:

$$\bar{M} = \begin{bmatrix} m_{00} & \bar{m}_{0r} & \bar{m}_{0v} & \bar{m}_{0\lambda} & m_{0\tau} & m_{0\epsilon} \\ \bar{m}_{r0} & M_{rr} & M_{rv} & M_{r\lambda} & \bar{m}_{r\tau} & \bar{m}_{r\epsilon} \\ \bar{m}_{v0} & M_{vr} & M_{vv} & M_{v\lambda} & \bar{m}_{v\tau} & \bar{m}_{v\epsilon} \\ \bar{m}_{\lambda 0} & M_{\lambda r} & M_{\lambda v} & M_{\lambda\lambda} & \bar{m}_{\lambda\tau} & \bar{m}_{\lambda\epsilon} \\ \bar{m}_{\tau 0} & \bar{m}_{\tau r} & \bar{m}_{\tau v} & \bar{m}_{\tau\lambda} & \bar{m}_{\tau\tau} & m_{\tau\epsilon} \\ m_{\epsilon 0} & \bar{m}_{\epsilon r} & \bar{m}_{\epsilon v} & \bar{m}_{\epsilon\lambda} & \bar{m}_{\epsilon\tau} & m_{\epsilon\epsilon} \end{bmatrix} \qquad (\text{II}\text{-}8)$$

The elements denoted by capital M are n x n matrices, and $\bar{m}$'s denote vectors. The elements appearing in (II-8) — not all of which are required for quasi-optimum control law — are to be found with the aid of the auxiliary equations for $\bar{\psi}$ and $\bar{\xi}$

$$\begin{aligned} \dot{\bar{\xi}} &= H_{xp}\,\bar{\xi} + H_{pp}\,\bar{\psi} \\ \dot{\bar{\psi}} &= -H_{xx}\,\bar{\xi} - H_{px}\,\bar{\psi} \end{aligned} \qquad (\text{II}\text{-}9)$$

or, by use of the matrix Riccati equation:

$$-d\bar{M}/d\tau = M H_{xp} + H_{px} M + M H_{pp} M + H_{xx} \qquad (\text{II}\text{-}10)$$

The coefficient matrices H_{xp}, H_{px}, H_{pp} and H_{xx} in (II-9) and (II-10) are obtained by partial differentiation of the Hamiltonian h in (II-2) with respect to $\bar{x}$ and $\bar{p}$ where the resulting derivatives are evaluated at $\bar{x}_s$ and $\bar{p}_s$. The first partials of h are:

$$\frac{\partial h}{\partial r_0} = 0$$

$$\frac{\partial h}{\partial \vec{r}} = p_0 \epsilon \frac{\partial L}{\partial \vec{r}}$$

$$\frac{\partial h}{\partial \vec{v}} = \bar{p}_r$$

$$\frac{\partial h}{\partial \bar{\lambda}} = -\bar{u}_c' \left[\frac{\partial F}{\partial \bar{\lambda}}\right]' [F']^{-1} \bar{p}_\lambda - \bar{a}_c' \left[\frac{\partial C}{\partial \bar{\lambda}}\right]' C \bar{p}_v \qquad \text{(II-11)}$$

$$\frac{\partial h}{\partial \tau} = p_0 \left[\frac{\partial M_\beta}{\partial \tau} + k \frac{\partial M_\omega}{\partial \tau} + \epsilon \frac{\partial L}{\partial \tau}\right]$$

$$\frac{\partial h}{\partial \epsilon} = p_0 L$$

$$\frac{\partial h}{\partial \bar{p}_0} = M_\beta + k M_\omega + \epsilon L$$

$$\frac{\partial h}{\partial \bar{p}_r} = \vec{v}$$

$$\frac{\partial h}{\partial \bar{p}_v} = \vec{a}$$

$$\frac{\partial h}{\partial \bar{p}_\lambda} = \bar{u} \qquad \text{(II-12)}$$

$$\frac{\partial h}{\partial p_\tau} = 1$$

$$\frac{\partial h}{\partial p_\epsilon} = 0$$

In order to evaluate the second partial matrices about the "simplified" solution, it is noted that for the simplified problem we have

$$\epsilon = 0$$

$$\vec{\beta} = \vec{\alpha} = \vec{\omega} = 0 \tag{II-13}$$

$$\vec{\alpha}_c = \vec{\alpha} + \vec{\alpha}_A = C'(\bar{\lambda}_c)\vec{\alpha}_A$$

$$\bar{u}_c = \bar{u} + \bar{u}_A = F^{-1}(\bar{\lambda}_c)\vec{\omega}_A \tag{II-14}$$

$$p_0(\tau) = -1$$

$$\bar{p}_r(\tau) = 0$$

$$\bar{p}_v(\tau) = 0$$

$$\bar{p}_\lambda(\tau) = 0 \tag{II-15}$$

$$\bar{p}_\tau(\tau) = \bar{p}(t+T)$$

$$\bar{p}_\epsilon(\tau) = \int_t^\tau L(\vec{r}(\tau))\,d\tau$$

$$r_0(\tau) = 0$$

$$\vec{r}(\tau) = \vec{r}(t) + \vec{v}(t)(\tau - t)$$

$$\vec{v}(\tau) = \vec{v}(t) \tag{II-16}$$

$$\bar{\lambda}(\tau) = \bar{\lambda}(t)$$

$$\tau(\tau) = \tau$$

$$\epsilon(\tau) = \epsilon$$

where the subscript "s" has been omitted in (II-13) – (II-16). In the subsequent development, we will be using only the "simplified" solution, and hence for convenienc the subscript "s" will be omitted unless otherwise indicated. Thus,

$$H_{px} = \left.\frac{\partial h}{\partial \bar{x}\,\partial \bar{p}}\right|_{\epsilon = 0} = H'_{xp} =$$

0	0	0	0	0	0
0	0	0	0	0	0
0	I	0	0	0	0
0	0	$-\vec{a}'_c\left[\frac{\partial C}{\partial \bar{\lambda}}\right]' C$	$-\bar{u}'_c\left[\frac{\partial F}{\partial \bar{\lambda}}\right]' [F]^{-1}$	0	0
0	0	$\left[\frac{\partial \vec{a}}{\partial \tau}\right]'$	$\left[\frac{\partial \bar{u}}{\partial \tau}\right]'$	0	0
L	0	0	0	0	0

(II-17)

$$H_{pp} = \left. \frac{\partial^2 h}{\partial \bar{p}^2} \right|_{\epsilon = 0} =$$

0	0	0	0	0	0
0	0	0	0	0	0
0	0	$\frac{\partial \vec{\alpha}}{\partial \bar{p}_\nu}$	0	0	0
0	0	0	$\frac{\partial \bar{\upsilon}}{\partial \bar{p}_\lambda}$	0	0
0	0	0	0	0	0
0	0	0	0	0	0

(II-18)

$$H_{xx} = \frac{\partial^2 h}{\partial \bar{x}^2} \quad \epsilon = 0 \quad =$$

0	0	0	0	0	0
0	0	0	0	0	$-\frac{\partial L}{\partial \vec{r}}$
0	0	0	0	0	0
0	0	0	0	0	0
0	0	0	0	0	$-\frac{\partial L}{\partial \tau}$
0	$-\frac{\partial L}{\partial \vec{r}}$	0	0	$-\frac{\partial L}{\partial \tau}$	0

(II-19)

Substitution of (II-17) — (II-19) into the auxiliary equations (II-9) results in

$$\dot{\xi}_0 = L\xi_\epsilon \qquad \text{(a)}$$

$$\dot{\bar{\xi}}_r = \bar{\xi}_v \qquad \text{(b)}$$

$$\dot{\bar{\xi}}_v = -\left\{\vec{a}_c'\left[\frac{\partial C}{\partial \bar{\lambda}}\right]' C\right\}\bar{\xi}_\lambda + \frac{\partial \vec{a}}{\partial \tau}\xi_\tau + \frac{\partial \vec{a}}{\partial \bar{p}_v}\bar{\psi}_v \qquad \text{(c)}$$

$$\dot{\bar{\xi}}_\lambda = -\left\{\bar{u}_c'\left[\frac{\partial F}{\partial \bar{\lambda}}\right]'[F']^{-1}\right\}\bar{\xi}_\lambda + \frac{\partial \bar{u}}{\partial \tau}\xi_\tau + \frac{\partial \bar{u}}{\partial \bar{p}_\lambda}\bar{\psi}_\lambda \qquad \text{(d)} \qquad \text{(II-20)}$$

$$\dot{\xi}_\tau = 0 \qquad \text{(e)}$$

$$\dot{\xi}_\epsilon = 0 \qquad \text{(f)}$$

$$\dot{\psi}_0 = 0 \qquad \text{(a)}$$

$$\dot{\bar{\psi}}_r = \frac{\partial L}{\partial \vec{r}}\xi_\epsilon \qquad \text{(b)}$$

$$\dot{\bar{\psi}}_v = -\bar{\psi}_r \qquad \text{(c)}$$

$$\dot{\bar{\psi}}_\lambda = \vec{a}_c'\left[\frac{\partial C}{\partial \bar{\lambda}}\right]' C\,\bar{\psi}_v + \bar{u}_c'\left[\frac{\partial F}{\partial \bar{\lambda}}\right]'[F']^{-1}\bar{\psi}_\lambda \qquad \text{(d)} \qquad \text{(II-21)}$$

$$\dot{\psi}_\tau = \frac{\partial L}{\partial \tau}\xi_\epsilon - \left[\frac{\partial \bar{a}}{\partial \tau}\right]'\bar{\psi}_v - \left[\frac{\partial \bar{u}}{\partial \tau}\right]'\bar{\psi}_\lambda \qquad \text{(e)}$$

$$\dot{\psi}_\epsilon = \frac{\partial L}{\partial \bar{r}}\bar{\xi}_r + \frac{\partial L}{\partial \tau}\xi_\tau - L\psi_0 \qquad \text{(f)}$$

with boundary conditions

$$t_0(t+T) = -\dot{p}_0(t+T)\,d(t+T) = 0 \qquad \text{(a)}$$

$$\bar{\psi}_r(t+T) = -\dot{\bar{p}}_r(t+T)\,d(t+T) = 0 \qquad \text{(b)}$$

$$\bar{\psi}_v(t+T) = -\dot{\bar{p}}_v(t+T)\,d(t+T) = 0 \qquad \text{(c)}$$

$$\bar{\psi}_\lambda(t+T) = -\dot{\bar{p}}_\lambda(t+T)\,d(t+T) = 0 \qquad \text{(d)} \qquad \text{(II-22)}$$

$$\bar{\psi}_\epsilon(t+T) = -\dot{p}_\epsilon(t+T)\,d(t+T) = 0 \qquad \text{(e)}$$

$$\xi_\tau(t+T) = -\dot{\tau}(t+T)\,d(t+T) = -d(t+T) \qquad \text{(f)}$$

and $\dot{\bar{p}}'(t+T)\,\bar{\xi}(t+T) = \dot{\bar{x}}'(t+T)\,\bar{\psi}(t+T)$ or

$$\psi_\tau(t+T) = 0 \qquad \text{(g)}$$

Since the optimum control laws $\vec{a}$ and $\bar{u}$ in (2. 53) and (2. 54) are only a function $\bar{p}_v$ and $\bar{p}_\lambda$, respectively, the elements in the $\bar{M}$ matrix (II-8) of primary interest are those affecting the correction of $\bar{p}_v$ and $\bar{p}_\lambda$. The correction factors $\bar{\psi}_r$ and $\bar{\psi}_\lambda$ are written in terms of the elements of $\bar{M}$ from (II-6) to give

$$\bar{\psi} = \bar{M}\,\bar{\xi} \qquad \text{(II-23)}$$

$$\bar{\psi}_v = \bar{M}_{v0}\,\xi_0 + M_{vr}\,\bar{\xi}_r + M_{vv}\,\bar{\xi}_v + M_{v\lambda}\,\bar{\xi}_\lambda + \bar{m}_{v\tau}\,\xi_\tau + \bar{m}_{v\epsilon}\,\xi_\epsilon \qquad \text{(II-24)}$$

$$\bar{\psi}_\lambda = \bar{M}_{\lambda 0}\,\xi_0 + M_{\lambda r} + M_{\lambda v}\,\bar{\xi}_v + M_{\lambda\lambda}\,\bar{\xi}_\lambda + \bar{m}_{\lambda\tau}\,\xi_\tau + \bar{m}_{\lambda\epsilon}\,\xi_\epsilon \qquad \text{(II-25)}$$

Those elements of the matrix $\bar{M}$, appearing in (II-24) and (II-25) will be evaluated as follows:

From (II-21a), (II-22a) and (II-23), and the fact that $\bar{M}$ is symmetric, it is evident that the first row and column of $\bar{M}$ vanish. Hence:

$$\psi_0 = 0 \qquad \text{(II-26)}$$

$$\bar{m}_{v0} = \bar{m}_{\lambda 0}$$

From (II-21b) and the fact that $\xi_\epsilon = \epsilon$, we have:

$$\bar{\psi}_r(\tau) = \bar{\psi}_r(t) + \epsilon \int_t^\tau \frac{\partial L}{\partial \vec{r}}\, d\lambda \qquad \text{(II-27)}$$

and hence, from (II-21c), we have:

$$\bar{\psi}_v(\tau) = \bar{\psi}_v(t) - \bar{\psi}_r(t)\tau - \epsilon \int_t^\tau \int_t^\mu \frac{\partial L}{\partial \vec{r}}\, d\gamma\, d\mu \qquad \text{(II-28)}$$

Using boundary conditions (II-22b) and (II-22c) in (II-27) and (II-28) yields:

$$\bar{\psi}_r(t) = -\epsilon \int_t^{t+T} \frac{\partial L}{\partial \vec{r}}\, d\lambda = \bar{m}_{r\epsilon}\,\epsilon$$

and

$$\bar{\psi}_v(t) = -\left[T \int_t^{t+T} \frac{\partial L}{\partial \vec{r}}\, d\lambda - \int_t^{t+T} \int_t^\tau \frac{\partial L}{\partial \vec{r}}\, d\lambda\, d\tau \right] \epsilon \qquad \text{(II-29)}$$

$$= \bar{m}_{v\epsilon}\,\epsilon$$

A comparison of (II-29) and (II-24) indicates that,

$$M_{vr} = M_{vv} = M_{v\lambda} = M_{v\tau} = 0$$

Therefore, from (II-6) and (II-15), we have the quasi-optimum solution for $\bar{p}_v$.

$$\bar{p}_v \cong \bar{\psi}_v = -\epsilon \left[T \int_t^{t+T} \frac{\partial L}{\partial \vec{r}} \, d\lambda - \int_t^{t+T} \int_t^{\tau} \frac{\partial L}{\partial \vec{r}} \, d\lambda \, d\tau \right] \qquad \text{(II- 30)}$$

To obtain $\bar{\psi}_\lambda$, it is observed from (II-21d) that the differential equation governing $\bar{\psi}_\lambda$ is exactly the same as the original equation for $\bar{p}_\lambda$ in (II- 3), which, as was shown in Section 2.5.1, can be simplified by the transformation defined in (2- 64). Therefore, proceed by letting

$$\bar{\gamma}_q = [F'(\bar{\lambda}_c)]^{-1} \bar{\psi}_\lambda \qquad \text{(II- 31)}$$

then, from (2. 66) - (2. 68), (II- 21d) is transformed into

$$\dot{\bar{\gamma}}_q = -C(\bar{\lambda}_c) [\vec{a}_c \times \bar{\psi}_r] \qquad \text{(II- 32)}$$

and integration of (II- 32) yields

$$\bar{\gamma}_q(\tau) = \bar{\gamma}_q(t) - \int_t^{\tau} C(\bar{\lambda}_c) [\vec{a}_c \times \bar{\psi}_v] \, d\tau \qquad \text{(II- 33)}$$

Since from (II- 6) and (II- 15), we have the original $\bar{p}_\lambda$ as

$$\bar{p}_\lambda \cong \bar{\psi}_\lambda$$

it immediately follows that

$$\bar{\gamma}(\tau) \cong \gamma_q(\tau) = \bar{\gamma}(t) - \int_t^{\tau} C(\bar{\lambda}_c) [\vec{a}_c \times \bar{p}_v] \, d\tau \qquad \text{(II- 34)}$$

The quasi-optimum approximations of $\bar{p}_v$ and $\bar{\gamma}$ in (II- 30) and (II- 34) respectively are the necessary terms in deriving the quasi-optimum control law in Section 2.5.3.

APPENDIX III

Singular Optimum Control

Consider the optimum control problem described by (2. 45) - (2. 50). If $k = 0$, then the Hamiltonian becomes

$$h = p_0(M_\beta + \epsilon L) + \bar{p}_r' \vec{v} + \bar{p}_v \vec{a} + \bar{p}_\lambda' \bar{u} + p_\tau \qquad \text{(III- 1)}$$

Using (2. 61), the adjoint equation (2. 49) can now be rewritten as

$$p_0 = -1 \qquad \text{(III- 2)}$$

$$\dot{\bar{p}}_r = \epsilon \frac{\partial L}{\partial \vec{r}} \qquad \text{(III- 3)}$$

$$\dot{\bar{p}}_v = -\bar{p}_r \qquad \text{(III- 4)}$$

$$\dot{\bar{p}}_\lambda = \frac{\partial M_\beta}{\partial \bar{\lambda}} = \vec{a}_c' \left[\frac{\partial C(\bar{\lambda}_c)}{\partial \bar{\lambda}}\right]' C(\bar{\lambda}_c)\,\bar{p}_v \qquad \text{(III- 5)}$$

$$\dot{p}_\tau = \frac{\partial M_\beta}{\partial \tau} + \epsilon \frac{\partial L}{\partial \tau} \qquad \text{(III- 6)}$$

$$\dot{p}_\epsilon = L \qquad \text{(III- 7)}$$

The optimum controls $\vec{a}$ and $\bar{u}$ are obtained by computing the partial derivatives of the Hamiltonian h with respect to $\vec{a}$ and $\bar{u}$ and equating the derivatives to zero.

$$-\frac{\partial M_\beta}{\partial \bar{a}} + \bar{p}_v = 0 \qquad \text{(III- 8)}$$

$$\bar{p}_\lambda \equiv 0 \qquad \text{(III- 9)}$$

Substitution of (III- 9) into (III- 5) results in the relation

$$\vec{\alpha}_c' \left[\frac{\partial C(\bar{\lambda}_c)}{\partial \bar{\lambda}}\right]' C(\bar{\lambda}_c)\,\bar{p}_v = 0 \qquad \text{(III- 10)}$$

which can be rewritten as

$$\vec{\alpha}_c' \; C(\bar{\lambda}_c) \left[\frac{\partial C(\bar{\lambda}_c)}{\partial \bar{\lambda}}\right]' C(\bar{\lambda}_c)\,\bar{p}_v = 0$$

or, using (2. 71) with $K_\beta = 0$, it becomes

$$\vec{\alpha}_c' \; C(\bar{\lambda}_c) \left[\frac{\partial C(\bar{\lambda}_c)}{\partial \bar{\lambda}}\right]' \vec{\alpha}_A = 0 \qquad \text{(III- 11)}$$

After performing the matrix multiplication, (III- 11) can be reduced to the component form

$$\alpha_{cy}\alpha_{Az} - \alpha_{cz}\alpha_{Ay} = 0$$

$$(\alpha_{cy}\alpha_{Ax} - \alpha_{cx}\alpha_{Ay}) \sin\Phi_c \cos\psi_c + (\alpha_{cz}\alpha_{Ax} - \alpha_{cx}\alpha_{Az}) \cos\Phi_c \cos\psi_c$$

$$+ (\alpha_{cy}\alpha_{Az} - \alpha_{cz}\alpha_{Ay}) \sin\psi_c = 0 \qquad \text{(III- 12)}$$

$$(\alpha_{cx}\alpha_{Ay} - \alpha_{cy}\alpha_{Ax}) \cos\Phi_c + (\alpha_{cz}\alpha_{Ax} - \alpha_{cx}\alpha_{Az}) \sin\Phi_c = 0$$

Since the set of equations in (III- 12) should be satisfied for all values of Φ_c and ψ_c, it follows that

$$\alpha_{cx}\alpha_{Ay} - \alpha_{cy}\alpha_{Ax} = 0$$

$$\alpha_{cy}\alpha_{Az} - \alpha_{cz}\alpha_{Ay} = 0 \qquad \text{(III- 13)}$$

$$\alpha_{cz}\alpha_{Ax} - \alpha_{cx}\alpha_{Az} = 0$$

which implies that

$$\vec{\alpha}_c \times \vec{\alpha}_A = 0 \qquad \text{(III- 14)}$$

It is noted that for the singular case, the control $\bar{a}$ is solved from (III- 8) in exactly the same way as for the nonsingular case. The control $\bar{u}$, however, can not be obtained by a direct application of the maximum principle. The equation (III- 9) obtained by the maximum principle results in an indeterminate value of $\bar{u}$. To obtain $\bar{u}$ for the singular case, first solve the set of equations (III-12) for the cab attitude θ_c, Φ_c and ψ_c. Next, differentiate the expressions for θ_c, Φ_c, and ψ_c and use the definition (2. 8) to obtain $\bar{u}$.

It is noted that the cross product relation (III- 14) can also be obtained by neglecting the angular error dynamics and treating the angle error $\bar{\lambda}$ as a control variable. In this case, the system dynamics (2. 45) become

$$\begin{aligned} \dot{r}_0 &= M_\beta + \epsilon L \\ \dot{\vec{r}} &= \vec{v} \\ \dot{\vec{v}} &= \vec{a} \\ \dot{\tau} &= 1 \\ \dot{\epsilon} &= 0 \end{aligned} \qquad \text{(III- 15)}$$

for which $\vec{a}$ and $\bar{\lambda}$ (which is implicit in M_β) are the control variables. The formulation given by (III- 15) can be interpreted as determining $\vec{a}$ and $\bar{\lambda}$ so that good translational perception of the motion is obtained without regard to angular perception.

APPENDIX IV

FORTRAN SUBROUTINE OF THE SIMULATOR CONTROL SYSTEM

A FORTRAN subroutine called WASHFL was developed for implementing the simulator control system design shown in Figure 2-19 and given by (2.94), (2.95), (2.97) - (2.101). This subroutine was used in the computer simulation study described in Section 3 and also has the capability of being used on the computer facility at NASA-AMES to generate the actual drive commands for the moving base simulator.

This appendix contains program listings of the WASHFL subroutine and two other subroutines, GINTR and DRPRC, required by WASHFL to perform the numerical integration of state variables of the simulator control system. In addition to the program listings, a brief description of how to use the WASHFL subroutine and a description of all computer variables are given.

SUBROUTINE WASHFL

Purpose: Implement the simulator control system design.

Procedure: See the block diagram of the simulator control system design in Figure 2-19.

Usage: CALL WASHFL (IMODE, H, APHI, ATHT, APSI, AXFM, AYFM, AZFM, PA, QA, RA, CPX, CPY, CPZ, CPHI, CTHT, CPSI)

where the inputs are

IMODE	index controlling the mode of operation; = 0, bypass; = -1, initialization; = +1, simulation.
H	integration step size (sec).
APHI	aircraft roll angle (rad).
ATHT	aircraft pitch angle (rad).
APSI	aircraft yaw angle (rad).
AXFM	aircraft inertial acceleration in the x direction (ft/sec^2).
AYFM	aircraft inertial acceleration in the y direction (ft/sec^2).
AZFM	aircraft inertial acceleration in the z direction (ft/sec^2).
PA	aircraft roll rate (rad/sec).
QA	aircraft pitch rate (rad/sec).
RA	aircraft yaw rate (rad/sec).

and where the outputs are

CPX	cab inertial displacement command in the x direction (ft).
CPY	cab inertial displacement command in the y direction (ft).
CPZ	cab inertial displacement command in the z direction (ft).
CPHI	cab roll angle command (rad).
CTHT	cab pitch angle command (rad).
CPSI	cab yaw angle command (rad).

Remarks :

The input aircraft Euler angles APHI, ATHT, and APSI are defined according to the conventional sequence of rotations: yaw-pitch-roll. Since the simulator control system was designed using the sequence of rotations: pitch-yaw-roll, a transformation is included in WASHFL to convert the aircraft Euler angles from the former sequence to the latter sequence. The FORTRAN statements containing the transformation are designated by the word MAYBE in columns 74-78. If the aircraft Euler angles defined according to latter sequence are available in the computer simulation of the aircraft then, by deleting the FORTRAN statements identified by MAYBE in columns 74-78, those Euler angles can be used in the calling argument.

The output cab Euler angles are defined according to the rotational sequence: pitch-yaw-roll.

An improved first-order Euler method is used to perform the numerical integration. An integration step size of $H = 0.05$ sec was used in computer simulation studies.

Subroutines required: GINTR

A list of all computer variables used in the WASHFL subroutine is given below where the variables are partitioned according to scaler or array type.

Scaler Computer Variables

Computer Variable	Mathematical Symbol	Description
TIME	t	Double precision value of T.
H2	Δt	Double precision value of H.
TFIN	T	$t + T$ is the terminal time in the performance index.

Scaler Computer Variables, contd

Computer Variable	Mathematical Symbol	Description
CK	K_β	Weighting factor in the performance index.
FK	K_ω	Weighting factor in the performance index.
EPS	ϵ	Weighting factor in the performance index.
WEIGT	k	Weighting factor in the performance index.
XMAX	d_x	Translation limit of the cab motion in the x direction.
YMAX	d_y	Translation limit of the cab motion in the y direction.
ZMAX	d_z	Translation limit of the cab motion in the z direction.
FNΦRM	$\beta^2_{A\,max}$	Normalization factor used in the approximation of $\bar{P}_v$.
RCA		$= \cos \Phi_A$.
APHI	Φ_A	Aircraft roll angle.
RSA		$= \sin \Phi_A$.
PCA		$= \cos \theta_A$.
ATHT	θ_A	Aircraft pitch angle.
PSA		$= \sin \theta_A$.
YCA		$= \cos \psi_A$.
APSI	ψ_A	Aircraft yaw angle.
YSA		$= \sin \psi_A$.
RNUM		$= \sin \Phi_A \cos \psi_A - \cos \Phi_A \sin \theta_A \sin \psi_A$.
RDEN		$= \cos \Phi_A \cos \psi_A + \sin \Phi_A \sin \theta_A \sin \psi_A$.
PNUM		$= \sin \theta_A$.
PDEN		$= \cos \theta_A \cos \psi_A$.
YARG		$= \cos \theta_A \sin \psi_A$.
IMODE		Index for control of subroutine computational mode.

See (2.4)

Scaler Computer Variables, contd

Computer Variable	Mathematical Symbol	Description
T	t	Current time.
H	Δt	Time increment used for numerical integration.
IFRST		Index used to initialize the numerical integration.
TF2		$= T^2$.
TF3		$= T^3$.
TF4		$= T^4$.
		See TFIN
CPX	x_c	Cab inertial displacement command in x direction.
CPY	y_c	Cab inertial displacement command in y direction.
CPZ	x_c	Cab inertial displacement command in z direction.
CVX	$\dot{x}_c$	Cab inertial velocity in x direction.
CVY	$\dot{y}_c$	Cab inertial velocity in y direction.
CVZ	$\dot{z}_c$	Cab inertial velocity in z direction
CPHI	Φ_c	Cab roll angle command.
CTHT	θ_c	Cab pitch angle command.
CPSI	ψ_c	Cab yaw angle command.
GAMM1	γ_x	x - component of the new costate variable γ.
GAMM2	γ_y	y - component of the new costate variable γ.
GAMM3	γ_z	z - component of the new costate variable γ.
ATO		$= \tan\psi_A$.
APHID	$\dot{\Phi}$	$= p_A - (q_A \cos\Phi_A - r_A \sin\Phi_A) \tan\psi_A$; roll gimbal rate. (See 2.7)
PA	p_A	Aircraft roll rate.
QA	q_A	Aircraft pitch rate.
RA	r_A	Aircraft yaw rate.
ATHTD	$\dot{\theta}_A$	$= (q_A \cos\Phi_A - r_A \sin\Phi_A) / \cos\psi_A$; pitch gimbal rate.
APSID	$\dot{\psi}_A$	$= q_A \sin\Phi_A + r_A \cos\Phi_A$; yaw gimbal rate.

Scaler Computer Variables, contd

Computer Variable	Mathematical Symbol	Description
AXFM	$\ddot{x}_A$	Aircraft inertial acceleration in x direction.
AYFM	$\ddot{y}_A$	Aircraft inertial acceleration in y direction.
AZFM	$\ddot{z}_A$	Aircraft inertial acceleration in z direction.
CTO		$= \tan\psi_c$.
ABETA2		$= \beta_A^2$.
CK2		$= K_\beta^2$.
PV2		$= p_v^2$.
XXX		$= \xi / \beta_A^2$.
I		Do loop index.
CAX	$\ddot{x}_c$	x - component of the cab acceleration.
CAY	$\ddot{y}_c$	y - component of the cab acceleration.
CAZ	$\ddot{z}_x$	z - component of the cab acceleration.
CAZZ	$a_c(3)$	$= \ddot{z}_c + g$.
GAM1		$= \gamma_x / k$.
GAM2		$= \gamma_y / k$.
GAM3		$= \gamma_z / k$.
PQR2	$\dot{\omega}_A^2$	Magnitude squared of the aircraft angular rate.
FK2	K_ω^2	Square of the weighting factor in the performance index.
GAMMM2		$= (\gamma / k)^2$.
PQRGAM		$= \vec{\omega}_A \bullet \bar{\gamma} / k$.

Scaler Computer Variables, contd

Computer Variable	Mathematical Symbol	Description
OOO		$= \Omega / \omega_A$.
PC	p_c	Cab roll rate.
QC	q_c	Cab pitch rate.
RC	r_c	Cab yaw rate.
CPHID	$\dot{\Phi}_c$	Derivative of the cab roll angle command.
CTHID	$\dot{\Phi}_c$	Derivative of the cab pitch angle command.
CPSID	$\dot{\psi}_c$	Derivative of the cab yaw angle command.

Array Computer Variables

Computer Variable	Mathematical Symbol	Dimension	Description
VC		12	Simulator control system state vector.
YC		9	Derivative of the simulator control system state vector.
AF	$\vec{a}_A$	3	Specific force acting on the aircraft.
AALFA	$\vec{\alpha}_A$	3	Sensed specific force acting on the aircraft.
ABETA	$\vec{\beta}_A$	3	Unbiased sensed specific force acting on the aircraft.
ACO		3	$= \cos \bar{\lambda}_A$.
ASO		3	$= \sin \bar{\lambda}_A$.
TFM	$C(\bar{\lambda}_A)$	3x3	Coordinate transformation of the aircraft Euler angles.
CCO		3	$= \cos \bar{\lambda}_c$.
CSO		3	$= \sin \bar{\lambda}_c$.
CFM	$C(\bar{\lambda}_c)$	3x3	Coordinate transformation of the cab Euler angles.
CALFA	$\vec{\alpha}_c$	3	Sensed specific force acting on the cab.

Array Computer Variables, contd

Computer Variable	Mathematical Symbol	Dimension	Description
PV	$\vec{p}_v$	3	Costate of the velocity error.
ROA		3	$= C'(\bar{\lambda}_c)\vec{\alpha}_A$.
ROB		3	$= C'(\bar{\lambda}_c)\vec{\beta}_A$.
W	$\vec{a}$	3	Error in the specific force.
ETA	$\bar{\eta}$	3	Intermediate variable used in the angular washout computation.
D		3	Diagonal elements of the matrix D in the penalty function $L(\vec{r}_c)$.

Listing of Subroutine WASHFL

```
      SUBROUTINE WASHFL(IMODE, H, APHI,ATHT,APSI, AXFM,AYFM,AZFM,
     *                  PA,QA,RA, CPX,CPY,CPZ, CPHI,CTHT,CPSI )
      DIMENSION VC(12),YC(9)
      DIMENSION AF(3),AALFA(3),ABETA(3),ACO(3),ASO(3),TFM(3,3)
      DIMENSION CCO(3),CSO(3),CFM(3,3),CALFA(3)
      DIMENSION PV(3),ROA(3),ROB(3),W(3),ETA(3),D(3)
      DATA      TFIN/5.0       /
      DATA        CK/0.0       /
      DATA        FK/0.0       /
      DATA       EPS/0.16      /
      DATA     WEIGT/1.0       /
      DATA      XMAX/10.0      /
      DATA      YMAX/10.0      /
      DATA      ZMAX/10.0      /
      DATA     FNORM/350.0     /
      DOUBLE PRECISION TIME,H2
      RCA= COS(APHI)                                                  MAYBE
      RSA= SIN(APHI)                                                  MAYBE
      PCA= COS(ATHT)                                                  MAYBE
      PSA= SIN(ATHT)                                                  MAYBE
      YCA= COS(APSI)                                                  MAYBE
      YSA= SIN(APSI)                                                  MAYBE
      RNUM = -RCA*PSA*YSA + RSA*YCA                                   MAYBE
      RDEN = RSA*PSA*YSA + RCA*YCA                                    MAYBE
      PNUM = PSA                                                      MAYBE
      PDEN = PCA*YCA                                                  MAYBE
      YARG = PCA*YSA                                                  MAYBE
       APHI = ATAN2(RNUM,RDEN)                                        MAYBE
       ATHT = ATAN2(PNUM,PDEN)                                        MAYBE
       APSI = ASIN(YARG)                                              MAYBE
      IF (IMODE) 1000, 3000, 2000
C
C    ***************
C    INITIALIZATION
C    ***************
C
 1000 CONTINUE
      T = 0.0
      TIME = DBLE(T)
      T = SNGL(TIME)
      H2 = DBLE(H)
      IFRST = 0
         TF2 = TFIN**2
         TF3 = TFIN**3
         TF4 = TF2**2
       D(1) = 1.0/(XMAX**2)
       D(2) = 1.0/(YMAX**2)
       D(3) = 1.0/(ZMAX**2)
```

Listing of Subroutine WASHFL (Continued)

```
      CPX = 0.0
      CPY = 0.0
      CPZ = 0.0
      CVX = 0.0
      CVY = 0.0
      CVZ = 0.0
      CPHI = APHI
      CTHT = ATHT
      CPSI = APSI
      GAMM1 = 0.0
      GAMM2 = 0.0
      GAMM3 = 0.0
      GO TO 3000
C
C
C
C    ****************************
C    DEFINING AIRCRAFT VARIABLES
C    ****************************
C
 2000 CONTINUE
       ACO(1) = COS(APHI)
       ACO(2) = COS(ATHT)
       ACO(3) = COS(APSI)
       ASO(1) = SIN(APHI)
       ASO(2) = SIN(ATHT)
       ASO(3) = SIN(APSI)
       ATO = TAN(APSI)
       APHID = PA - (QA*ACO(1) - RA*ASO(1))*ATO
       ATHTD = (QA*ACO(1) - RA*ASO(1))/ACO(3)
       APSID = QA*ASO(1) + RA*ACO(1)
C
        TFM(1,1) = ACO(2)*ACO(3)
        TFM(2,1) = ASO(1)*ASO(2) - ACO(1)*ASO(3)*ACO(2)
        TFM(3,1) = ACO(1)*ASO(2) + ASO(1)*ASO(3)*ACO(2)
        TFM(1,2) = ASO(3)
        TFM(2,2) = ACO(1)*ACO(3)
        TFM(3,2) = -ASO(1)*ACO(3)
        TFM(1,3) = -ACO(3)*ASO(2)
        TFM(2,3) = ASO(1)*ACO(2) + ACO(1)*ASO(3)*ASO(2)
        TFM(3,3) = ACO(1)*ACO(2) - ASO(1)*ASO(3)*ASO(2)
C
      AF(1) = AXFM
      AF(2) = AYFM
      AF(3) = AZFM - 32.2
      AALFA(1) = TFM(1,1)*AF(1) + TFM(1,2)*AF(2) + TFM(1,3)*AF(3)
      AALFA(2) = TFM(2,1)*AF(1) + TFM(2,2)*AF(2) + TFM(2,3)*AF(3)
      AALFA(3) = TFM(3,1)*AF(1) + TFM(3,2)*AF(2) + TFM(3,3)*AF(3)
```

Listing of Subroutine WASHFL (Continued)

```
      ABETA(1) = AALFA(1)
      ABETA(2) = AALFA(2)
      ABETA(3) = AALFA(3) + 32.2
C
C
C     ************************
C     DEFINING CAB VARIABLES
C     ************************
C
      CCO(1) = COS(CPHI)
      CCO(2) = COS(CTHT)
      CCO(3) = COS(CPSI)
      CSO(1) = SIN(CPHI)
      CSO(2) = SIN(CTHT)
      CSO(3) = SIN(CPSI)
      CTO = TAN(CPSI)
        CFM(1,1) = CCO(2)*CCO(3)
        CFM(2,1) = CSO(1)*CSO(2) - CCO(1)*CSO(3)*CCO(2)
        CFM(3,1) = CCO(1)*CSO(2) + CSO(1)*CSO(3)*CCO(2)
        CFM(1,2) = CSO(3)
        CFM(2,2) = CCO(1)*CCO(3)
        CFM(3,2) = -CSO(1)*CCO(3)
        CFM(1,3) = -CCO(3)*CSO(2)
        CFM(2,3) = CSO(1)*CCO(2) + CCO(1)*CSO(3)*CSO(2)
        CFM(3,3) = CCO(1)*CCO(2) - CSO(1)*CSO(3)*CSO(2)
C
C
C     ****************************************
C     COMPUTES TRANSLATIONAL WASHOUT CONTROLS
C     ****************************************
C
      PV(1) = -EPS*D(1)*(CPX*TF2/2.0 +CVX*TF3/3.0 +AXFM*TF4/(8.0*FNORM))
      PV(2) = -EPS*D(2)*(CPY*TF2/2.0 +CVY*TF3/3.0 +AYFM*TF4/(8.0*FNORM))
      PV(3) = -EPS*D(3)*(CPZ*TF2/2.0 +CVZ*TF3/3.0 +AZFM*TF4/(8.0*FNORM))
      ROA(1) = AALFA(1)*CFM(1,1) + AALFA(2)*CFM(2,1) + AALFA(3)*CFM(3,1)
      ROA(2) = AALFA(1)*CFM(1,2) + AALFA(2)*CFM(2,2) + AALFA(3)*CFM(3,2)
      ROA(3) = AALFA(1)*CFM(1,3) + AALFA(2)*CFM(2,3) + AALFA(3)*CFM(3,3)
      ABETA2 = ABETA(1)**2 + ABETA(2)**2 + ABETA(3)**2
C
      IF (CK.EQ.0.0) GO TO 100
      CK2 = CK**2
      PV2 = PV(1)**2 + PV(2)**2 + PV(3)**2
      ROB(1) = ABETA(1)*CFM(1,1) + ABETA(2)*CFM(2,1) + ABETA(3)*CFM(3,1)
      ROB(2) = ABETA(1)*CFM(1,2) + ABETA(2)*CFM(2,2) + ABETA(3)*CFM(3,2)
      ROB(3) = ABETA(1)*CFM(1,3) + ABETA(2)*CFM(2,3) + ABETA(3)*CFM(3,3)
      XXX = ABETA2*PV2 + CK2 + 2.*CK *(PV(1)*ROB(1)+PV(2)*ROB(2)
     *                                 +PV(3)*ROB(3))
      XXX = SQRT(XXX)
```

Listing of Subroutine WASHFL (Continued)

```
      DO 5 I=1,3
      ETA(I) = -((1.0 + CK/(-CK+XXX))*AALFA(I) + CK*ABETA(I))/ABETA2
    5 W(I) = (1.0 - CK/XXX)*(ABETA2*PV(I) + CK*ROB(I)) + ROA(I) - AF(I)
      GO TO 200
  100 CONTINUE
C
      DO 6 I=1,3
      ETA(I) = -AALFA(I)/ABETA2
    6 W(I) = ABETA2*PV(I) + ROA(I) - AF(I)
  200 CONTINUE
      CAX = AXFM + W(1)
      CAY = AYFM + W(2)
      CAZ = AZFM + W(3)
      CAZZ = CAZ - 32.2
      CALFA(1) = CFM(1,1)*CAX   + CFM(1,2)*CAY   + CFM(1,3)*CAZZ
      CALFA(2) = CFM(2,1)*CAX   + CFM(2,2)*CAY   + CFM(2,3)*CAZZ
      CALFA(3) = CFM(3,1)*CAX   + CFM(3,2)*CAY   + CFM(3,3)*CAZZ
C
C
C   ***********************************
C   COMPUTES ANGULAR WASHOUT CONTROLS
C   ***********************************
C
C
      GAM1 = GAMM1/WEIGT
      GAM2 = GAMM2/WEIGT
      GAM3 = GAMM3/WEIGT
      PQR2 = PA*PA + QA*QA + RA*RA
C
      IF (FK.EQ.0.0) GO TO 700
      FK2 = FK*FK
      GAMMM2 = GAM1**2 + GAM2**2 + GAM3**2
      PQRGAM = PA*GAM1 + QA*GAM2 + RA*GAM3
      OOO = PQR2*GAMMM2 + 2.0*FK*PQRGAM + FK2
      OOO = SQRT(OOO)
      PC = PA + (1.0 - FK/OOO)*(PQR2*GAM1 + FK*PA)
      QC = QA + (1.0 - FK/OOO)*(PQR2*GAM2 + FK*QA)
      RC = RA + (1.0 - FK/OOO)*(PQR2*GAM3 + FK*RA)
      GO TO 800
  700 CONTINUE
C
      PC = PA + PQR2*GAM1
      QC = QA + PQR2*GAM2
      RC = RA + PQR2*GAM3
  800 CONTINUE
C
      CPHID =PC - QC*CCO(1)*CTO + RC*CSO(1)*CTO
      CTHTD =QC*CCO(1)/CCO(3) - RC*CSO(1)/CCO(3)
```

Listing of Subroutine WASHFL (Continued)

```
      CPSID =QC*CSO(1) + RC*CCO(1)
C
C
C     ************************************
C     COMPUTES INPUTS TO THE INTEGRATORS
C     ************************************
C
      YC(1) = CAX
      YC(2) = CAY
      YC(3) = CAZ
      YC(4) = CPHID
      YC(5) = CTHTD
      YC(6) = CPSID
      YC(7) = CALFA(3)*ETA(2) - CALFA(2)*ETA(3)
      YC(8) = CALFA(1)*ETA(3) - CALFA(3)*ETA(1)
      YC(9) = CALFA(2)*ETA(1) - CALFA(1)*ETA(2)
C
      VC(1) = CPX
      VC(2) = CVX
      VC(3) = CPY
      VC(4) = CVY
      VC(5) = CPZ
      VC(6) = CVZ
      VC(7) = CPHI
      VC(8) = CTHT
      VC(9) = CPSI
      VC(10) = GAMM1
      VC(11) = GAMM2
      VC(12) = GAMM3
C
C
C     ***********************
C     PERFORMING INTEGRATION
C     ***********************
C
      CALL GINTR(T, H, VC, YC, IFRST)
C
      CPX = VC(1)
      CPY = VC(3)
      CPZ = VC(5)
      CVX = VC(2)
      CVY = VC(4)
      CVZ = VC(6)
      CPHI = VC(7)
      CTHT = VC(8)
      CPSI = VC(9)
      GAMM1 = VC(10)
      GAMM2 = VC(11)
```

Listing of Subroutine WASHFL (Continued)

```
      GAMM3 = VC(12)
C
      TIME = TIME + H2
      T = SNGL(TIME)
C
 3000 CONTINUE
      RETURN
      END
```

Listing of Subroutine GINTR

```
      SUBROUTINE GINTR(T, H, Y, YC, IFRST)
      DIMENSION Y(12),YD(12),YC(9),XXX(12)
      DIMENSION STATE(12), STATET(12)
      COMMON/DOUBLE/ STATE, STATET
      DOUBLE PRECISION STATE, STATET, DTT, DBLT
      TMAX = T + H
      IF (IFRST.NE.0) GO TO 900
      IFRST = 1
      EPSIL = 1.E-4
      CALL DRPRC(YD, Y, YC)
  900 CONTINUE
  101 CONTINUE
      DBLT = DBLE(T)
      DTT = DBLT + 0.5D0 * DBLE(H)
      TT = SNGL ( DTT )
      DO 105 I=1,12
      STATE(I) = DBLE(Y(I))
      XXX(I) = 0.5*H*YD(I)
      STATET(I)=STATE(I)+DBLE(XXX(I))
       Y(I)=SNGL(STATET(I))
  105 CONTINUE
      CALL DRPRC(YD, Y, YC)
      DO 205 I=1,12
      XXX(I) = H*YD(I)
      STATE(I)=STATE(I)+DBLE(XXX(I))
      Y(I)=SNGL(STATE(I))
  205 CONTINUE
      DBLT = DBLT + DBLE(H)
      T = SNGL ( DBLT )
      CALL DRPRC(YD, Y, YC)
      IF ( T. LT . ( TMAX - EPSIL )) GO TO 101
      RETURN
      END
```

Listing of Subroutine DRPRC

```
      SUBROUTINE DRPRC(DXP,ZP,VP)
      DIMENSION DXP(12),ZP(12),VP(9)
C
C
      DXP(1) = ZP(2)
      DXP(2) = VP(1)
      DXP(3) = ZP(4)
      DXP(4) = VP(2)
      DXP(5) = ZP(6)
      DXP(6) = VP(3)
      DXP(7) = VP(4)
      DXP(8) = VP(5)
      DXP(9) = VP(6)
         DXP(10) = VP(7)
         DXP(11) = VP(8)
         DXP(12) = VP(9)
C
C
      RETURN
      END
```

*U.S. GOVERNMENT PRINTING OFFICE: 1973-739-153/49

"The aeronautical and space activities of the United States shall be conducted so as to contribute . . . to the expansion of human knowledge of phenomena in the atmosphere and space. The Administration shall provide for the widest practicable and appropriate dissemination of information concerning its activities and the results thereof."

—NATIONAL AERONAUTICS AND SPACE ACT OF 1958

NASA SCIENTIFIC AND TECHNICAL PUBLICATIONS

TECHNICAL REPORTS: Scientific and technical information considered important, complete, and a lasting contribution to existing knowledge.

TECHNICAL NOTES: Information less broad in scope but nevertheless of importance as a contribution to existing knowledge.

TECHNICAL MEMORANDUMS: Information receiving limited distribution because of preliminary data, security classification, or other reasons. Also includes conference proceedings with either limited or unlimited distribution.

CONTRACTOR REPORTS: Scientific and technical information generated under a NASA contract or grant and considered an important contribution to existing knowledge.

TECHNICAL TRANSLATIONS: Information published in a foreign language considered to merit NASA distribution in English.

SPECIAL PUBLICATIONS: Information derived from or of value to NASA activities. Publications include final reports of major projects, monographs, data compilations, handbooks, sourcebooks, and special bibliographies.

TECHNOLOGY UTILIZATION PUBLICATIONS: Information on technology used by NASA that may be of particular interest in commercial and other non-aerospace applications. Publications include Tech Briefs, Technology Utilization Reports and Technology Surveys.

Details on the availability of these publications may be obtained from:

SCIENTIFIC AND TECHNICAL INFORMATION OFFICE

NATIONAL AERONAUTICS AND SPACE ADMINISTRATION

Washington, D.C. 20546